DEVELOPMENT OF GRAPHENE OXIDE BASED AEROGELS

A THESIS SUBMITTED TO
THE GRADUATE SCHOOL OF NATURAL AND APPLIED SCIENCES
OF
MIDDLE EAST TECHNICAL UNIVERSITY

BY

ÖZNUR DOĞAN

IN PARTIAL FULFILLMENT OF THE REQUIREMENTS
FOR
THE DEGREE OF MASTER OF SCIENCE
IN
CHEMICAL ENGINEERING

AUGUST 2017

Approval of thesis:

DEVELOPMENT OF GRAPHENE OXIDE BASED AEROGELS

submitted by **ÖZNUR DOĞAN** in partial fulfillment of the requirements for the degree of **Master of Science in Chemical Engineering Department, Middle East Technical University** by,

Prof. Dr. Gülbin Dural Ünver
Dean, Graduate School of **Natural and Applied Sciences** _____

Prof. Dr. Halil Kalıpçılar
Head of Department, **Chemical Engineering** _____

Asst. Prof. Dr. Erhan Bat
Supervisor, **Chemical Engineering Dept., METU** _____

Examining Committee Members:

Prof. Dr. Levent Yılmaz _____
Chemical Engineering Dept., METU

Asst. Prof. Dr. Erhan Bat _____
Chemical Engineering Dept., METU

Assoc. Prof. Dr. Bora Maviş _____
Mechanical Engineering Dept., Hacettepe University

Asst. Prof. Dr. Emre Büküşoğlu _____
Chemical Engineering Dept., METU

Asst. Prof. Dr. Bahar İpek _____
Chemical Engineering Dept., METU

Date: 18.08.2017

I hereby declare that all information in this document has been obtained and presented in accordance with academic rules and ethical conduct. I also declare that, as required by these rules and conduct, I have fully cited and referenced all material and results that are not original to this work.

Name, Last Name: Öznur Doğan

Signature:

ABSTRACT

DEVELOPMENT OF GRAPHENE OXIDE BASED AEROGELS

Doğan, Öznur
M.Sc., Department of Chemical Engineering
Supervisor: Asst. Prof. Dr. Erhan Bat

August 2017, 101 pages

Owing to their large surface area, high hydrophobicity and porous structure, graphene oxide based aerogels have been proposed as feasible and economic solutions for the increasing water pollution caused by crude oils, petroleum products and toxic organic solvents. In this study, graphene oxide based aerogels were prepared via two different routes. In the first route, random copolymers of glycidyl methacrylate and styrene were used as crosslinkers in the aerogel. In the second route, 1,3-diaminopropane was used to obtain crosslinked hydrogel precursors. Graphene oxide was synthesized using Tour Method and characterized. Morphology of graphene oxide was assessed using Scanning Electron Microscopy (SEM) and Transmission Electron Microscopy (TEM) analyses. Copolymers of glycidyl methacrylate and styrene were synthesized using free radical polymerization and chemical characterizations were performed. Copolymers were used along with graphene oxide in order to synthesize the precursor hydrogels. Graphene oxide concentration in the hydrogels was kept at 5.0 mg/mL while copolymer concentrations were varied from 0 to 5.0 mg/mL. After freeze-drying and thermal reduction, morphologies of the aerogels were assessed using SEM analysis. To determine the oil absorption capacity of the prepared aerogels,

chloroform, toluene and sunflower oil were used. The prepared aerogels were found to have absorption capacities in the range of 90 to 175 g/g for toluene and 90 to 200 g/g for sunflower oil. In the case of chloroform, aerogels with higher styrene content had absorption capacities ranging from 170 to 315 g/g, whereas this range was between 145-260 g/g for aerogels with lower styrene content. 1,3-diaminopropane and reduced graphene oxide based aerogels were found to have absorption capacities in the range of 230 to 534 g/g for chloroform, 109 to 202 g/g for toluene and lastly 173 to 270 g/g for sunflower oil. Aerogels with initial graphene oxide concentration of 3 mg/mL showed better absorption capacities compared to that of 4 mg/mL and 5 mg/mL. Aerogels produced by either route offer efficient absorption for oil and are promising candidates to be used in oil-water separation.

Keywords: Graphene oxide, aerogel, hydrogel, separation, polymer

ÖZ

GRAFEN OKSİT ESASLI AEROJELLERİN GELİŞTİRİLMESİ

Doğan, Öznur
Yüksek Lisans, Kimya Mühendisliği Bölümü
Tez Yöneticisi: Yrd. Doç. Dr. Erhan Bat

Ağustos 2017, 101 sayfa

Geniş yüzey alanları, yüksek hidrofobiklikleri ve gözenekli yapıları sayesinde grafen oksit esaslı aerojeller ham petrol, petrol ürünleri ve toksik organik çözücülerden kaynaklı artan su kirliliğini için uygulanabilir ve ekonomik çözümlerdir. Bu çalışmada iki farklı yöntem kullanılarak oxit esaslı aerojeller üretilmiştir. İlk yöntemde glisidil metakrilat ve stirenin random kopolimerleri aerojelde çapraz bağlayıcı olarak kullanılmıştır. İkinci yöntemde ise 1,3-diaminopropan çapraz bağlı öncül hidrojel eldesinde kullanılmıştır. Başlangıç olarak Tour yöntemi ile grafen oksit sentezlenerek kimyasal karakterizasyonları yapılmıştır. Üretilen grafen oksitin morfolojisi Taramalı Elektron Mikroskopu (SEM) ve Geçirmeli Elektron Mikroskopu (TEM) kullanılarak incelenmiştir. Glisidil metakrilat ve stiren kopolimerleri serbest radikal polimerizasyon kullanılarak sentezlenmiş ve karakterizasyonları yapılmıştır. Kopolimerler grafen oksitle birlikte öncül hidrojellerin üretilmesinde kullanılmıştır. Kopolimer konsantrasyonları 0 ile 5 mg/mL arasında değişirken 5 mg/mL'lik grafen oksit konsantrasyonu kullanılmıştır. Liyofilizasyon ve termal indirgemenin ardından aerojel morfolojileri SEM analizi ile tayin edilmiştir. Hazırlanan aerojellerin yağ emme kapasitelerini bulmak amacı ile kloroform, toluen ve ayçiçeği yağı

kullanılmıştır. Hazırlanan aerojellerin toluene için 90 ile 170 g/g aralığında ve sebze yağı için 90 ile 200 g/g aralığında emme kapasitesine sahip oldukları görülmüştür. Kloroformda ise yüksek oranda stiren içeren aerojellerin 170 ile 315 g/g arasında emme kapasitesine sahip oldukları görülmüşken, bu aralık düşük oranda stiren içeren aerojeller için 145 ile 260 g/g olmuştur. 1,3-diaminopropan ve indirgenmiş grafen oksit esaslı aerojeller kloroform için 230 ile 534 g/g arasında, toluen için 109 ile 202 g/g arasında ve son olarak ayçiçeği yağı için 173 ile 270 g/g arasında emme kapasitesi göstermişlerdir.

3 mg/mL'lik başlangıç grafen oksit konsantrasyonuna sahip aerojeller 4 ve 5 mg/mL başlangıç grafen oksit konsantrasyonuna sahip aerojellere göre daha yüksek emme kapasitesi göstermişlerdir. Kullanılan yöntemlerden herhangi biriyle üretilen aerojeller etkili yağ emme özelliği göstermişlerdir ve yağ-su ayrıştıma için gelecek vaat eden adaylardır.

Anahtar Kelimeler: Grafen oksit, aerojel, hidrojel, ayrıştırma, polimer

To my dearest family,

ACKNOWLEDGMENTS

I would like to start with expressing my sincere appreciation and gratitude towards my supervisor Dr. Erhan Bat for his guidance and support. It has been a great experience for me to be a part of his research group.

I finally have a chance to thank Dr. Canan Özgen and Dr. Cevdet Öztin; without their encouragement, it would have been much harder for me to graduate. Dr. Hayrettin Yücel, Dr. Güngör Gündüz and Dr. Levent Yılmaz also believed in me and encouraged me when I consider a M.Sc. degree in Chemical Engineering, I owe them a sincere appreciation. I am also grateful for the support that Dr. İnci Ayrancı provided.

I would like to thank Dr. Gülay Ertaş and Dr. Bora Maviş for letting me use their laboratory equipment. I am appreciatory for the humanity and kindness of İsa Çağlar and Gazi Saranay at all times. I am also thankful for the help and understanding that METU Central Laboratory staff especially S. Kaan Kirdeciler provided.

I would like to thank my lab partners; Ayşe Elif Kıratlı, Gözde Şahin, Zeynep Cansu Özçınar, Hatice Özyetiş, Cemre Avşar, Seda Sivri, Cansu Çaylan and Duygu Sezen Polat for their support and friendship. I would also like to thank Sibel Öztürk, Damla Hüccetoğulları, Yiğit Akgün, Erdem Boy and Zeynep Erova for their friendships and the cheers that they gave me. I would like to thank C-Block residents also for the support they provided.

I appreciate invaluable friendships of Semanur Kandil and Emre Altınkaynak. They have been bearing me out in every step I took. I have always felt special with the intimacy and support they provided.

My special thanks to Muhammed Kavak for standing up with me at all time. Everything would be much harder without his endless patience and support.

Last but not the least, I would like to thank my family. In every achievement that I made, my family especially my mother has a great share. They have always encouraged me to believe in myself and I am more than lucky to have them.

TABLE OF CONTENTS

LIST OF TABLES

TABLES

LIST OF FIGURES

FIGURES

LIST OF ABBREVIATIONS

Abbreviation	Definition
1,3-DAP	1,3-diaminopropane
AIBN	Azobisisobutyronitrile
CdS	Cadmium sulfide
CdSe	Cadmium selenide
CGS	Compressible graphene sponge
ClO_2	Chlorine dioxide
CO	Carbon monoxide
CO_2	Carbon dioxide
CNT	Carbon nanotube
CuO	Copper(I) oxide
DMF	N,N-dimethylformamide
$Fe(C_5H_5)_2$	Ferrocene
GA	Graphene aerogel
GMA	Glycidyl methacrylate
GO	Graphene oxide
HCl	Hydrochloric acid
HNO_3	Nitric acid
H_2O_2	Hydrogen peroxide
H_2SO_4	Sulfuric acid
H_3PO_4	Orthophosphoric acid
IC	Integrated circuit
ICF	Inertial confinement fusion
$KClO_3$	Potassium chlorate
$KMnO_4$	Potassium permanganate
K_2FeO_4	Potassium ferrate

M_n	Number average molecular weight
Mn_2O_7	Dimanganeseheptoxide
M_w	Weight average molecular weight
$NaBH_4$	Sodium borohydride
$NaClO_3$	Sodium chlorate
$NaNO_3$	Sodium nitrate
NbC	Nobium carbide
NMP	N-methyl-2-pyrrolidone
PbS	Lead(II) sulfide
PDI	Polydispersity index
PDMS	Poly(dimethylsiloxane)
pGcSt	Poly(glycidyl methacrylate-co-styrene)
RF	Pesorcinol-formaldehyde
rGO	Reduced graphene oxide
Sty	Styrene
THF	Tetrahydrofuran
TiC	Titanium carbide
TiO_2	Titanium dioxide
ULGA	Ultralight graphene aerogel
ZnS	Zinc sulfide

CHAPTER 1

INTRODUCTION

Industrialization has improved life in many ways. Use of technology in agriculture, health etc. created a better life quality for humans. As technology evolves in many areas including fabrication of goods and transportation, more challenges to deal with arise. Pollution, one of the biggest challenge, in many aspects of the nature created harsh conditions to live in. Release of waste products, chemical contaminants and harmful gases through environment create harmful and even fatal effects to any living organism[1].

Industrial wastes together with spills due to industrial accidents and sinking of oil tankers are very important challenges to consider and there is no universal solution for those problems[2,3]. Oil based effluent wastes to sea-water have endangered not only the marine environment, but also most of the living organism as well as the soil. In Figure 1.1, animals affected by an oil spill in an ocean can be seen. In the figure on the left, soil which is contaminated by oil can also be seen.

Figure 1.1: Animals affected by an oil spill in an ocean[4].

Industrial wastes and tanker spills are not the only sources for the contamination of water with oil. Domestic waste oil is more than 15 million tons annually[5]. Its disposal happens through the drains, which joins to the waste water eventually and makes the waste-water treatment problematic in many aspects including the difficulties in separation and increase in cost[6]. Diseases, and deaths become inevitable in an environment without a clean water resource, since it affects food chain as a whole. As a result in the upcoming decades, the problems related with water are expected to grow [7,8].

In order to preserve nature as well as the future, people are prompt to seek for remediation strategies for water, especially for removal of oil from water. There are increasing number of research to find new water purification methods which cost less money, spend less energy, minimize use of chemicals, and minimize effect of chemicals on the environment[7]. Different kinds of materials such as polystyrene, carbon nanotube, fatty acid were used for the purpose of oil removal due to their oleophilic nature[9]. Absorptive and/or reactive strategies have been proposed in many studies. There are some conventional methods for oil/water separation including air flotation, ultrasonic separation etc. yet, use of nanotechnology combined with those strategies is thought to be more effective than conventional techniques[9,10]. It is mainly attributed to superior properties of nanomaterials such as high surface area, and limitations caused by conventional methods such as secondary pollutants generated, large sizes, low efficiencies[9,10].

There are numerous materials proposed for the separation oily water and some of the nanomaterials can be listed as[10]:

- Nanodispersants
- Magnetic nanocomposites
- Filters/pads
- Foams and meshes
- Micro- and nano-TiO_2
- Membranes

- Carbon nanostructures
- Nanostructured hydrophobic organoclays
- Aerogels.

There are some critical issues that should be considered while choosing appropriate nanomaterial for oil-water separation. These issues can be listed as environmental factors, multifunctional synergies, commercial viability, engineering aspects, performance criteria and cost aspects[11]. Among all of the nanomaterials listed above, aerogels are among the most important materials for oil spill cleanup, yet the critical issues hold for aerogels also. On the other hand, aerogels are advantageous in terms of cost aspects: aerogels' cost per kilograms is likely to decrease in the near future[10].

Aerogels are very similar to hydrogels and they can be obtained by removing water from the precursor hydrogel using supercritical drying, freeze-drying etc. They have open pore structure, low density and high surface area which also make them preferable in many applications as well as in oil-water separation. In order to increase the absorbance capacity as well as to increase surface area of the aerogels, carbon based materials including activated carbon, carbon nanotube, and graphene oxide have been used for the production of aerogels. A graphene oxide based aerogel with low density on a flower (dog's tail) can be seen in Figure 1.2.

Figure 1.2: A graphene oxide based aerogel with low density[12].

Among the carbon based materials, graphene oxide is more preferable considering the cost of production and scalable production. In addition, aerogels of different shapes and properties can be obtained by changing production conditions and ingredients used to obtain aerogels. In terms of water remediation, graphene oxide has been used together with,

- Polyethyleneimine[13], biopolymers[14], chitosan/silver[15] for dye removal,
- Chitosan[16], poly(N,N-dimethylaminoethyl methacrylate)[17] for the removal of ions,
- Ethylene diamine[18,19], polypyrole[20], poly(acrylic acid)[21] for water-oil separation.

By increasing oleophilicity and hydrophobicity of graphene oxide based aerogels, oil absorption capacity can be increased, and consecutively environmental wealth can be recovered. Both polymers, and materials that have nitrogen in their structures such as ethylene diamine have been used for the production of graphene oxide based aerogels. Use of oleophilic polymers, such as polystyrene, in the production of hydrogels may improve the oil absorption capacity of aerogels. By extending the chain length of the crosslinker, the distance between crosslinks increases. Using longer chains of diamine based crosslinkers may increase the absorption capacity as well.

In this study, we set out to develop reduced graphene oxide based aerogels with enhanced oil absorption properties. To achieve this goal, aerogels were prepared by using two different crosslinker molecules: In the first approach, random copolymers of glycidyl methacrylate and styrene were used. Here the styrene residues were expected to impart oleophilicity while glycidyl methacrylate residues were expected to react with the functional groups on graphene oxide to form a network. In the second approach, instead of the commonly used crosslinker ethylenediamine, 1,3-diaminopropane was used as the crosslinker molecule.

CHAPTER 2

BACKGROUND AND LITERATURE SURVEY

2.1. Aerogels

2.1.1. Definition

Aerogels are porous materials in which the liquid inside the wet gel is replaced with air leading to small shrinkage and without causing any damage in its structure[22,23]. Following the invention of aerogel in 1931 by Kistler, interest in the subject aroused and number of the research on the subject have increased[22,24]. Aerogels are well known with their low densities and large surface areas, but the features of the aerogels are specified with their applications[25–29].

2.1.2. Classification of Aerogels

Although there are quite a few methods for the classification of aerogels, common classification is gathered under four categories as indicated below in Figure 2.1 according to the literature[23].

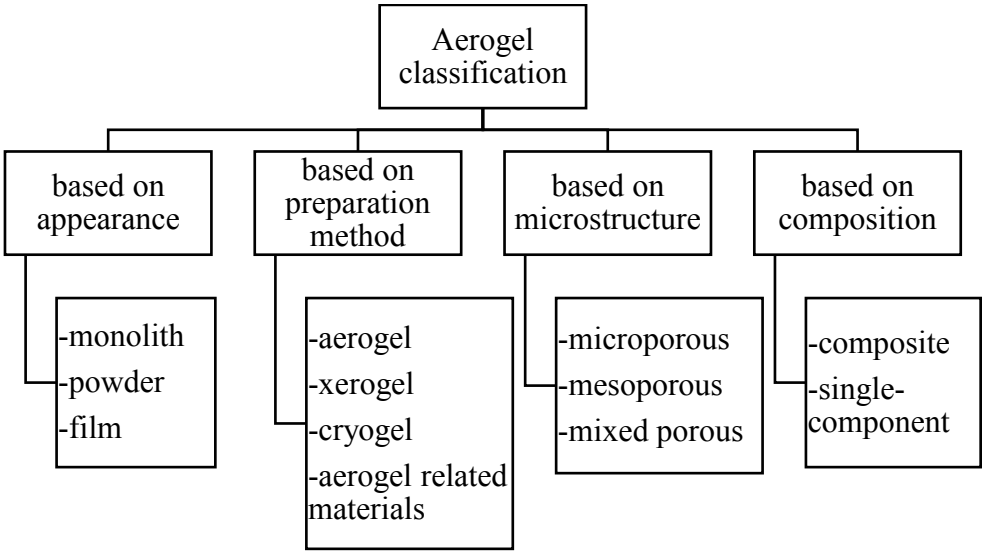

Figure 2.1: Classification of aerogels[23].

Among all methods, the most common way to classify aerogels is to consider their compositions as single-component aerogel and aerogel composites[23]. Oxide aerogels, organic aerogels, carbon aerogels, chalcogenide aerogels and others can be considered in single component aerogels, whereas multi-composition aerogels, gradient aerogels and micro-/nano- aerogel composites are given as aerogel composites as indicated in Figure 2.2.

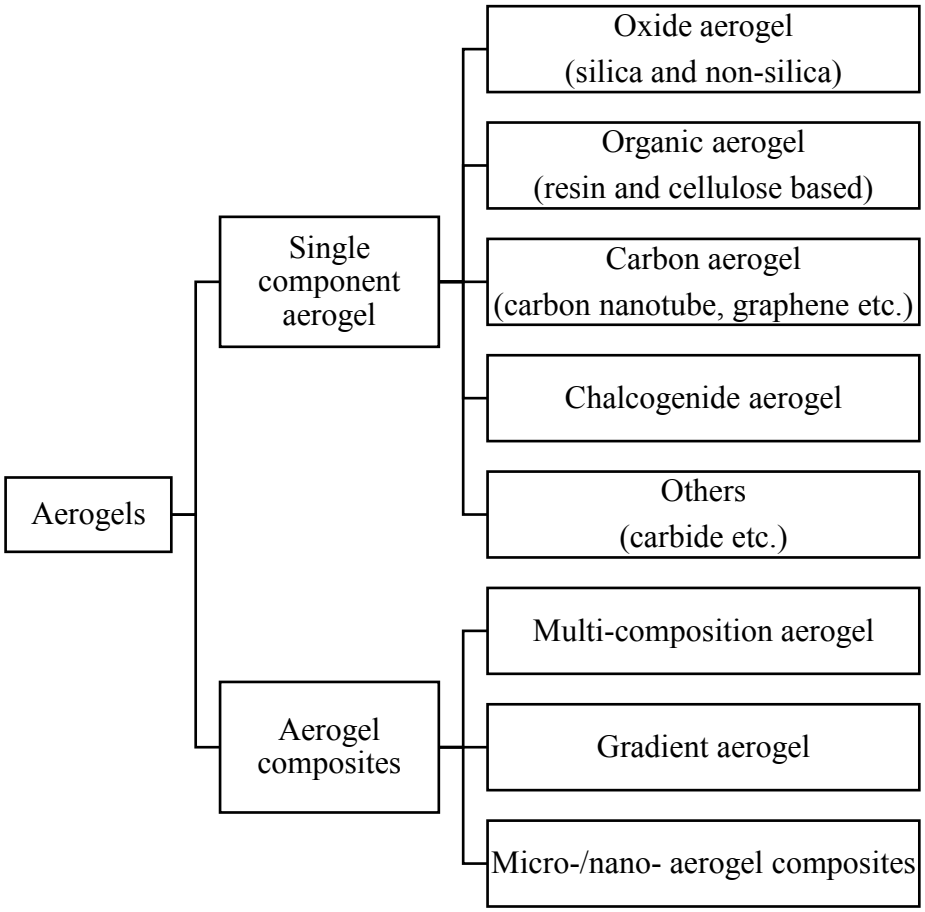

Figure 2.2: Classification of aerogels based on composition[23].

By knowing the preparation problems and their corresponding solutions for single component aerogels, in principle, it is likely to produce composite aerogels, hence there are still ongoing studies for both single component aerogels and aerogel composites[23]. In Table 2.1, some of the common examples of each category are provided.

Table 2.1: Examples from literature on aerogels classified based on composition.

	Type of Aerogel	Examples from Literature
Single componentt aerogels	Oxide aerogels	Silica[30–33], alumina[34–36], titania[37,38], chromia[39–41], nickel oxide[42,43], zirconia[44,45]
	Organic aerogels	Resorcinol-formaldehyde (RF)[46,47], cellulose[48,49]
	Carbon aerogels	Carbon nanotube[50], graphene oxide[13,51,52]
	Chalcogenide aerogels	Chalcogenide aerogels based on PbS, CdSe, CdS, and ZnS[53]
	Others	TiC, NbC[54]
Aerogel composites	Multi-composition aerogel	CuO-RF[55]
	Gradient aerogel	Silica[56]
	Micro-/nano- aerogel composites	Graphene oxide based[27,57–59], silica based[60,61]

2.1.3. Applications of Aerogels

Features and properties of the aerogels can be arranged according to their application areas. For capacitors electrical properties gain importance in the synthesis of aerogels, whereas if aerogel is to be used for insulation purposes as shown in Figure 2.3 thermal conductivity is the key property to consider for the production. As in the case of sorbers such as in Figure 2.4, density and porosity are both important for improved sorption capacity.

Figure 2.3: A bare foot standing on aerogel based insulation material[62].

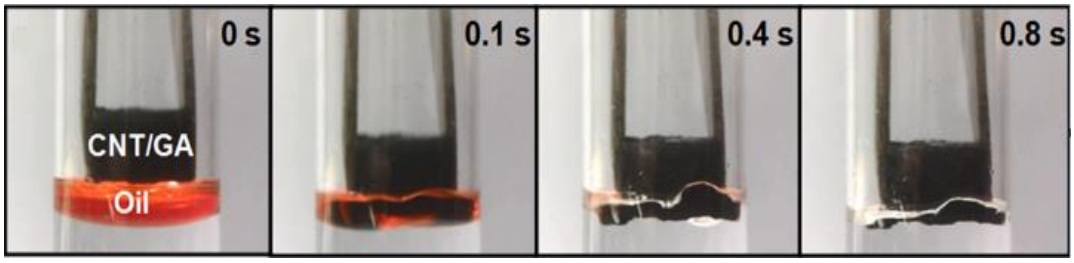

Figure 2.4: Diesel fuel sorption by an aerogel[63].

From absorption to catalysis, there are various application areas for aerogels. Some of the many application areas of the aerogels as well as desired properties in related areas and corresponding features are listed in Table 2.2. Based on the application area and the desired property, features can be tuned according to the table.

Table 2.2: Aerogel properties and features, with their applications[25].

Property	**Features**	**Applications**
Thermal conductivity	• Best insulating solid • Transparent • High temperature • Lightweight	• Architectural and appliance insulation, portable coolers, transport vehicles, pipes, cryogenic, skylights • Space vehicles and probes, casting molds
Density/porosity	• Lightest synthetic solid • Homogeneous • High specific surface area • Multiple compositions	• Catalysts, sorbers, sensors, fuel storage, ion exchange • Targets for ICF, X-ray laser
Optical	• Low refractive index solid • Transparent • Multiple compositions	• Cherenkov detectors, lightweight optics, lightguides, special effect optics
Acoustic	• Lowest sound speed	• Impedance matchers for transducers, range finders, speakers
Mechanical	• Elastic • Lightweight	• Energy absorber, hypervelocity particle trap
Electrical	• Lowest dielectric constant • High dielectric strength • High surface area	• Dielectrics for ICs, spacers for vacuum electrodes, vacuum display spacers, capacitors

2.2.Graphene Oxide

2.2.1. Background on Graphene Oxide

Graphene is a two dimentional and one-atom thick material in which carbon atoms are arranged in a honeycomb lattice[64]. Following the isolation of graphene and identification of its properties by Andre Geim and Konstantin Novoselov in 2004, graphene and related materials have become the focus of research in different fields owing to their superior properties such as high surface area, high modulus, and high thermal and electrical conductivity[65]. Nanomaterials based on graphene are shown in Figure 2.5.

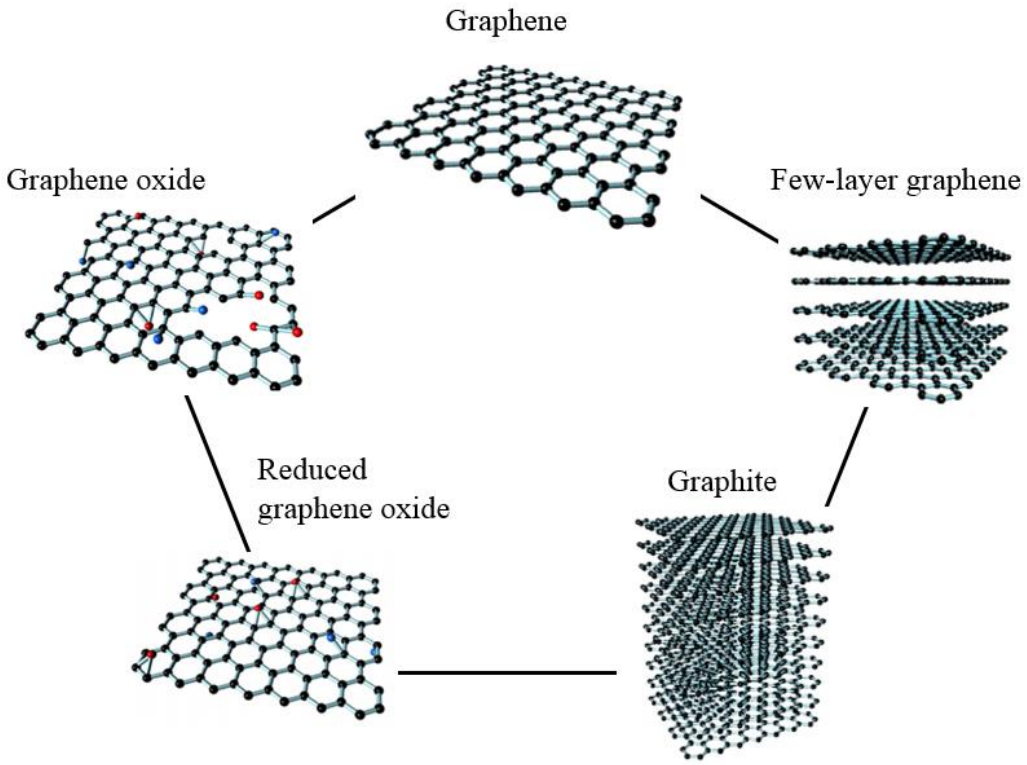

Figure 2.5: Graphene based nanomaterials[66].

The studies[67] of Geim and Novoselov was awarded with a Nobel Prize in 2010. In order to obtain graphene, many methods have been developed including[68,69]:

- micro-mechanical exfoliation of pyrolytic graphite,

- chemical vapor deposition,
- epitaxial growth on electrically insulating surface,
- reduction of graphene oxide.

All of the first three methods above provide high quality graphene; however, use of all three methods individually to produce graphene results in lower productivities compared to that of reduction of graphene oxide[69,70]. Therefore, graphene oxide reduction can be considered as a suitable method to acquire graphene. Low raw material cost for the synthesis, simple synthesis methodology make graphene oxide reduction route available for the large-scale applications[69,70]. Also, graphene oxide sheets are easy to work with since they do not form aggregates, can be dispersed in water and in most of the polar solvents.

2.2.2. Structure of Graphene Oxide

Graphene oxide has three main features in its structure as[71,72]:

- Graphitic regions due to incomplete oxidation of the raw material, graphite
- Holes, less than 5 nm^2 generally, which are formed during oxidation and exfoliation due to CO and CO_2 release
- Disordered regions which are considered as the areas of high oxidation.

Graphene oxide stays as a grey area in terms of its chemical and physical structure despite enormous research interest in the subject. It is hard to define a certain structure for the graphene oxide since the composition of material strongly depends on the synthesis conditions. Strong hygroscopy, decomposition above 60-80 °C and nonstoichiometry of the reaction also preclude the structure definition[73].

Graphene oxide has a layered structure as in the case of its raw material, graphite, but layers contain oxygen containing functional groups enabling further modifications, yet there is no exact structure for graphene oxide[71,74,75]. On the other hand, there are some structural models proposed for the structure of graphene oxide:

- Hofmann,
- Ruess,

- Scholz-Boehm,
- Nakajima-Matsuo,
- Lerf-Klinowski,
- Décány.

In 1939, the first known model was proposed for the structure of graphene oxide by Hofmann and Holst, indicating that epoxy groups are present on the surface of graphene oxide[76,77]. Following Hofmann and Holst's model, Ruess proposed a new model that includes hydroxyl groups in the structure and suggested that the basal planes, consisting of carbon layers, were wrinkled[76,77]. Later in Sholtz and Boehm's model, corrugated carbon layers and ketone groups were said to be present in graphene oxide structure[76,77]. In 1988, Nakajima and Matsuo proposed stage 2-type model for graphite fluoride and they predicated graphene oxide structure based upon this[76]. By the use of solid state NMR technique, Lerf and Klinowski proposed in 1998 that epoxy and hydroxyl groups are present in the basal plane, whereas carboxyl groups are located at the edges[77]. In the Décány's Model, corrugated layers of carbon layers were also present, in addition they included ethers into the graphene oxide structure[76]. In Figure 2.6, summary of the aforementioned structural models of graphene oxide is provided.

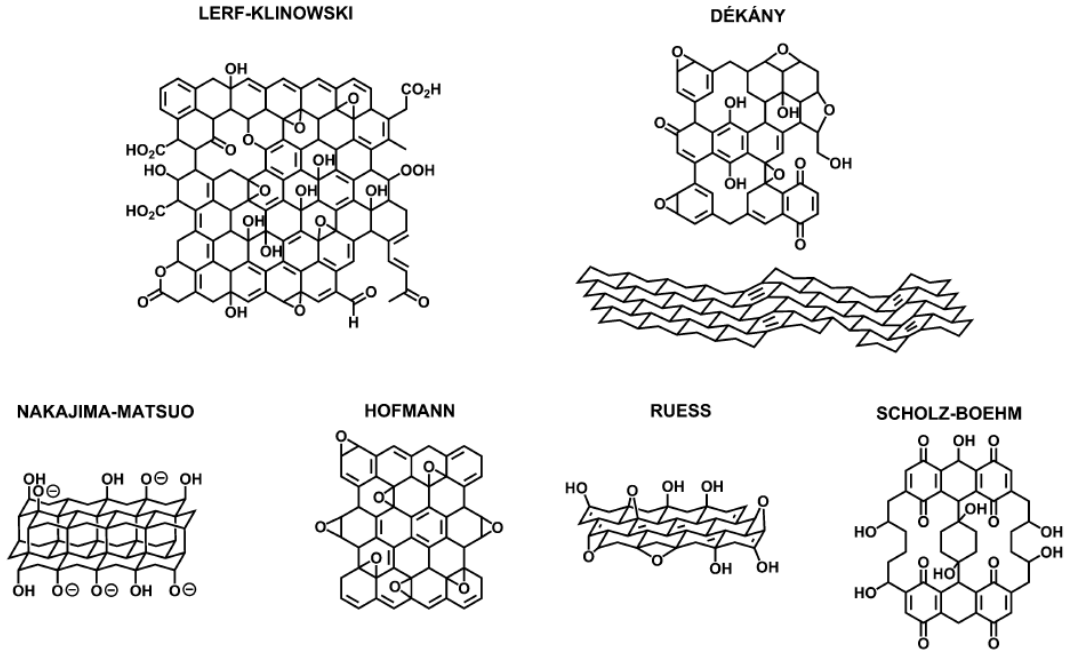

Figure 2.6: Summary of proposed structural models of graphene oxide[78].

2.2.3. Synthesis Methods and Purification of Graphite Oxide

Graphene oxide can be acquired by oxidation graphene or graphite by chemical methods. Hitherto methods as Brodie[77,79,80], Staudenmaier[81,82], Hofmann[82], Hummers[83], Tour[84,85], Peng[86] and modified versions of Hummers method[69,82,87–89] have been used extensively for the synthesis of graphene oxide. Graphite source, reaction conditions as well as the oxidation agent used affect graphite oxides produced; in other words products may have different properties[68]. Duration for the reaction varies from 1 hour (Peng's Method[86]) up to 5 days (modified Hummers Method[87]). The methods have some other differences in the choice of the reaction media as well as the oxidation agent. Core synthesis methods, oxidants used in corresponding methods and reaction media are provided below in Figure 2.7, respectively.

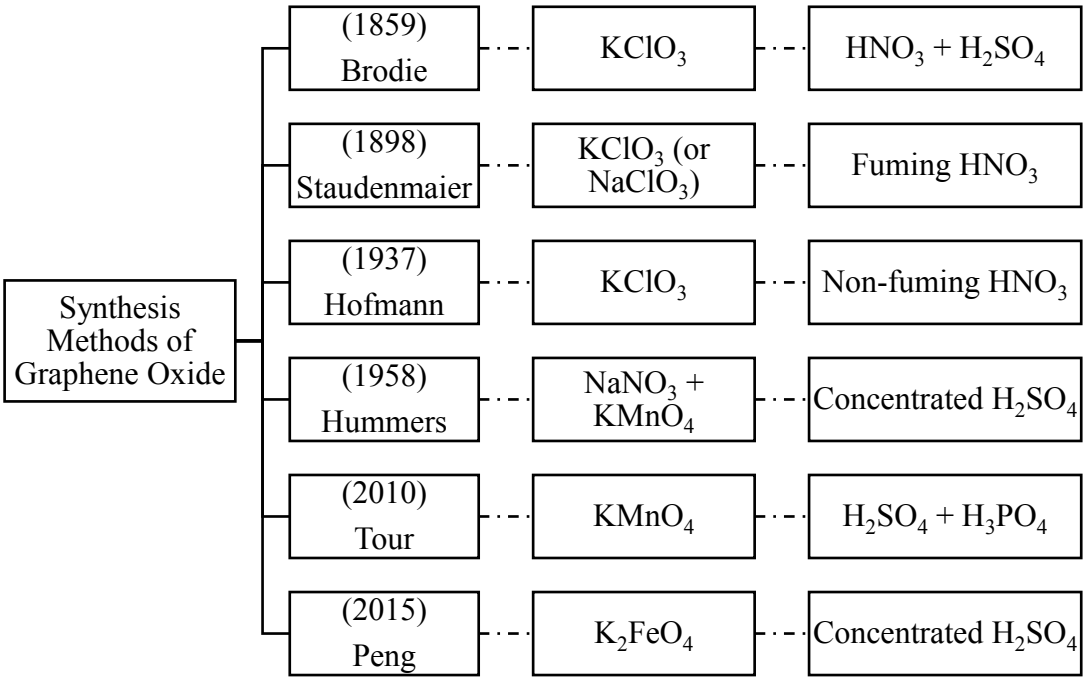

Figure 2.7: Synthesis methods of graphene oxide, corresponding oxidants and reaction media, respectively.

The problems with most of the methods are the generation of the toxic gases during reaction and risk of explosion. For example, Brodie, Staudenmaier and Hofmann methods create, chlorine dioxide, ClO_2 as a toxic gas. Nitric acid, HNO_3, which is used by Hummers method and a modified version of this method[87], can react strongly with aromatic carbon surfaces and its oxidation causes release of nitrogen oxides, NO_x as toxic gases[68,86]. Furthermore, potassium chlorate, $KClO_3$ is used in Brodie, Staudenmaier and Hofmann methods; and dimanganeseheptoxide, Mn_2O_7, formation whose reaction scheme is provided in Figure 2.8, in Hummers method and its modified versions[87,88], and in Tour method possess a risk for explosion[68,86]. As can be seen Peng's method have neither exploder nor toxic gas involvement within the synthesis, yet the prices for the oxidant is higher than that of other methods.

$$KMnO_4 + 3H_2SO_4 \rightarrow K^+ + MnO_3{}^+ + H_3O^+ + 3HSO_4{}^-$$

$$MnO_3{}^+ + MnO_4{}^- \rightarrow Mn_2O_7$$

Figure 2.8: Reaction scheme of Mn_2O_7 formation[90].

More modifications can be performed to improve any aforementioned methods such as using microwave heating for pre-exfoliation prior to synthesis[71]. Tour method can be wise choice for the synthesis since well-set experimental conditions (temperature of 50 °C) eliminate the risk of explosion. Addition of H_3PO_4 to the synthesis media is useful to sustain the carboxylic acid ring structure[91]. In addition, H_2O_2 addition and efficient washing prevents the resultant graphene oxide from the contamination with excess permanganate ions[92].

Hitherto many washing procedures for the graphene oxide purification have been used in the literature. It is important to note that efficient washing is as important as the synthesis. As-synthesized graphene oxide goes into volume expansion and gelation when it is washed with water, causing problems in centrifugation and filtration[93]. Hence, in order to suppress the gelation behavior, use of two step washing procedure that involves 3.4% HCl and acetone was found to be more efficient[93]. Schematic comparison of both washing procedures is provided in Figure 2.9. Aforementioned gelation behavior of graphene oxide can easily be observed in the washing procedure with water.

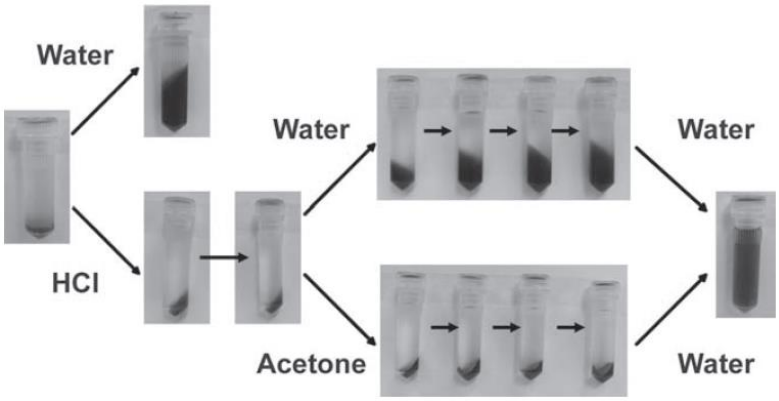

Figure 2.9: Schematic illustration of purification of graphene oxide[93].

2.2.4. Dispersion Behavior of Graphene Oxide

Graphite oxide consists of "stacked sheets of graphene oxide[94]" that contains oxygen containing groups. These groups not only increase interlayer distance but also enable intercalation of water molecules, hence even under mild sonication exfoliation of the stack layers can be performed in water[70,94].

Aqueous dispersions of the graphene oxide have been prepared in many studies since graphene oxide is known with its hydrophilic nature, yet it should be noted that both the size and the pH value have impact on hydrophilicity of graphene oxide[95]. It is important to have better dispersibility not only in water but also in other organic solvents for the processing[68,96]. Covalent functionalization via polymers and different molecules has been performed to assist dispersibility in many studies, hence some more studies emerged to explain the dispersion of graphene oxide in organic solvents[96,97]. The dispersion behavior of graphene oxide in different solvents can be seen in Figure 2.10. It can be seen that in addition to water, graphene oxide can form stable dispersions in N,N-dimethylformamide DMF), N-methyl-2-pyrrolidone (NMP) and tetrahydrofuran (THF) and ethylene glycol even after 2 weeks.

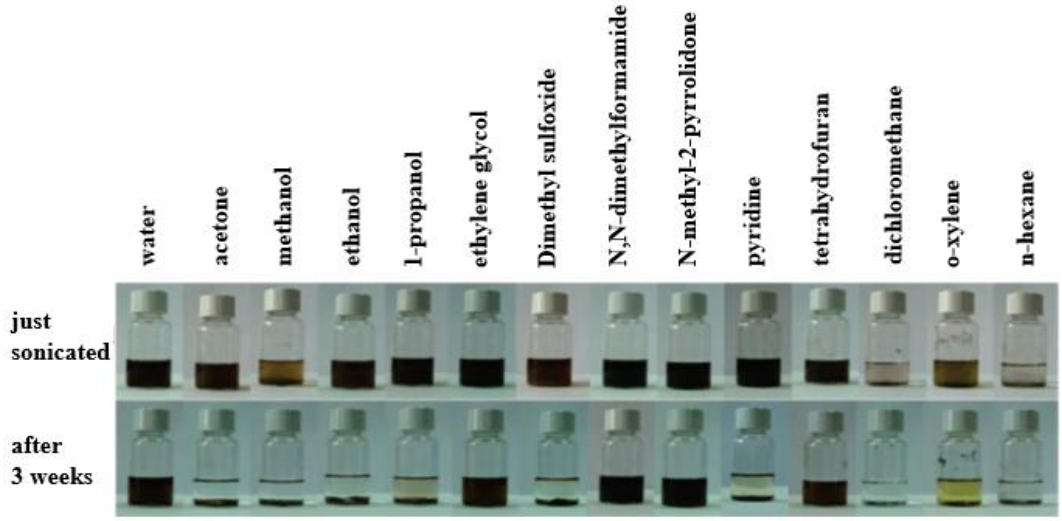

Figure 2.10: Digital photographs of as-prepared graphite oxide dispersed in water and 13 organic solvents through bath ultrasonication of 1 hour[96].

2.2.5. Reduction of Graphene Oxide

In order to attain the superior properties of graphene such as high surface area, high modulus, high thermal and electrical conductivity; reduction of graphene oxide has been performed. There are many methods for the reduction of graphene oxide to graphene or to reduced graphene oxide including chemical, thermal and solvothermal methods. Reduction using hydrazine has been used widely in the literature[98,99]. On the other hand, due to the toxicity and flammability of hydrazine, studies have continued to increase rapidly[100].

Ascorbic acid (Vitamin C) is thought to be a good alternative and used for the reduction[101–103], however its high price and reactivity towards water have become the major problems. Dispersions of unreduced graphene oxide and vitamin C reduced graphene oxide are provided in Figure 2.11. It is noteworthy that graphene oxide can form stable dispersions in water, DMF and NMP even after reduction.

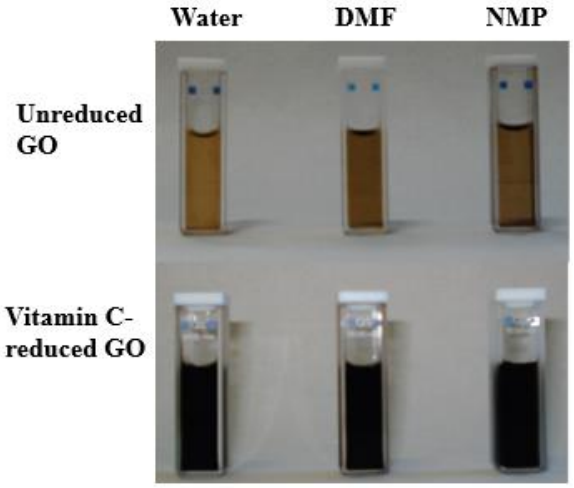

Figure 2.11: Digital photographs of unreduced graphene oxide suspensions (top), and their vitamin C reduced versions 4 weeks after reduction (bottom)[103].

Many other chemicals including sodium borohydride ($NaBH_4$)[98], benzylamine[104], hydroxylamine[105] were also used for GO reduction and it is claimed that in terms of poisonous and explosive properties as well as cost, hydroxylamine is a suitable candidate for the chemical reduction. Proposed mechanism for the reduction of graphene oxide with hydroxylamine is given in the scheme provided in Figure 2.12.

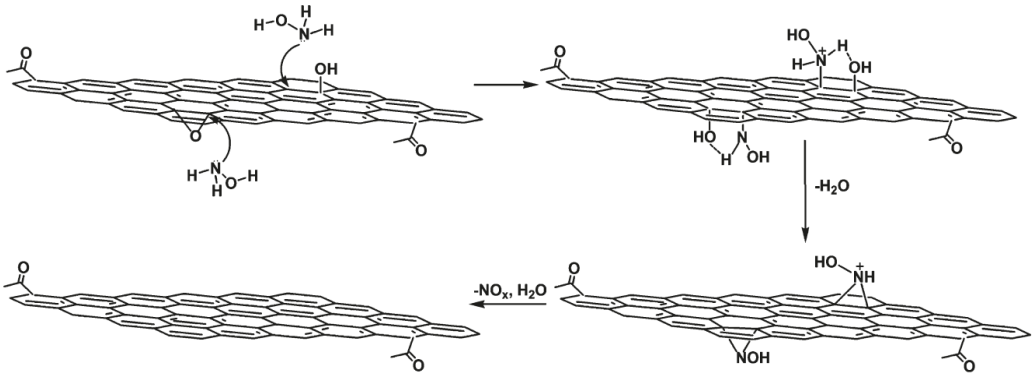

Figure 2.12: Schematic representation of the proposed mechanism for the reduction of graphene oxide with hydroxylamine[105].

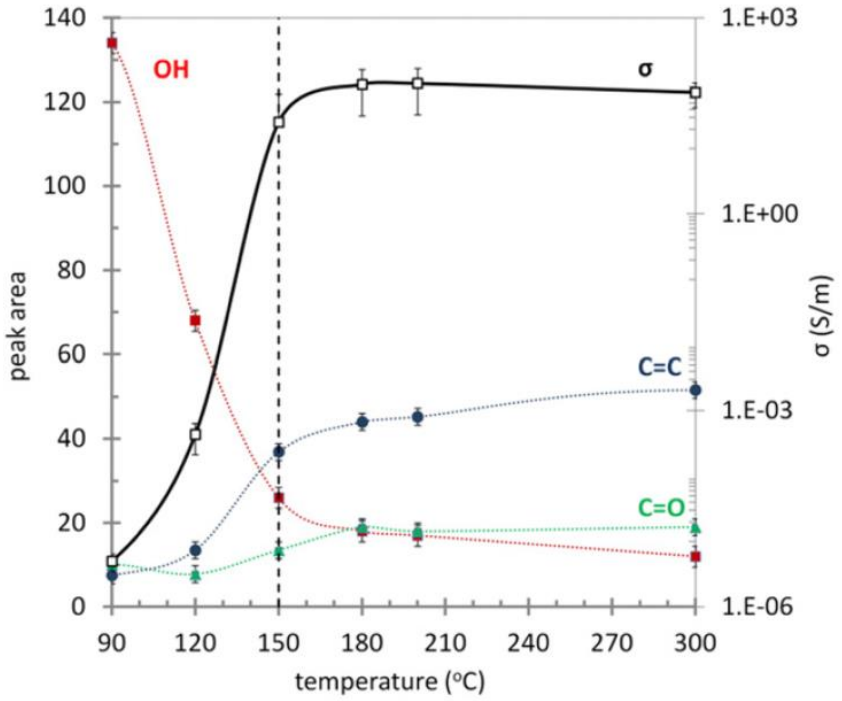

Figure 2.13: Removal of hydroxyl functionalities, formation of carbonyl groups and restoration of sp^2 graphene network along with electrical conductivity[106].

In terms of thermal reduction, thermal annealing[107], microwave treatments[108–110], and solvothermal/hydrothermal reduction in various media[111–115] have been used. Thermal reduction of graphene oxide can eliminate the aggregation problem that is caused by chemical reduction and hence is a useful method to employ[100]. Chemical changes almost diminish at a critical transition temperature of 150 °C[106] as can be seen from Figure 2.13. So, low temperature reduction of graphene oxide can be considered as an alternative in thermal reduction methods.

2.2.6. Applications of Graphene Oxide

Graphene and its derivatives have been used in various applications. Acting as a precursor for graphene synthesis, graphene oxide has been used for the purposes of flow reactor technologies, environmental protection, energy conversion and storage, biomedicine and biotechnology[78,116–118].

In biomedical applications, graphene oxide (GO) has been used as a nanocarrier[119–121] for anticancer drug delivery (doxorubicin); in addition, combinations of GO

with different molecules showed high loading efficiency as well as targeted drug delivery to the tumor area[122]. Graphene so as GO can also be used in sensors[65,123–126]. A sensor that is produced using reduced graphene oxide (rGO), has been used for detection of explosives, recognition of a bacteria, detection of biomolecules etc[1,65]. On the other hand, GO membranes have been produced for seawater desalination[127], for removal of humic acid[128], wastewater treatment[129], drinking water purification[130] purposes. As an example, in Figure 2.14, performance of rGO-CNT nanofiltration membrane in removing fulvic acid from water can be seen. As indicated in the inset photograph, feed has a yellow color and permeate is clear and transparent, which indicates that rGO-CNT nanofiltration membrane has successfully reject the fulvic acid.

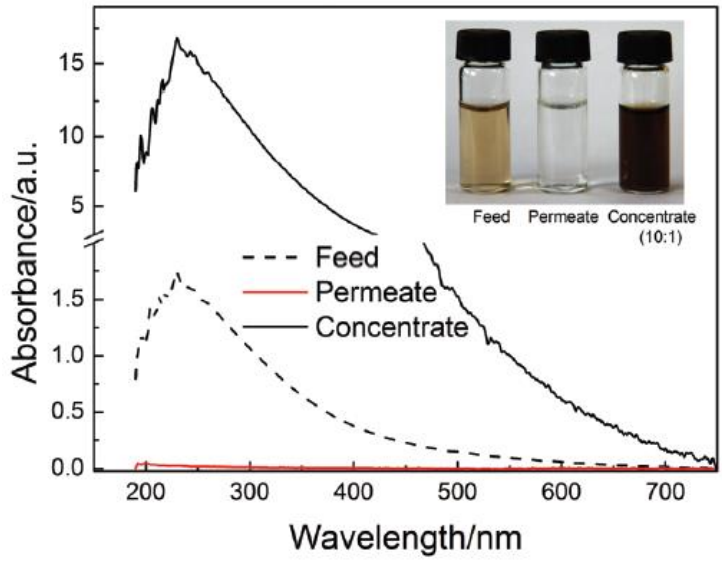

Figure 2.14: Performance of rGO–carbon nanotube hybrid nanofiltration membranes for removing fulvic acid (a type of humic acid) from water[130].

Further applications of the graphene oxide includes:

- Supercapacitors[117]
- Electrode in primary lithium cells[74]
- Photocatalyst for hydrogen production from water[117]
- Membranes[74,129–132]

- Clean energy devices[65]
- Transparent conductive films (which can be used as electrodes for dye-synthesized solar cells etc.)[65]
- Aerogels and hydrogels[18,51,133] etc.

2.3.Graphene Oxide Based Aerogels

Graphene oxide based aerogels have been produced for many applications. For example, Xu *et al.*[134] produced ultralight magnetic graphene/iron oxide aerogel which is stated as a candidate to be used in self-sensing soft actuators, remotely controlled oil absorption etc. The produced aerogel went under reversible deformation, and absorbed oil can be retracted from the aerogel with magnetic field induced compression[134] and original shape is retained as shown in Figure 2.15.

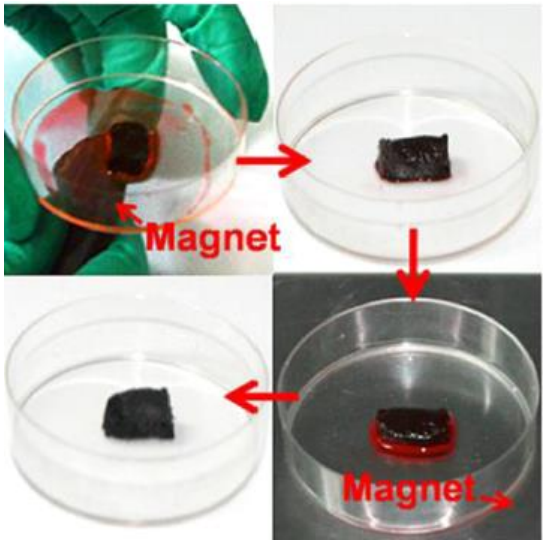

Figure 2.15: Aerogel absorbing oil with magnet guiding, and the oil-retracted version of the aerogel[134].

In the study of Yang *et al.*[135] magnetic graphene aerogels were produced with magnetite for the adsorption of oil and organic solvents, and schematic representation of the procedure is provided in Figure 2.16 and absorption capacities of the aerogels is presented in Figure 2.17.

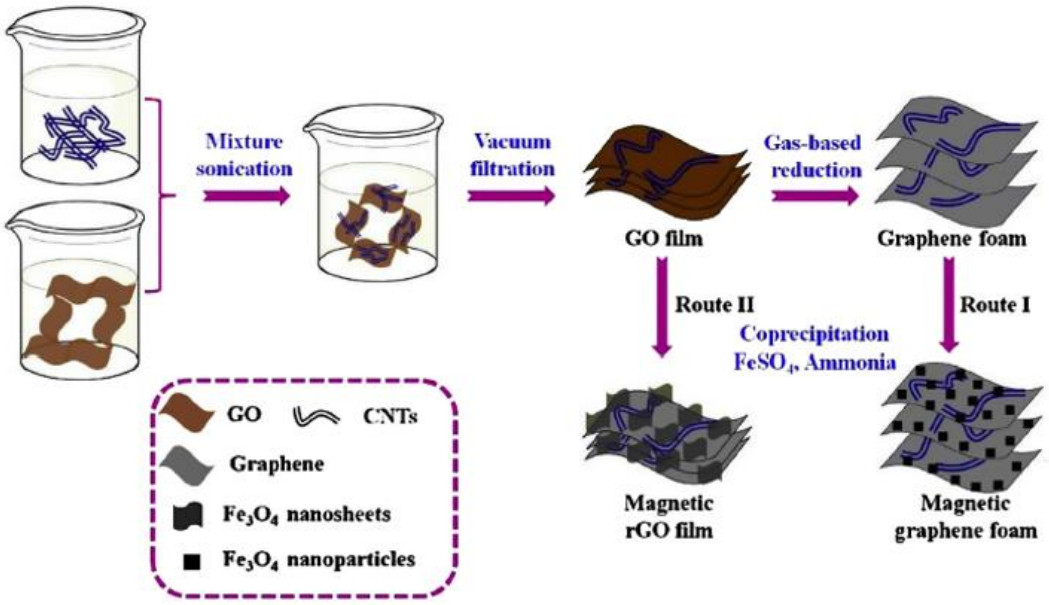

Figure 2.16: Preparation of graphene aerogel (foam)[135].

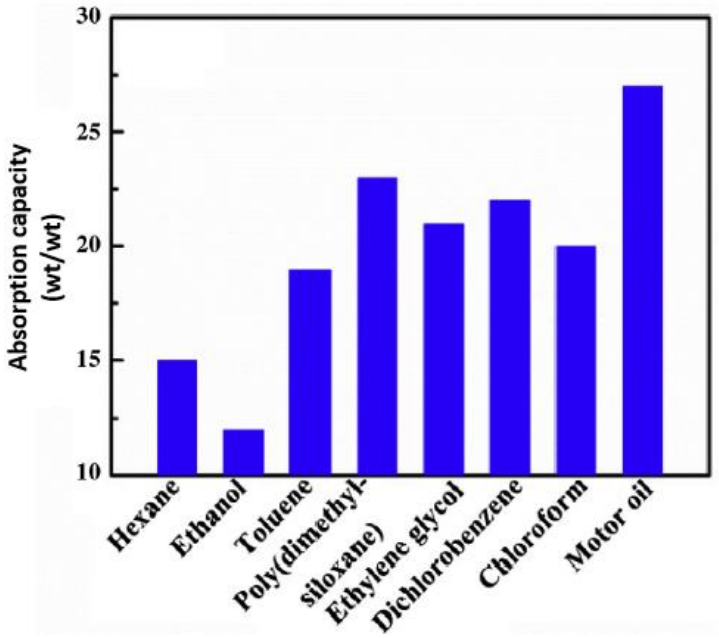

Figure 2.17: Absorption capacity of the magnetic aerogel produced[135].

In the study of Liu *et al.*[136] graphene oxide based aerogels were prepared graphene aerogels to be used in supercapacitors. Graphene oxide dispersions and different

alcohols (isopropanol, ethanol, ethylene glycol) were mixed well, desired amount was taken and reaction proceeded at 180 °C for 18 hours to give rise to graphene hydrogels[136]. After freeze-drying, resulting aerogels exhibited mechanical robustness and flexibility. Highest specific area and less degree of reduction was achieved with aerogel prepared with isopropanol; as a result it showed less ability to charge transport and less capability for energy storage[136].

Ethylene diamine (EDA) is a popular crosslinker used for the synthesis of graphene oxide based aerogels for various applications. Quan *et al.*[137] produced graphene-EDA hydrogels at 96 °C for 6 hours, treated with microwave radiation (800W) for 5 seconds after washing and solvent extraction. They used the resulting aerogel (cross-linked graphene sponge, CGS) as hemostat and compared the aerogels with gauze sponge. As it can be seen from Figure 2.18, CGSs can stop bleeding in 2-4 minutes whereas gauze sponge can stop bleeding in more than 10 minutes[137].

Figure 2.18: The hemostatic effect of the CGS and the control group of gauze sponge, just by contacting with the wound[137].

A number of studies also prepared aerogels that consisted of EDA and graphene oxide prior to production of graphene/polymer hybrid or composite aerogels to promote improved mechanical properties. For instance, Hu *et al.*[138] and Zhang et al.[126] both produced PDMS-graphene hybrid aerogels after the production of graphene-EDA aerogels. But in former study, graphene-EDA aerogels were prepared at 95 °C for 6 hours based on the study of Hu *et al.*[18]. After the infusion of PDMS into the structure, in order to remove the solvent and to promote polymerization, the infused gels were put under vacuum at 120 °C, and heated at 120 °C respectively[138]. On the other hand, in the study of Zhang *et al.*, hydrothermal

synthesis was conducted at 120 °C for 6 hours, resulting hydrogels can be seen in Figure 2.19.

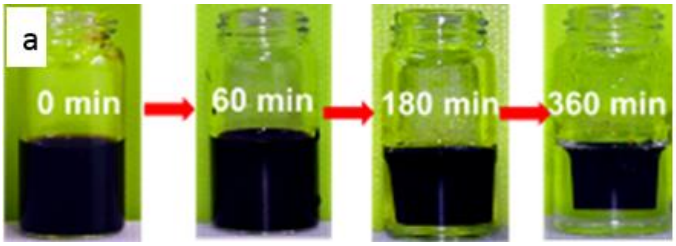

Figure 2.19: Hydrogel formation at different reaction times[126].

Li *et al.*[19] produced ultralight, compressible and fire-resistant aerogels that was acquired by using graphene oxide and ethylene diamine. Ethylene diamine in water is added to the graphene oxide dispersion in water under magnetic stirring. Resultant mixture was sealed and without the aid of stirring it was heated at 80 °C for 24 hours, time dependent change in the hydrogel formation is provided Figure 2.20, below[19].

Figure 2.20: Time dependent change in the hydrogel formation[19].

Aerogels produced with this method exhibit good absorption behaviour for organic liquids. In Figure 2.21, snapshots of removal of n-decane and dichloromethane dyed with 'Oil Red O' can be seen. When aerogels were squeezed after organic liquid is absorbed, it was seen that the original height can not be recovered unless re-absorption of the oil was provided[19]. The produced aerogel showed absorption capacities upto 250 g/g depending on the liquid density.

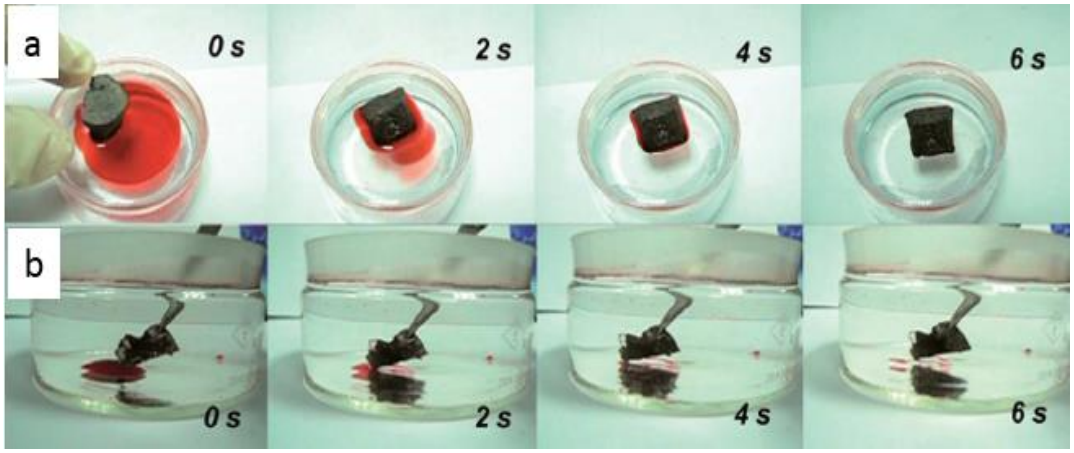

Figure 2.21: Snapshots of the removal process of (a) n-decane floating on water and (b) DCM sinking below water using aerogel[19].

In another study of Hu *et al*. graphene-EDA aerogels were produced again, for the purpose of enhanced oil sorption. The aerogels were coated with ferrocene and exposed to microwave radiation (800 W) for 1 minute to get CNT/graphene aerogel hybrid aerogels.

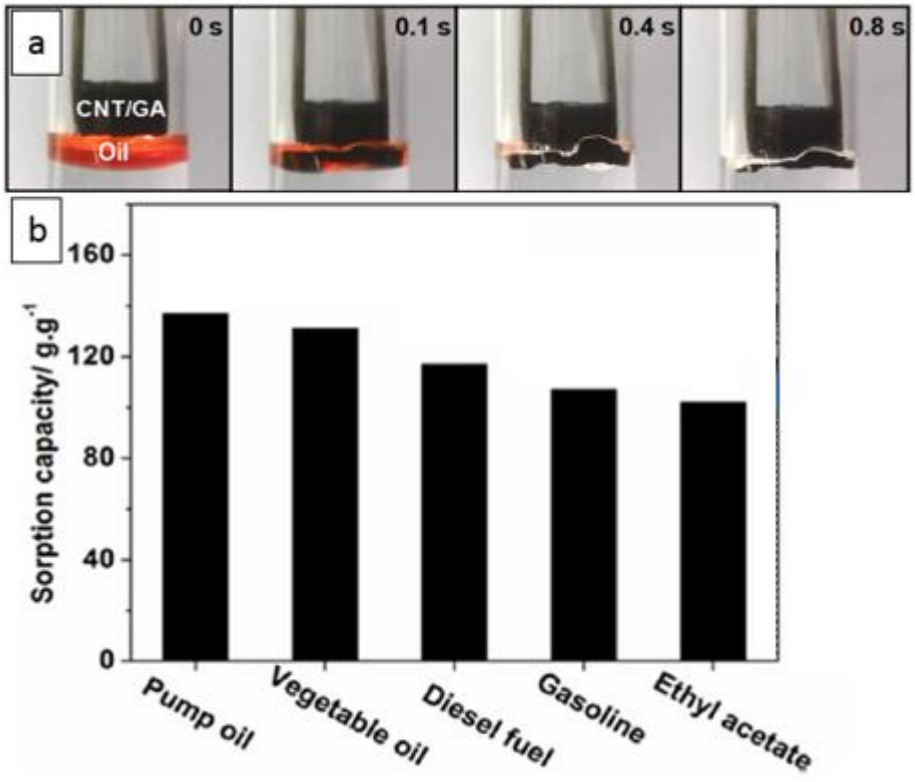

Figure 2.22: (a) Video snapshots of sorption of diesel fuel by CNT/graphene aerogel, (b) sorption capacities of aerogel produced [63].

As can be seen from Figure 2.22a, diesel fuel can be sorbed easily by the CNT/graphene aerogel and the aerogel showed a high absorption capacity for oils indicated in Figure 2.22b. CNT/graphene aerogels were also produced by Fan *et al.*[139] but without using graphene aerogels as the precursor for the hybrid aerogel in order to obtain good thermal and electrical properties. MWCNT and graphene oxide suspensions were mixed, using L-ascorbic acid as the reducing agent reaction was allowed to proceed for 5 hours at 95 °C and they showed 2.8 times higher electrical conductivity than the graphene aerogel[139].

Graphene oxide has also been used with polymers to produce aerogels. In the study of Mangadlao *et al.*[140] graphene oxide was modified with poly(ethylene glycol) methyl ether methacrylate (PEGMEMA) using RAFT and used for the synthesis of hydrogels. They also used graphene oxide and PEGMEMA for the hydrogel synthesis and compared physically mixed and covalently linked hydrogels in terms

of reinforcement and lubrication effect[140]. They observed that with graphene oxide concentrations more than 0.1 wt % the lubrication effect dominates, in addition covalently linked graphene oxide-PEGMEMA has less lubrication effect. Resiliency of the covalently linked graphene oxide-PEGMEMA hydrogel under load can be seen in Figure 2.23.

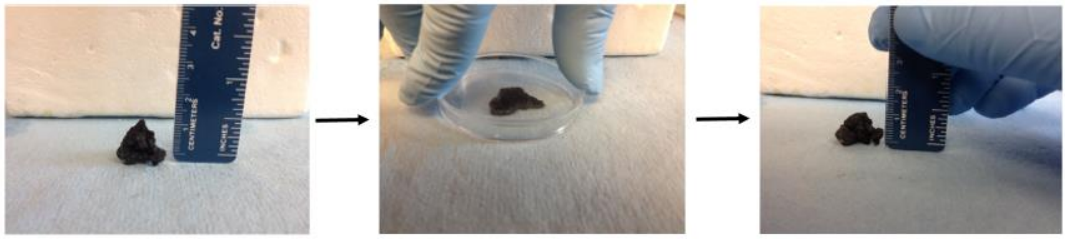

Figure 2.23: Resiliency of covalently linked graphene oxide-PEGMEMA under load[140].

Polydopamine was used in the study of Cheng *et al.*[141] for the pollutant disposal purpose. Both dopamine and graphene oxide were dissolved in pH 8.5 Tris.Cl buffer, and mixed. Reaction was conducted at 60 °C for 12 hours without stirring; adsorption capacities for different oils can be seen in Figure 2.24. After the oil uptake, the aerogels can be dried and reused for the same purpose. They have also used the produced aerogel for the efficient dye removal.

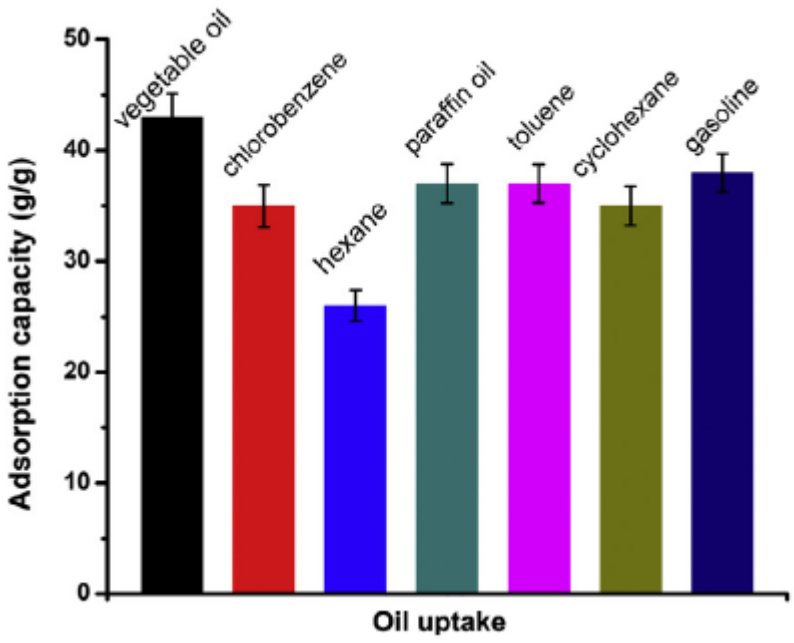

Figure 2.24: Adsorption capacities of graphene oxide based aerogels prepared by Cheng et al. for different oils and organic solvents at saturated state[141].

Polyvinylidene fluoride (PVDF) solution in DMF and graphene oxide dispersion in mixtures of water and DMF were used in the study of Li *et al.*[142]; they focused on the oleophilicity and hydrophobicity. They were mixed in a graphene oxide /PVDF ratio of 2/5, reaction proceeded at 160 °C for 10 h, and the aerogel was acquired after freeze-drying. In a broad range of different oils and organic solvents, they investigate the adsorption capacity and compare it with the graphene aerogel prepared in the similar conditions, results can be seen in Figure 2.26. Pictures of paraffin oil (with Sudan red G) absorbed by the aerogel with DMF/water=7/3 are provided in Figure 2.25.

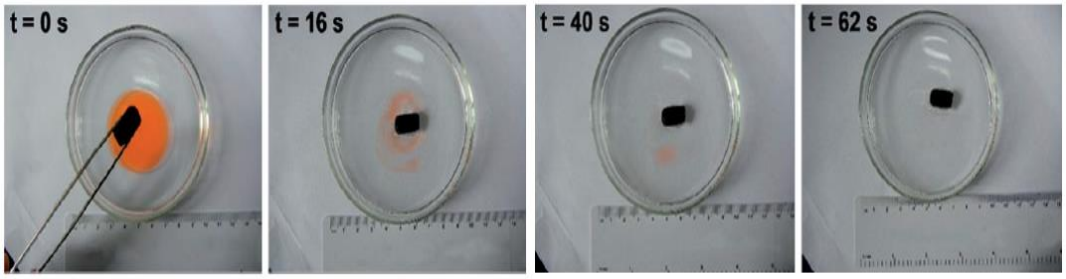

Figure 2.25: Absorption of paraffin oil by graphene oxide-polyvinylidene fluoride aerogel[142].

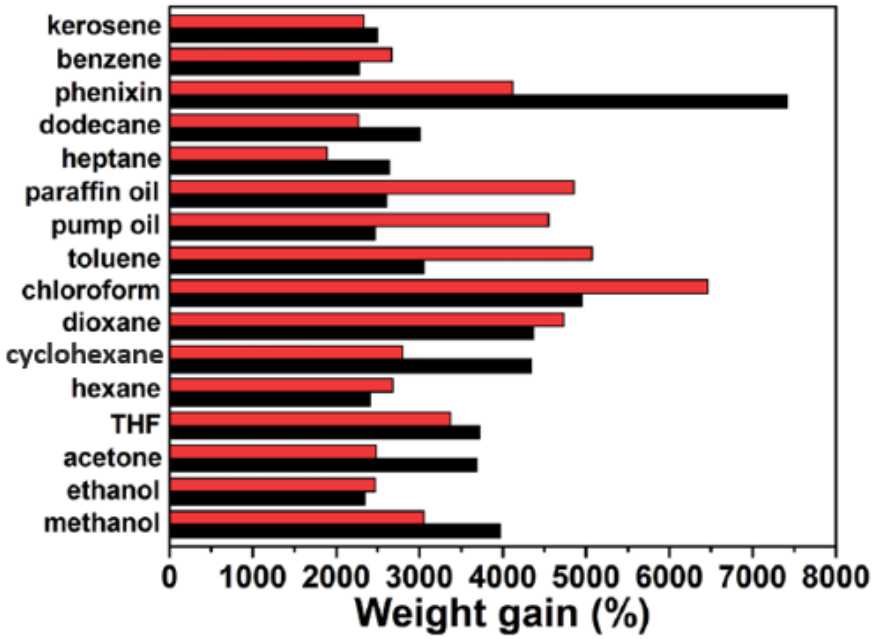

Figure 2.26: Adsorption capacitiy of polyvinylidene fluoride-graphene aerogels (red: DMF/water=8/2; black DMF/water=7/3)[142].

Alginate[143], chitosan[16,144], epoxy[58], poly(acrylic acid)[21], polypyrole[20,145], poly(methyl methacrylate)[146] and many more chemical have been used for the aerogel production with graphene oxide.

Hydrophobic aerogels can absorb oil 215 to 913 times of their own weight[12]. Materials in the production of aerogels along with graphene oxide have changed throughout the literature for the oil absorption purposes. However, studies offer

either low production cost but limited absorption capacity, or they offer expensive production cost with high absorption capacity. Therefore, it is still a need to find new methods for the production of aerogels to offer both low production costs and good absorption capacities.

2.4.Absorption Mechanism of Aerogels

Adsorption and absorption are commonly encountered in the literature on aerogels. When compared, absorption and adsorption referred in the literature are not the same as neither of definitions. Adsorption is a process that involves contact of liquid or gas mixture to the solid surface; upon the contact with solid surface, a component of mixture adheres to the solid surface[147].

Absorption, on the other hand, is a process in which a component of a gas mixture is dissolved in a liquid solvent upon the contact with it. Gas absorption or gas scrubbing is indeed used for the waste gas treatment[147]. Absorption columns have been used for this purpose. As indicated in Figure 2.27, gas mixture is fed to the tower from the bottom and it leaves the column from the top while the desired component in the mixture is absorbed by liquid which is flowing downwards.

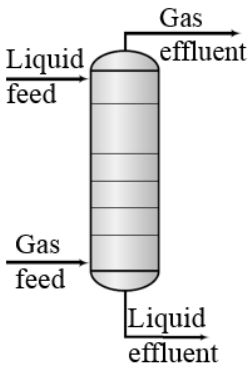

Figure 2.27: A representative image of an absorption column.

In the current study and in many other studies, absorption has been used to denote imbibition and adsorption of the liquid phase into the pores of aerogels. Therefore,

it is important to note that the process involves the replacement of air in the pores of aerogels by the liquid without dissolving in air.

CHAPTER 3

MATERIALS AND METHODS

3.1. Materials

Graphite with an average lateral size of 300 μm was kindly supplied by Asbury Carbons. Potassium permanganate ($KMnO_4$) was purchased from Yenilab. Sulfuric acid (H_2SO_4, 95-97%) was purchased from Honeywell. Orthophosphoric acid (H_3PO_4, 85%) and acetone (technical grade) were purchased from VWR Chemicals. Hydrochloric acid (HCl, fuming 37%), hydrogen peroxide (H_2O_2, 30%) and toluene were purchased from Merck. N,N-dimethylformamide (DMF), tetrahydrofuran (THF), methanol and styrene (Sty) were purchased from Sigma-Aldrich. Glycidyl methacrylate (GMA), azobisisobutyronitrile (AIBN) and 1,3-diaminopropane (1,3-DAP) were purchased from Aldrich. All of the chemicals were used as received.

3.2. Methods

3.2.1. Synthesis of Graphite Oxide

Graphite oxide was synthesized by using Tour Method[84]. Graphite flakes (1.2 grams, 1 wt equivalent) were mixed with $KMnO_4$ (7.2 grams, 6 wt equivalent) and 160 mL of H_2SO_4:H_3PO_4 (9:1) mixture was then added slowly to solid mixture under stirring. In order for oxidation reaction to proceed, reaction was stirred at 50 °C for 12 hours. Reaction scheme is provided below in Figure 3.1. At the end of 12 hours, reaction mixture was allowed to cool down to room temperature. Reaction mixture was to be poured onto ice, however viscosity of the reaction mixture increased significantly and therefore 160 mL of ice was added onto reaction mixture in a water bath. In order to get rid of the excess MnO_4^- ions[148], H_2O_2 was

added to the reaction mixture until a color change was observed from brownish purple to through bright yellow.

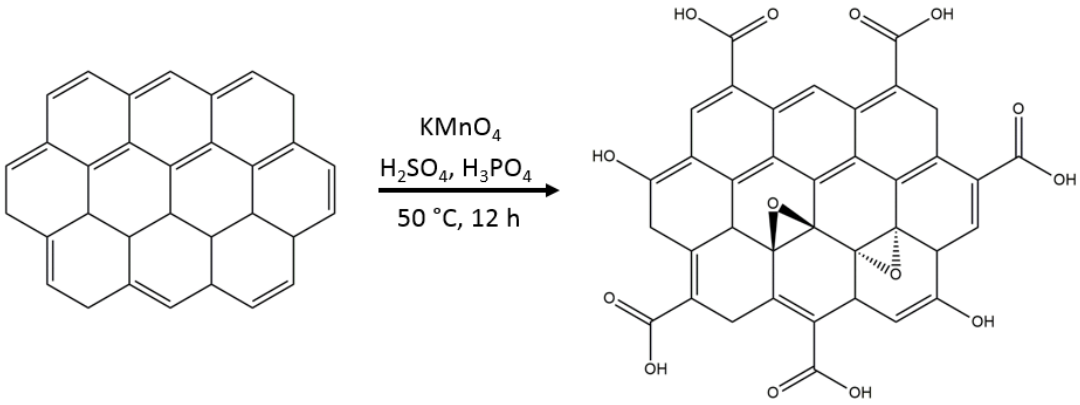

Figure 3.1: Reaction scheme of graphene oxide synthesis.

After the centrifugation, highly acidic supernatant of the product was decanted away. The remaining material was then washed with 3.4 wt % HCl (x3) and acetone (x4) [93]. The product which was acquired at the end of this washing procedure, was dried under vacuum and stored at -20 °C to minimize the environmental effects.

3.2.2. Synthesis of Poly(GMA-co-Styrene) Copolymers

GMA and styrene can react to give random copolymers according to the literature[149]. Copolymers of styrene and glycidyl methacrylate (pGcSt) were prepared using free radical polymerization with AIBN as the initiator. Two different copolymers were synthesized SG10 (Styrene:GMA:AIBN:Tolune being 90:10:1:150) and SG5 (Styrene:GMA:AIBN:Toluene being 95:5:1:150). Briefly, to the flask containing AIBN and toluene, monomers were introduced and flask was placed into an oil bath at a temperature of 80 °C. Reaction was allowed to proceed for 5 h, after which the mixture was diluted with THF and precipitated into cold methanol. Dissolving/precipitation was performed three times. Reaction scheme is provided in Figure 3.2.

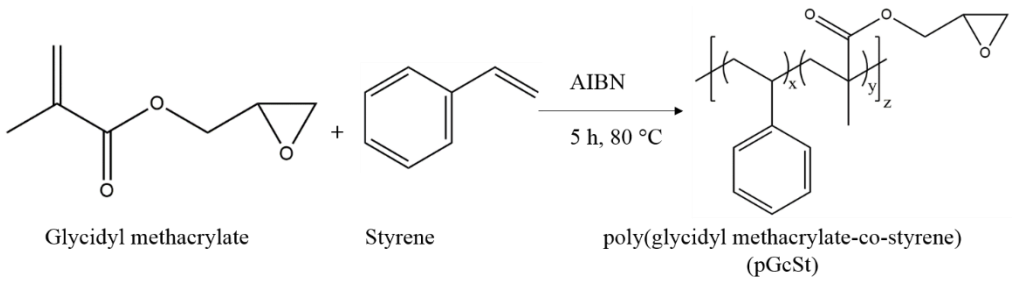

Figure 3.2: Copolymerization of GMA and styrene in the presence of free radical polymerization initiator, AIBN.

3.2.3. Production of Reduced Graphene Oxide and Copolymer Based Aerogels

GO dispersions of 5 mg/mL and pGcSt solutions were prepared in DMF and mixed in required amounts (0, 0.5, 1, 1.5, 2, 3, 4 or 5 mg/mL). After sonication (less than 2 minutes) in ice bath, vials were placed into an oven at 130 °C for 5 h. During this period, carboxylic acid and hydroxyl groups of graphene oxide react with glycidyl groups of the pGcSt copolymers promoting the gelation between GO and copolymers as illustrated in the scheme provided in Figure 3.3.

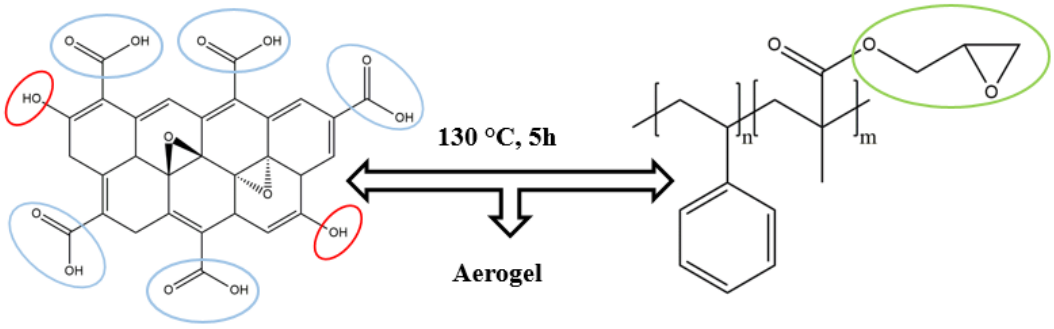

Figure 3.3: Reaction between the copolymers of GMA and styrene, and GO to produce hydrogels.

For the work up, 20%, 10%, 5%, 2.5% ethanol-water mixtures and finally water (several times) were used. Hydrogels were then freeze-dried at around -53 °C to obtain pGcSt/GO aerogels. Resulting aerogels were sealed and subjected to argon flow for at least 15 minutes prior to thermal treatment at 150 °C for 4 h in an oven.

At the end of this thermal treatment, graphene oxide is substantially reduced therefore it is referred to as rGO and the obtained aerogels are referred to as pGcSt/rGO aerogels.

3.2.4. Production of Reduced Graphene Oxide and 1,3-diaminopropane Based Aerogels

Into the GO dispersions with concentrations of 3, 4 or 5 mg/mL, 1,3-DAP was added in desired amounts (2.5, 5, 7.5, 10, 12.5 or 15 mg/mL). After a mild sonication (less than 10 seconds in ice bath conditions), vials were placed into an oven at 95 °C for 6 h. During this period, carboxyl, hydroxyl and epoxide groups of graphene oxide react with amine groups of 1,3-DAP promoting the gelation between GO and copolymers as illustrated in the scheme provided in Figure 3.4.

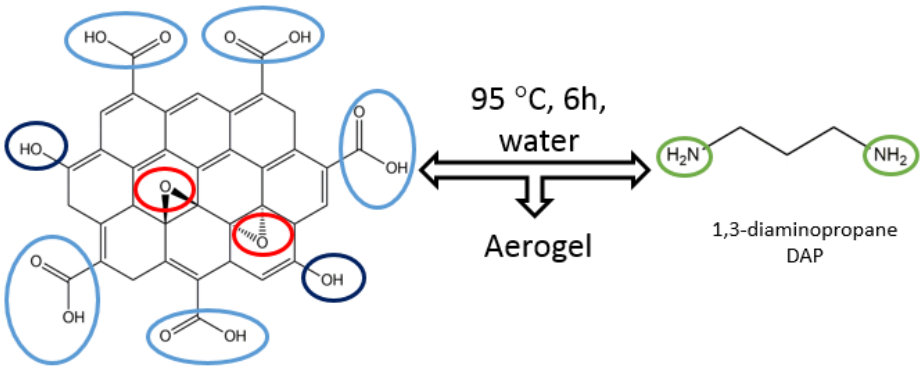

Figure 3.4: Reaction between 1,3-DAP and GO to produce hydrogels.

For washing the aerogels, 20%, 10%, 5%, 2.5% ethanol-water mixtures and finally water (several times) were used. When the aerogels were immersed into the liquid nitrogen directly, sudden volume expansion occurs and this promotes cracking in the structure upon freeze drying. Therefore, after decanting away the supernatant, hydrogels were placed into the freezer for an hour. Gels were then frozen in liquid nitrogen then freeze-dried for one day. The resulting aerogels were subjected to argon flow at least for 15 minutes then they were subjected to thermal treatment at 150 °C for 4 h in an oven to obtain DAP/rGO aerogels.

3.2.5. Absorption Experiments

Prior to the experiments, dry aerogels were weighed. Aerogels were then placed into containers having 15 mL of chloroform, toluene or sun flower oil. At the end of 2 hours, gels were taken out of the absorbate using a spoon and put onto paper towel. Absorbate on the surface of the gels were taken with the towel within 10 seconds. Gels were then weighed and their absorption capacities were calculated. Since the gels have low weights, weighing was performed on tared bottle caps. The absorption capacities of the aerogels were determined using the following formula.

$$Absorption\ capacity = \frac{weight\ of\ wet\ gel}{weight\ of\ dry\ gel}$$

3.3. Characterizations

3.3.1. Attenuated Total Reflectance-Fourier Transform Infrared Spectroscopy (ATR-FTIR)

All of the analyses were performed using Shimadzu IRPrestige-21 spectrophotometer in the wavenumber range of 500-4000 cm^{-1} with 64 scan. Solid samples were used for the analysis.

3.3.2. Ultraviolet-visible Spectroscopy (UV-Vis)

The analysis was conducted for graphene oxide using Shimadzu UV-2550 in a wavelength range of 200-800 nm. Dried graphite oxide was dispersed in water with the concentration of 1 mg/mL. Using Bandelin Solopuls HD 2200 with 33 % power (66 W) and 5 cycles for 30 minutes with 10 seconds of pause in each 5 minutes, ultrasonication was performed for the homogenization at 0 °C. Dispersion was then centrifuged at 2000 rpm for 10 minutes and supernatant was used for the analysis.

3.3.3. X-ray Photoelectron Spectroscopy (XPS)

SPECS EA 300 equipped with Al-monochromatic X-ray anode was used for overall scan of graphite and graphene oxide. Solid samples were use for the

analysis. Deconvolution of the C1s spectrum of the synthesized graphene oxide was performed after Shirley background correction using OriginPro software version 2016. Gaussian-Lorenzian correlation was used for the curve fitting.

3.3.4. Thermogravimetric Analysis (TGA)

Solid samples were prepared and analyses were conducted from room temperature to 600 °C with a heating rate of 10 °C/min in nitrogen environment. Shimadzu DTG-60H was used for analyses.

3.3.5. Gel Permeation Chromatography (GPC) Analysis

Copolymers of glycidyl methacrylate and styrene were dissolved in chloroform for the analysis. Analysis was performed with Shimadzu Prominence GPC System with a refractive index detector.

3.3.6. Proton Nuclear Magnetic Resonance (^{1}H-NMR) Analysis

Copolymers were dispersed in deuterated chloroform and analyzed using Bruker AVANCE III 400 MHz. Integral calculations were performed using MestReNova NMR Analysis software.

3.3.7. Atomic Force Microscopy (AFM)

Graphene oxide dispersion with the concentration of 0.5 mg/mL was prepared. After 1 hour of sonication, it was centrifuged at 8000 rpm for 5 minutes. 50 µL of the supernatant was taken and coated onto silicon wafer using Polos Spin 150i. Spinning of graphene oxide was performed at a speed of 3000 rpm for 30 seconds with an acceleration of 1000 rpm/s. The AFM analysis was then conducted by using Veeco Multimode V AFM on tapping mode.

3.3.8. Scanning Electron Microscopy (SEM)

FEI Nova NanoSEM 430 Field Emission SEM equipped with a secondary electron detector (Everhart-Thornley detector) with acceleration voltage of 10 kV was used for the analysis of graphene oxide which was spin coated onto the silicon wafer. Spinning of graphene oxide was performed at a speed of 3000 rpm for 30 seconds with an acceleration of 1000 rpm/s.

QUANTA 400F Field Emission SEM with acceleration voltage of 20 kV was used for the analysis of the aerogels. Aerogel samples were placed onto holders with the aid of carbon tape and coated with gold-palladium using Quorum 150R ES sputter coater.

3.3.9. Transmission Electron Microscopy (TEM)

FEI Nova NanoSEM 430 was used with an acceleration voltage of 20 kV for the analysis of graphene oxide.

CHAPTER 4

RESULTS AND DISCUSSIONS

Two routes were proposed in order to increase the oil absorption capacity of graphene oxide based aerogels. Sunflower oil, chloroform, and toluene were used to assess the oil absorption capacity of the aerogels. In the first route, graphene oxide and copolymers of glycidyl methacrylate and styrene were firstly synthesized. They were then mixed in required amounts and incubated for 5 hours at 130 °C to form precursor hydrogels. In the second route, the hydrogels were prepared using 1,3-DAP and graphene oxide and incubating the hydrogels for 6 hours at 95 °C. In both routes, hydrogels were washed, freeze-dried and thermally treated to obtain reduced graphene oxide based aerogels. The resultant aerogels were then tested for their absorption capacities.

4.1.Synthesis of Graphene Oxide

In order to convert graphite to graphene oxide intercalation and oxidation pay crucial role. In the synthesis, acids (H_2SO_4 and H_3PO_4) increase the spacing between graphene layers via intercalation and enable oxidizing agent ($KMnO_4$) to oxidize graphite. It is also important that addition of H_3PO_4 to the synthesis media is useful to sustain the carboxylic acid ring structure[91]. Further exfoliation can be obtained if microwave heating is used prior to synthesis[71]. The reaction mixture have some changes in color during the reaction. To start with, acid addition to the solid mixture results in dark-green color due to dimanganase heptoxide (Mn_2O_7) formation. At the end of 12 hours, reaction mixture became brownish purple as a result of the use of excess $KMnO_4$. In order to get rid of excess $KMnO_4$, hydrogen peroxide was used and the color of the reaction mixture then turned into bright yellow. Efficient wash after hydrogen peroxide addition eliminates the risk of

contamination of the graphene oxide with excess permanganate ions[92]. Aforementioned changes in the appearance of the reaction mixture at different stages of the reaction can be seen from Figure 4.1.

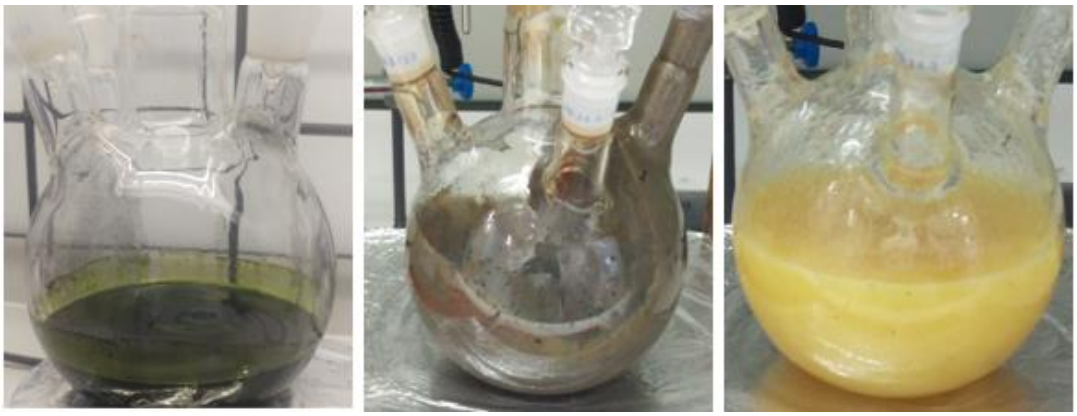

Figure 4.1: Photographs indicating the color changes during the synthesis of graphene oxide (left: graphite and $KMnO_4$ in acid mixture, middle: reaction mixture at the end of 12 hours, right: reaction mixture after H_2O_2 addition).

Efficient washing is extremely important for the synthesis. Water has been used for the purification, but it creates volume expansion and gelation which can be troublesome for centrifugation and filtration[93]. Use of 3.4% HCl and acetone prevent these problems by eliminating gelation behavior[93]. In order to confirm the oxidation of graphite into graphite oxide and to define the oxygen containing functional groups in the structure, ATR-FTIR analysis was conducted and the result of the analysis for both graphite and graphene oxide are provided in Figure 4.2.

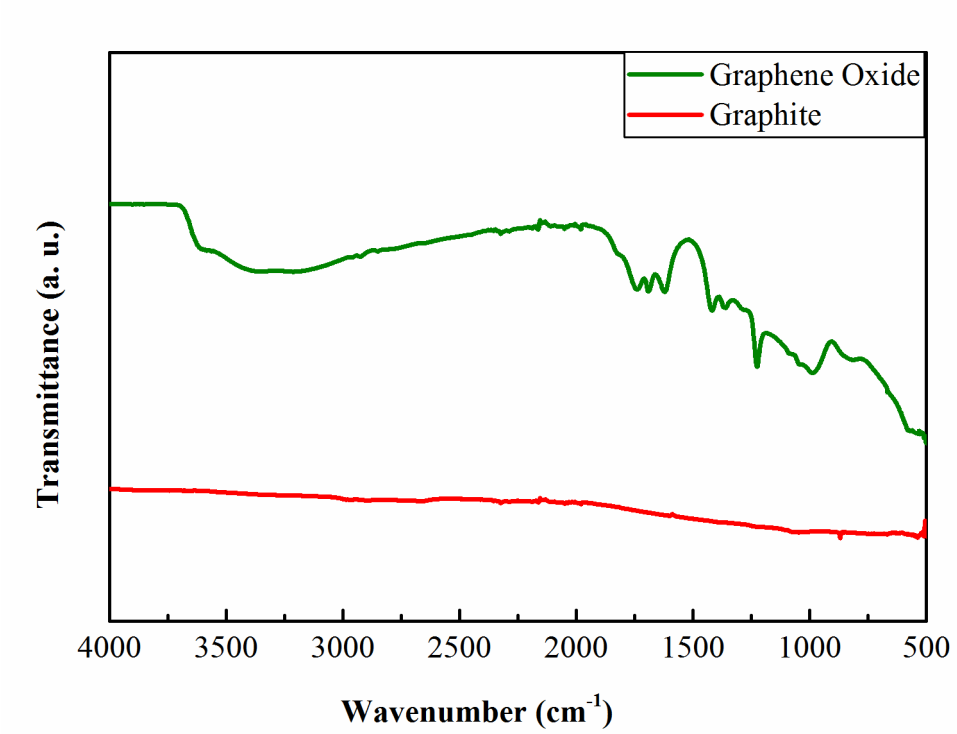

Figure 4.2: ATR-FTIR spectra of graphite and the synthesized graphite oxide.

In order to campare the result of the ATR-FTIR analysis with the literature, Table 4.1 was prepared and provided below. As can be seen the results are very similar to corresponding values from the literature.

Table 4.1: Comparison of experimental ATR-FTIR data with the literature.

Functional Group	Wavenumber (cm^{-1}) (Literature values[150])	Wavenumber (cm^{-1}) (Experimental values)
O-H streching vibrations	2500-3600	3430
C=O streching vibrations	1720-1750	1744
C=C from unoxidized sp^2 carbon to carbon bonds	1400-1680	1628
C-O vibrations	1050-1250	1227

UV-Vis analysis for the graphene oxide has two characteristics, which are a peak around 227-231 nm range due to $\pi \rightarrow \pi^*$ transitions of C=C bonding and a shoulder around 300 nm due to $n \rightarrow \pi^*$ transitions of carbonyl groups[84]. Figure 4.3 gives the UV-Vis spectra of the produced graphene oxide that shows both of the mentioned characteristics.

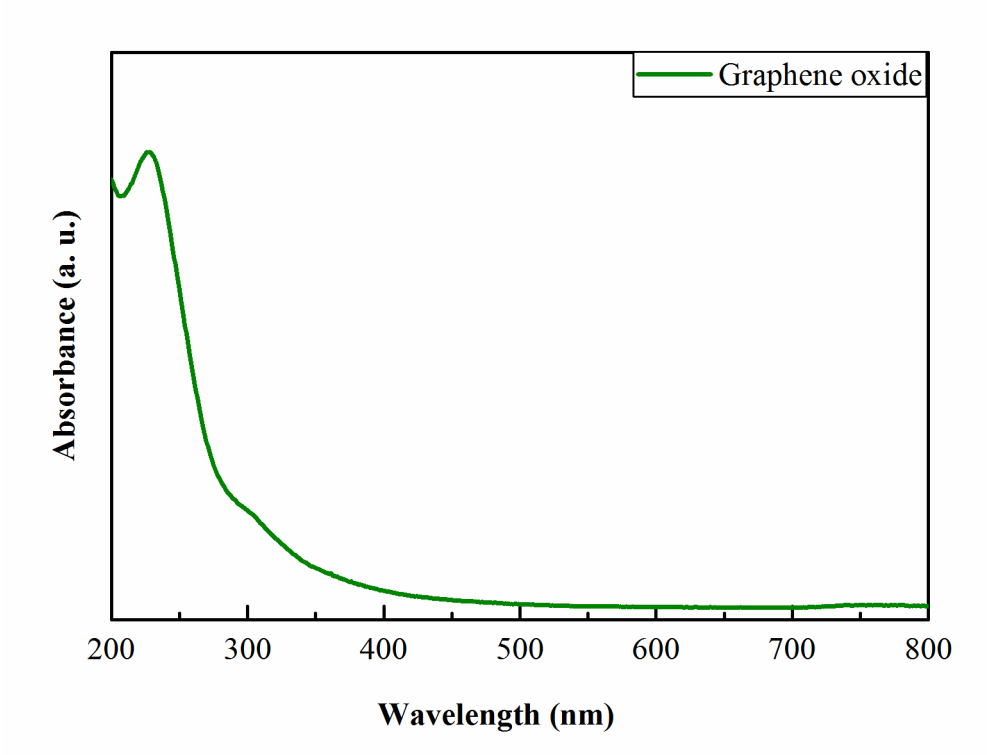

Figure 4.3: UV-Vis spectrum of the synthesized graphene oxide.

XPS spectrum of graphene oxide which represents the chemical bonding states is provided in Figure 4.4. C1s and O1s peaks peaks are detected at 285 and 531 eV, respectively and those values are compatible with the literature[151]. C/O ratio in the produced GO was found to be 1.56 by elemental analysis. C1s spectrum of the graphene oxide is also given in Figure 4.5. Deconvolution of C1s spectrum gave rise to 4 peaks that correspond to carbon sp^2 (C=C, 284 eV), epoxy/hydroxyls (C-O, 286 eV), carbonyl (C=O, 288 eV) and carboxylates (O-C=O, 289 eV) which are in agreement with the values from literature[3,52,84,152].

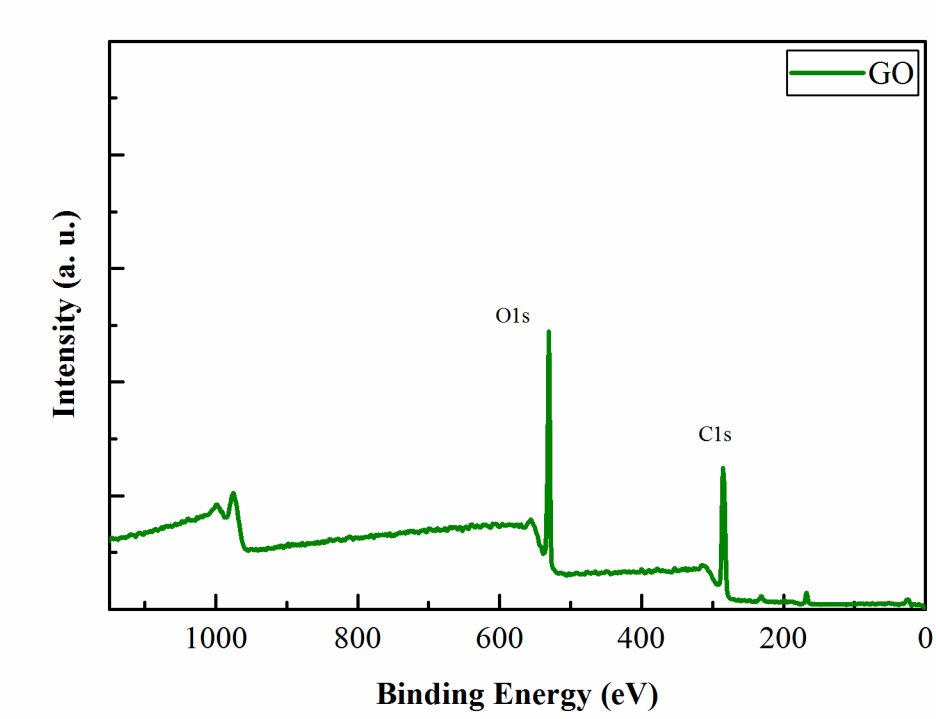

Figure 4.4: XPS spectrum of the synthesized graphite oxide.

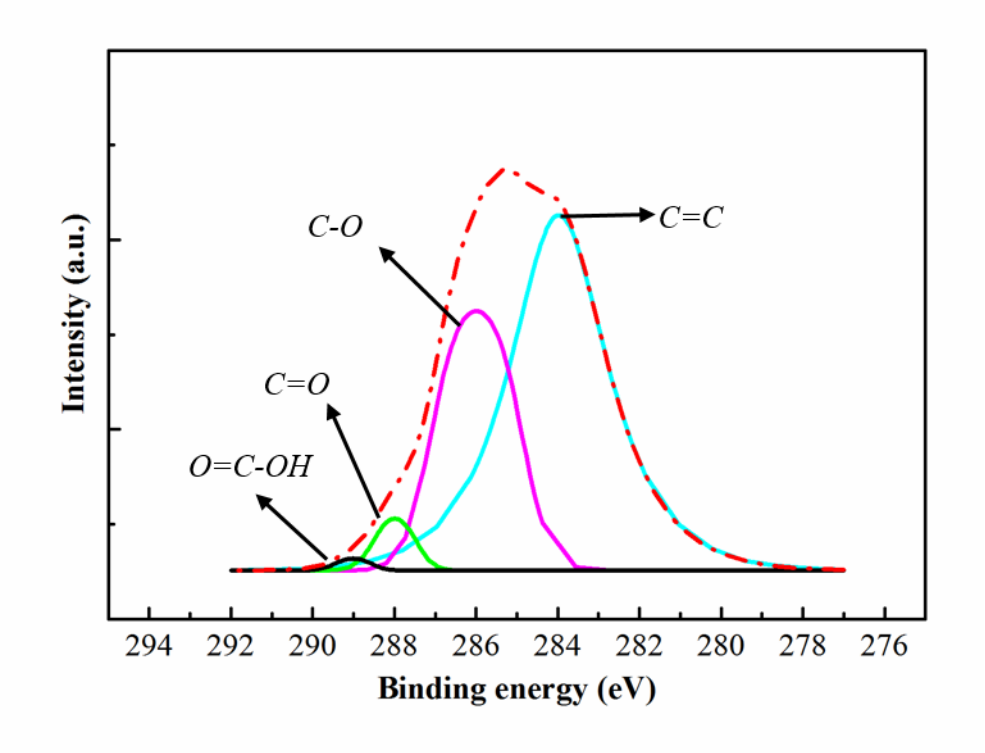

Figure 4.5: C1s spectrum of the synthesized graphite oxide.

After chemical characterization of GO, its morphology was investigated. Layered and sheet like structure of graphene oxide can be seen from SEM image provided in Figure 4.6 on the left, and it can be seen that graphene oxide has a broad range of the size. When GO was analyzed with TEM analysis; wrinkles in the structure were seen.

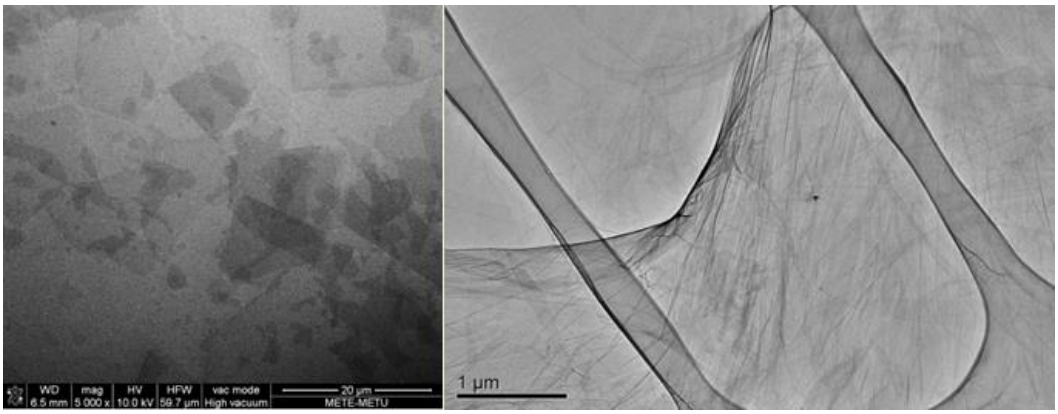

Figure 4.6: SEM (left) and TEM (right) images of graphene oxide.

GO was so thin that grid can be seen through it as indicated in TEM image on the right side of Figure 4.6, therefore to assess the thickness of GO; AFM analysis was conducted. It was seen from Figure 4.7 that lateral sizes of the flakes vary yet the thickness is around 1 nm, which indicates that the synthesized graphene oxide layers are single layers as the thickness is very close to atomic thickness[76].

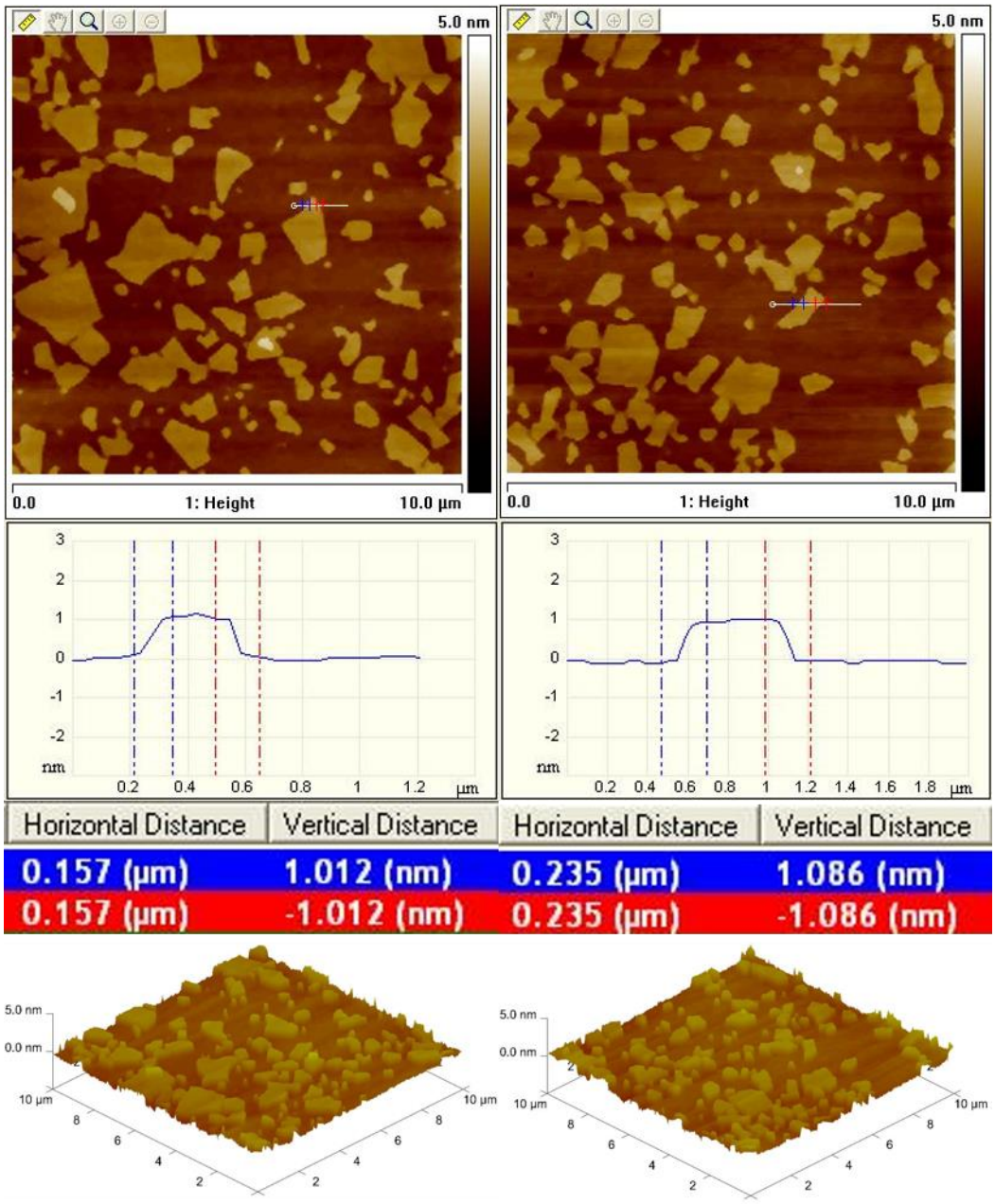

Figure 4.7: AFM analysis results of synthesized graphene oxide.

At elevated temperatures, oxygen containing groups of GO are liberated. Therefore, TGA is used as a tool to assess functionalization of graphite. In TGA, graphite showed very small weight loss which can be seen in Figure 4.8. GO however has a major weight loss around 65 % between 150-200 °C which can be attributed to CO, CO_2 and steam release[84]. This implies that in order to make use of oxygen containing functional groups in the hydrogel production, graphene oxide is required to be used at temperatures lower than 150 °C. Since graphene oxide is hygroscopic, the weight change until 100 °C corresponds to the evaporation of physically attached water molecules. More stable oxygen functionalities were continued to be removed after 200 °C. TGA thermograms used to construct TGA curves provided in Figure 4.8 are given in Appendix A.

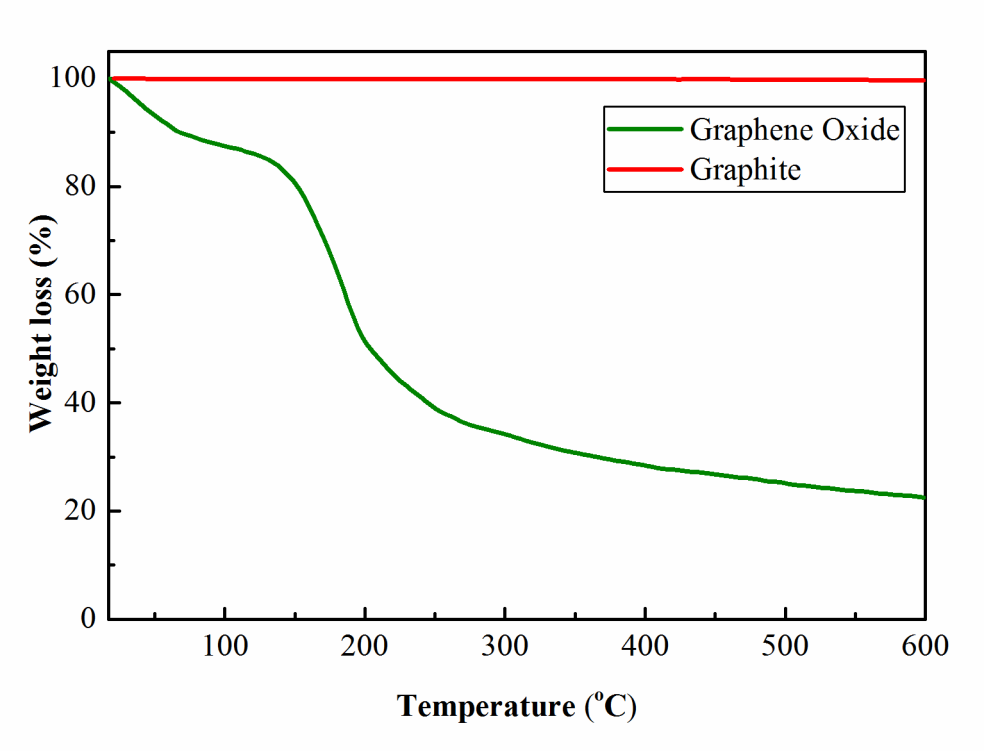

Figure 4.8: TGA curves of graphite and graphene oxide.

4.2. Reduced Graphene Oxide and Copolymer Based Aerogels

Many materials have been crosslinked into the three dimensional structures for oil absorption purposes[153]. In this study to crosslink graphene oxide a copolymer of styrene and GMA was used. Hence, copolymers of GMA and styrene were prepared and characterized prior to aerogel production. The copolymers were analyzed with ATR-FTIR, proton NMR, GPC, and TGA. They were then used in the production of reduced GO and copolymer based aerogels. Absorption experiments and SEM analysis were performed for the resultant aerogels.

4.2.1. Free Radical Copolymerization of GMA with Styrene

Copolymerization was performed with different molar ratios of the monomers charged to the reactor which can be seen in Table 4.2. Toluene was used as the solvent, and molar ratio of solvent to monomer was kept as 1.5.

Table 4.2: Molar ratios of the monomers and initiator used in free radical copolymerization of GMA and styrene.

Copolymer type	Sty	GMA	AIBN
SG5	95	5	1
SG10	90	10	1

ATR-FTIR analyses of both copolymers were conducted for chemical characterization of the copolymers. Consistent with the FTIR spectra from literature[154] provided in Figure 4.9, ATR-FTIR spectra of both copolymers in Figure 4.10 have peaks at wavenumbers of 1493 cm^{-1} and 1730 cm^{-1}, which correspond to aromatic rings of styrene and carbonyl groups of GMA, respectively.

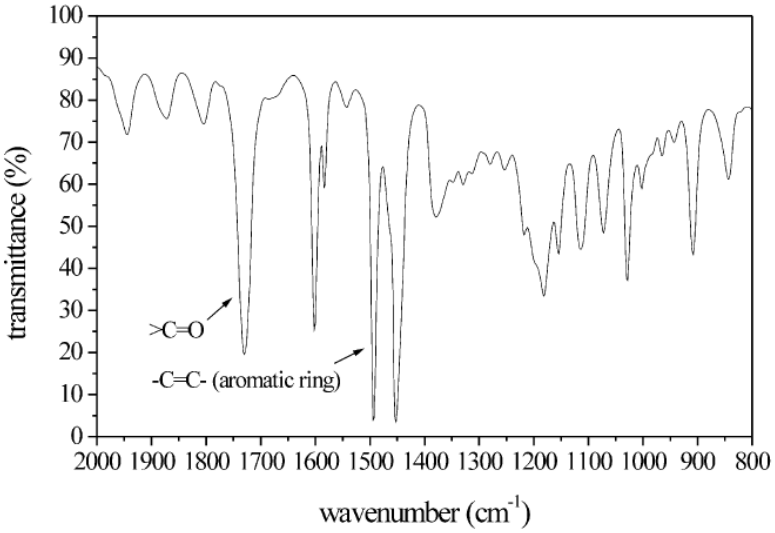

Figure 4.9: FTIR spectrum of a styrene-glycidyl methacrylate copolymer from the literature[154].

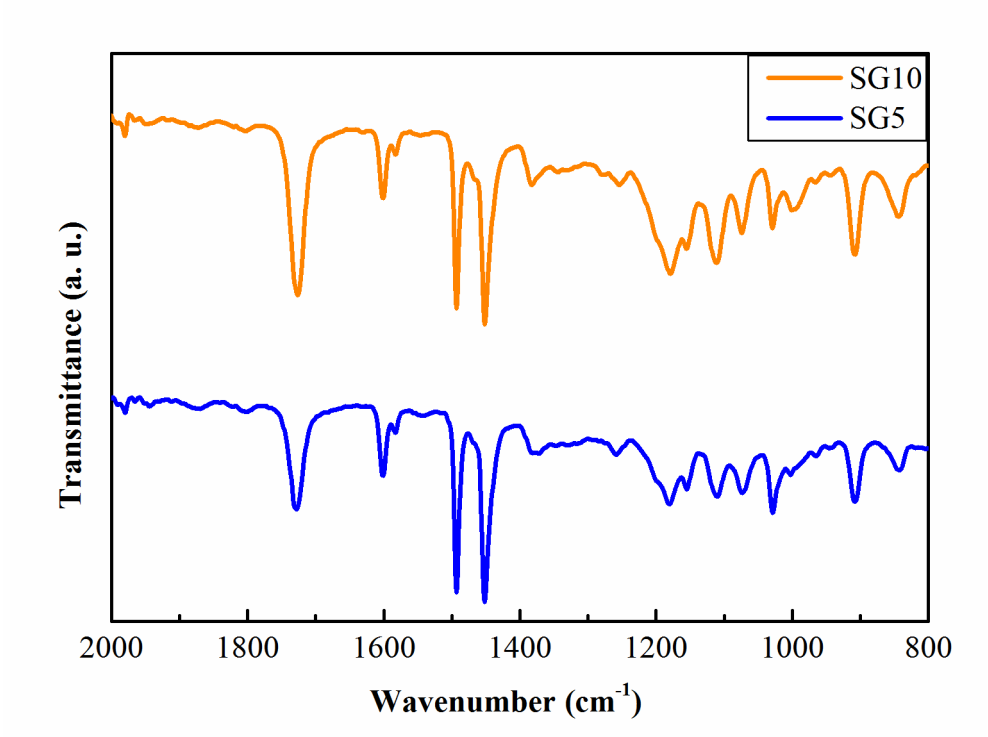

Figure 4.10: ATR-FTIR spectra of the synthesized copolymers of GMA and styrene.

Sty:GMA ratios charged to the copolymerization were 0.95 and 0.9 for SG5 and SG10, respectively. ^{1}H-NMR analysis was conducted to find the actual molar ratios

of the monomers in the resulting purified copolymers. The results of the analysis can be seen from Figure 4.11 for SG5 and Figure 4.12 for SG10.

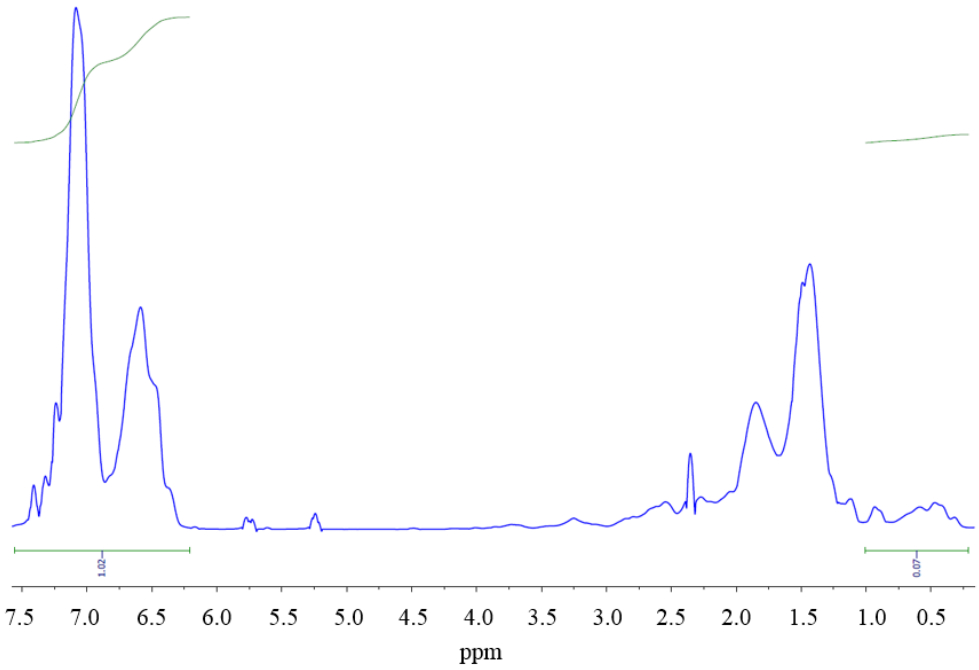

Figure 4.11: ^{1}H-NMR spectrum of SG5.

Ratios of styrene to GMA were calculated using the integrated areas that belong to protons in the aromatic ring of styrene (integral on the left side of both figure) and methyl (integral on the left side of both figure) group of GMA[155,156]. Based on the proton NMR results, the ratio of styrene to GMA residues were calculated as 0.9 and 0.83 for SG5 and SG10 respectively. The results show that the molar percentage of GMA in the copolymers is higher than the charged percentage. This indicates that GMA is more reactive than styrene. GMA and styrene show different reactivity depending upon the feed ratio of GMA to styrene according to the literature[157]. As illustrated in Table 4.3, GMA has increasing reactivity as the feed ratio of styrene to GMA increases. Ratio of styrene to GMA fed to the reactor was 19 for SG5 and it was 9 for SG10. Both values are in the range where the reactivity of GMA increases.

Table 4.3: Copolymer composition data for several styrene GMA copolymers from the literature[157].

Monomer mixture (Styrene/GMA)	Copolymer (Styrene/GMA)
0.0765	0.1573
0.2762	0.2853
1	0.6147
1.8531	0.5396
6.72	3.2637
24	9.1075

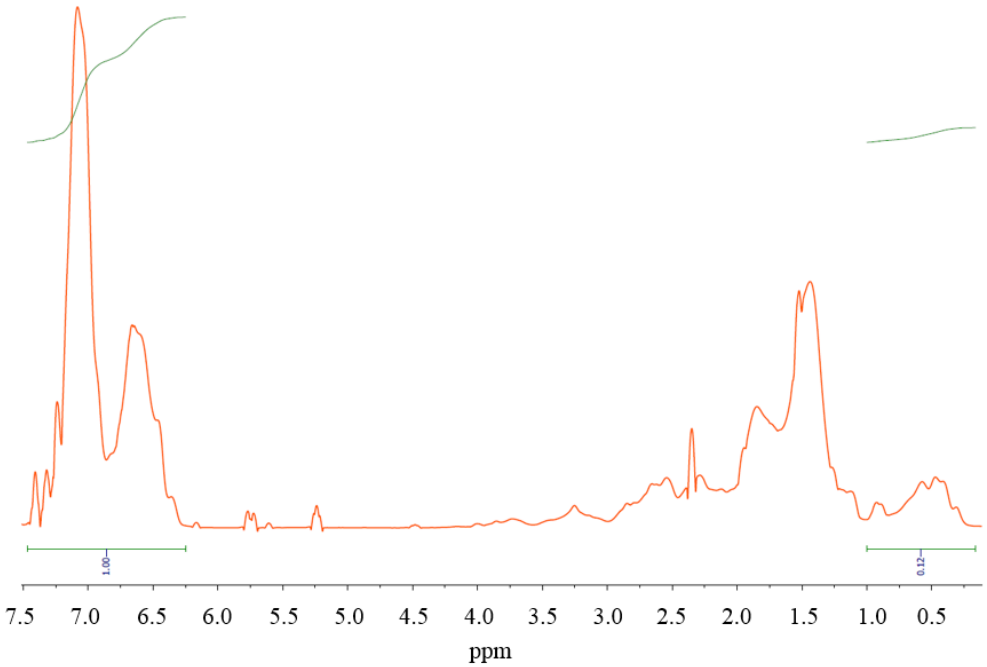

Figure 4.12: ^{1}H-NMR spectrum of SG10.

GPC was conducted to find out the corresponding molecular weights of the purified copolymers as well as their polydispercity indices. The results including polydispersity index (PDI), number average ($\bar{M}_n$) and weight average molecular weight ($\bar{M}_w$) along with charged and actual (determined by proton NMR) molar ratios of styrene to GMA are gathered below in Table 4.4.

Table 4.4: GPC results of copolymers along with molar ratios of styrene to GMA (Sty/GMA).

Copolymer type	Sty/GMA charged (mol ratio)	Sty/GMA actual (mol ratio)	$\bar{M}_n$ (g/mol)	$\bar{M}_w$ (g/mol)	PDI
SG5	95:5	90:10	20000	25000	1.25
SG10	90:10	83:17	26000	33000	1.28

When the PDI values are compared with the literature[154,158], it was seen that the values are lower than those values. Actually values were very close to literature PDI values[156] of copolymers synthesized using Atom Transfer Radical Polymerization. This indicates that the molecular weight distributions of the copolymers are comparable with the ones with controlled polymerization techniques.

TGA curves of the copolymers are given in Figure 4.13. As expected, the thermal properties of SG5 is slightly better than that of SG10 due to higher styrene content. Release of the moisture can be seen up to 100 °C. After that, two steps of weight loss can be seen in both copolymers. The one around 200 °C corresponds to the loss of oxygen containing functional groups of GMA, other one around 420 °C corresponds to the loss of benzene rings of styrene[159]. TGA thermograms used to construct TGA curves provided in Figure 4.13 are given in Appendix B.

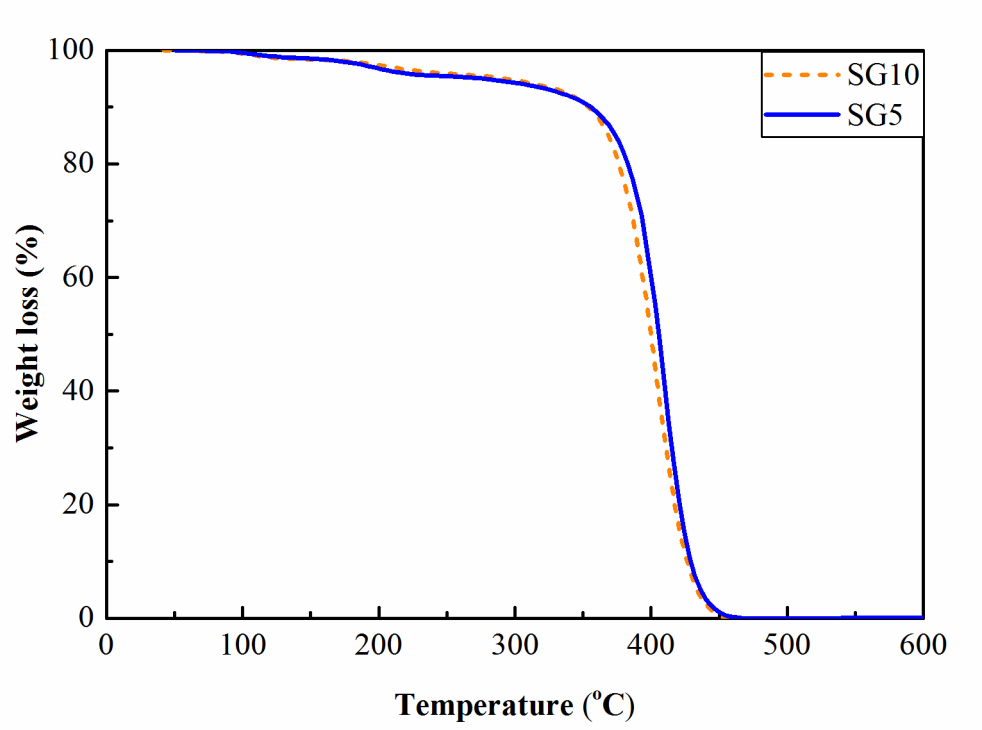

Figure 4.13: TGA curves of copolymers of styrene and GMA having different ratios of styrene and GMA (blue curve for SG5 with 5% GMA ratio charged to the feed and orange-dashed line for SG10 with 10% GMA ratio charged to the feed).

4.2.2. Reduced Graphene Oxide and Copolymer Based Aerogel Production

All of dispersions prepared in the given range (with GO concentration of 5 mg/mL and copolymer concentration of 0, 0.5, 1, 1.5, 2, 3, 4 or 5 mg/mL) gave rise to hydrogel formation at the end of 5 hours of incubation in the oven at 130 °C. During this period, carboxylic acid and hydroxyl groups of graphene oxide react with glycidyl groups of the pGcSt copolymers that promote the gelation between GO and copolymers as illustrated in the scheme provided in Figure 3.3. Mixtures of GO and copolymers of GMA and styrene are given on the top image in Figure 4.14, and hydrogels formed at the end of 5 hours of incubation are provided at the bottom image of the figure. Vials were held upside down in the image to show hydrogel formation. There was a small amount of solvent, *DMF,* at the end of 5 hours, however can not be seen in the figure due to the opacity of the rubber septum.

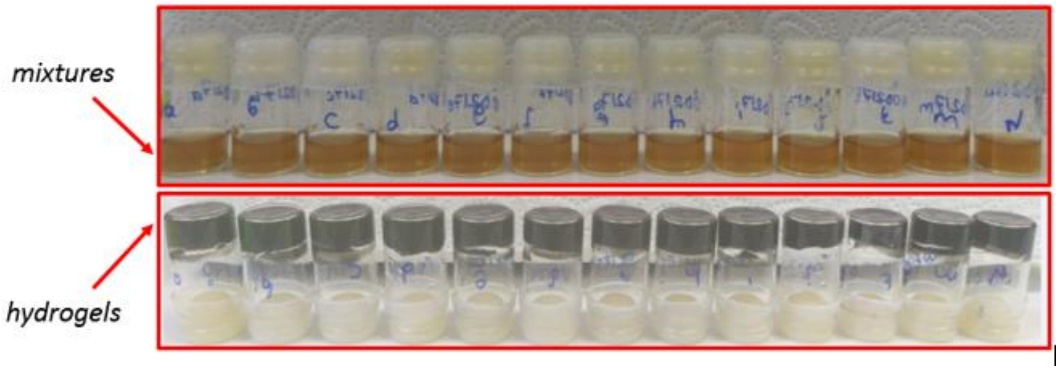

Figure 4.14: Mixtures of GO and copolymer before gelation (top) and hydrogels after gelation (bottom).

Color change from yellow to black implies that graphene oxide is reduced in gelation. Absorption tests and SEM analyses were conducted for the produced aerogels. SEM analysis of pristine rGO aerogel, *i.e.* without the addition of copolymers of GMA and styrene, is provided below in Figure 4.15. pGcSt/rGO aerogels' SEM images were given in Figure 4.16 and Figure 4.17.

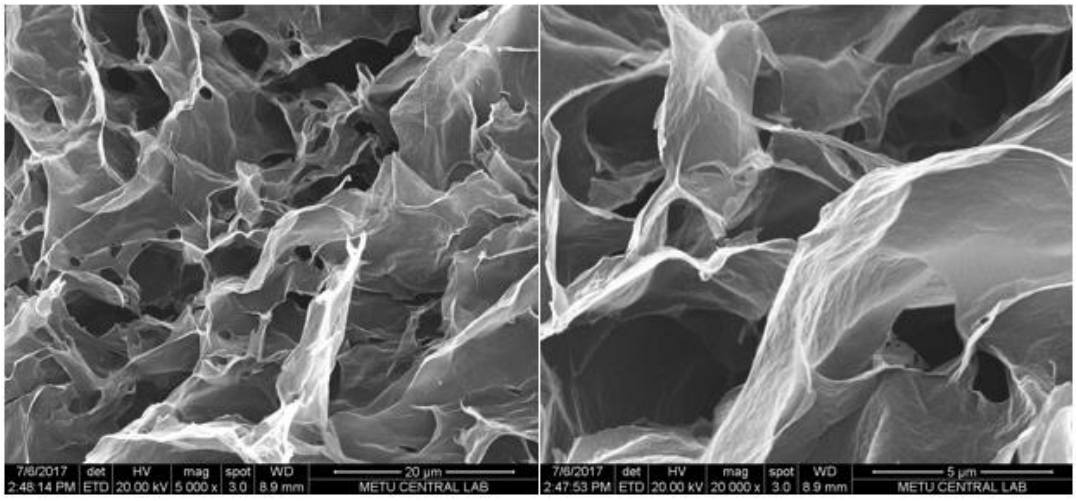

Figure 4.15: SEM images of rGO aerogels in low (left) and high (right) magnification.

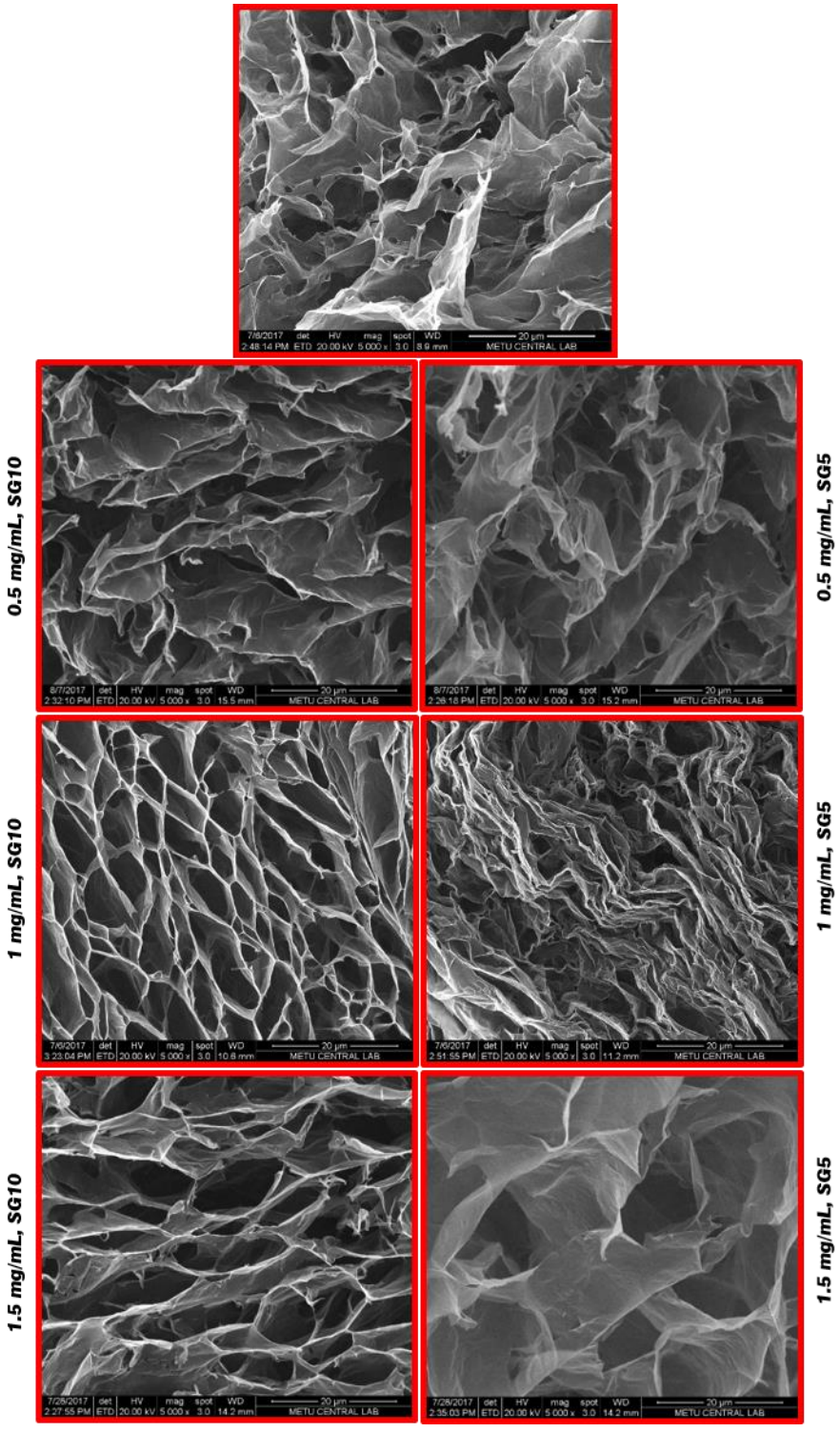

Figure 4.16: SEM images of cross-sections of pGcSt/rGO aerogels. In the hydrogel precursors used to prepare the aerogels GO concentrations were kept as 5 mg/mL and the copolymer concentrations ranged from 0 (top) to 1.5 mg/mL.

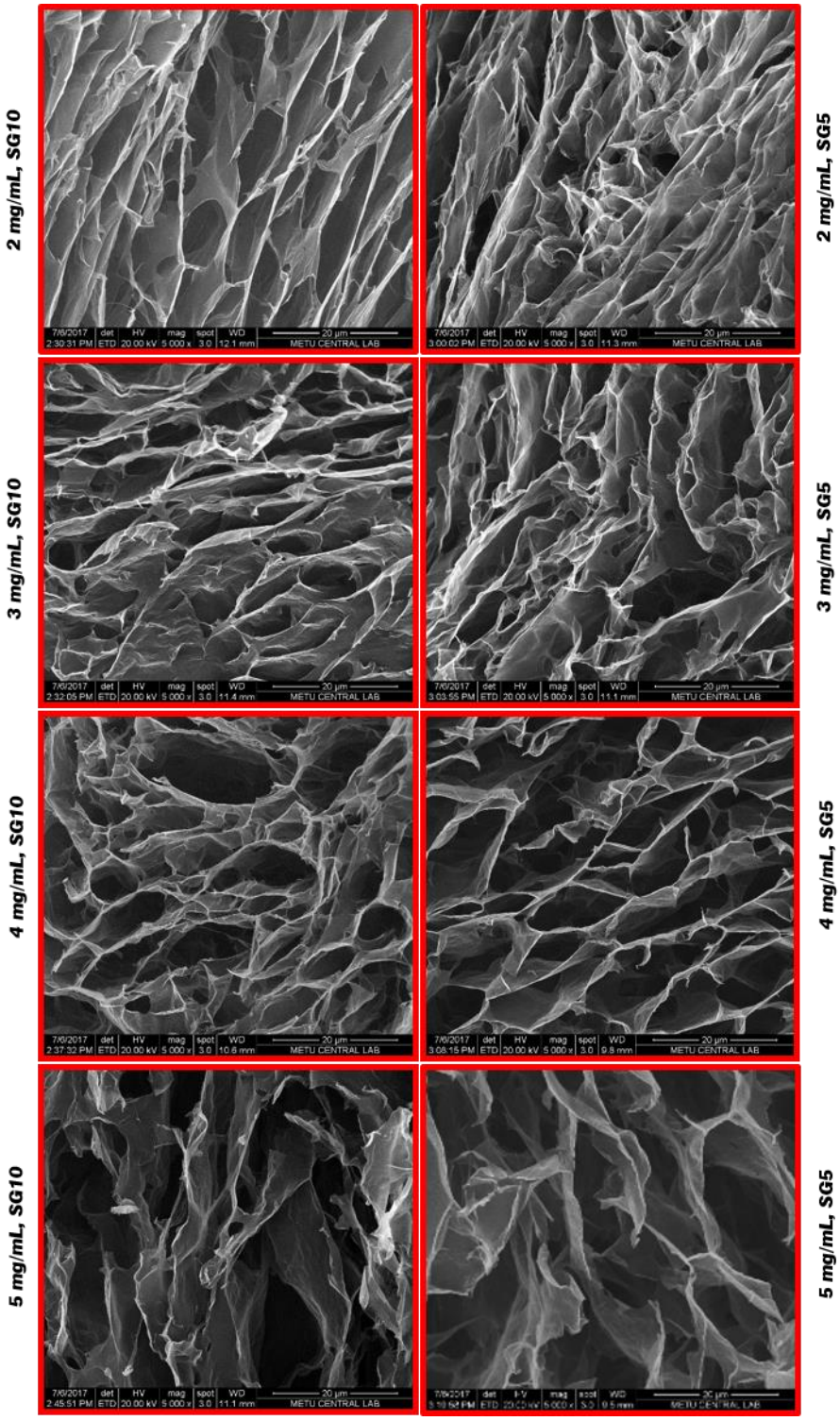

Figure 4.17: SEM images of cross-sections of pGcSt/rGO aerogels. In the hydrogel precursors used to prepare the aerogels GO concentrations were kept as 5 mg/mL and the copolymer concentrations ranged from 2 to 5 mg/mL.

All of the aerogels synthesized showed open pore structure as well as interconnection. Those are very important since open structure allows rapid transfer of the absorbed oil[160]. There exists a difference in between rGO aerogel and pGcSt/rGO aerogels in terms of pore structure and openness of the pore. Holes on the sheets and wrinkles are more obvious in rGO aerogel. However, generalization on the pore size and distribution can not be made for pGcSt/rGO aerogels.

Absorption capacities of aerogels for chloroform, toluene and vegetable oil are given in Figure 4.18, Figure 4.19 and Figure 4.20, respectively. Experiments were conducted to compare the absorption capacities of the produced aerogels. Based on the experimental observations on change of the mass of wet gel over time, absorption time was fixed at 2 hours for all of the aerogels. In order to construct the absorption capacity graphs, average absorption capacity of three samples from each aerogel type were used. Error bars were added by using standard deviations in the absorption capacities of aerogels.

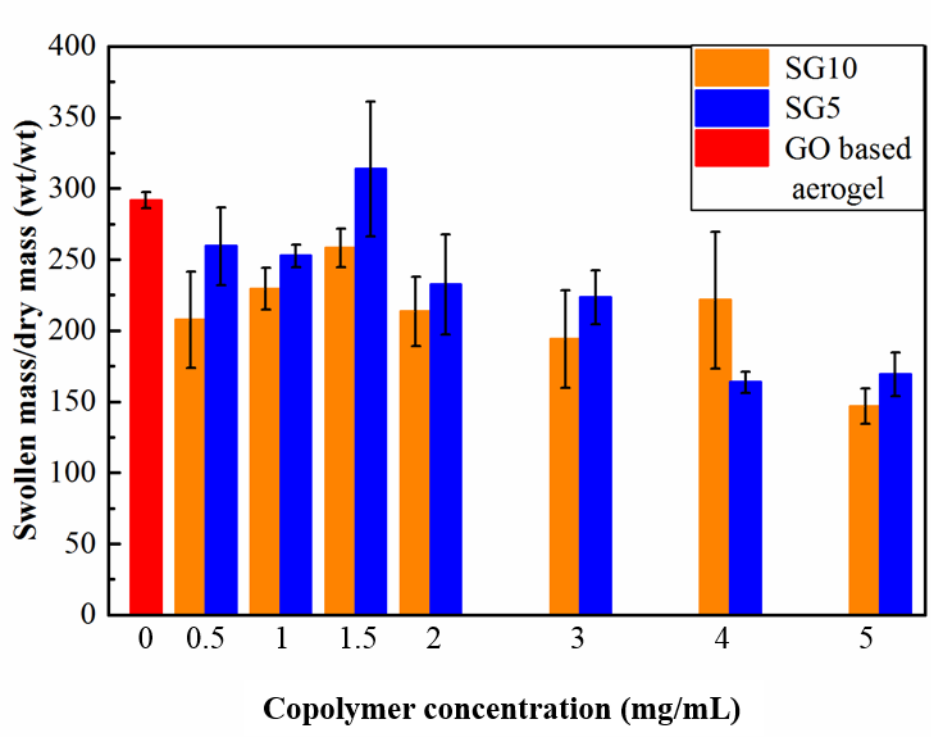

Figure 4.18: Absorption capacities of pGcSt/rGO aerogels for chloroform with respect to the concentration of styrene and GMA copolymers.

The prepared SG5 aerogels were found to have absorption capacities ranging from 170 to 315 g/g, whereas this range was between 145-260 g/g for SG10 aerogels in chloroform. Both aerogels had the highest absorption capacity at a polymer concentration of 1.5 mg/mL. It can be seen from Figure 4.18 that the absorption of chloroform with this aerogel is better than rest of the aerogels produced by using copolymers of styrene and glycidyl methacrylate. rGO based aerogels without the addition of crosslinker can be produced at the same conditions. This study completes a huge gap in terms of this comparison since both the graphene oxide aerogels produced with another ingredient and aerogels produced without any addition of crosslinking or reducing agent were subjected to the same conditions upon the completion of the hydrogel formation.

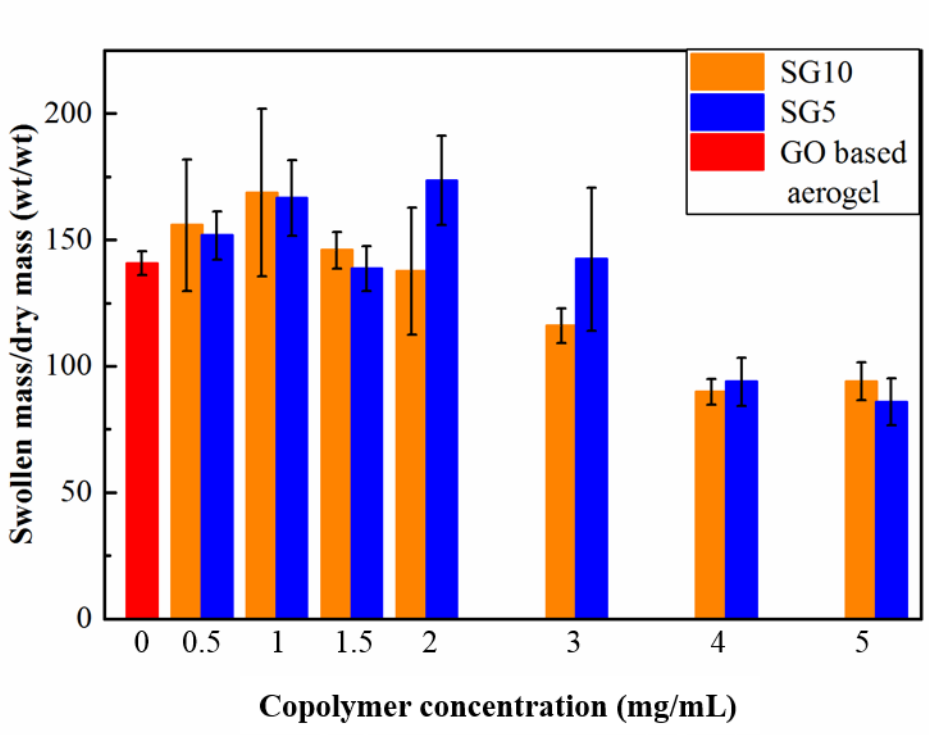

Figure 4.19: Absorption capacities of pGcSt/rGO aerogels for toluene with respect to the concentration of styrene and GMA copolymers.

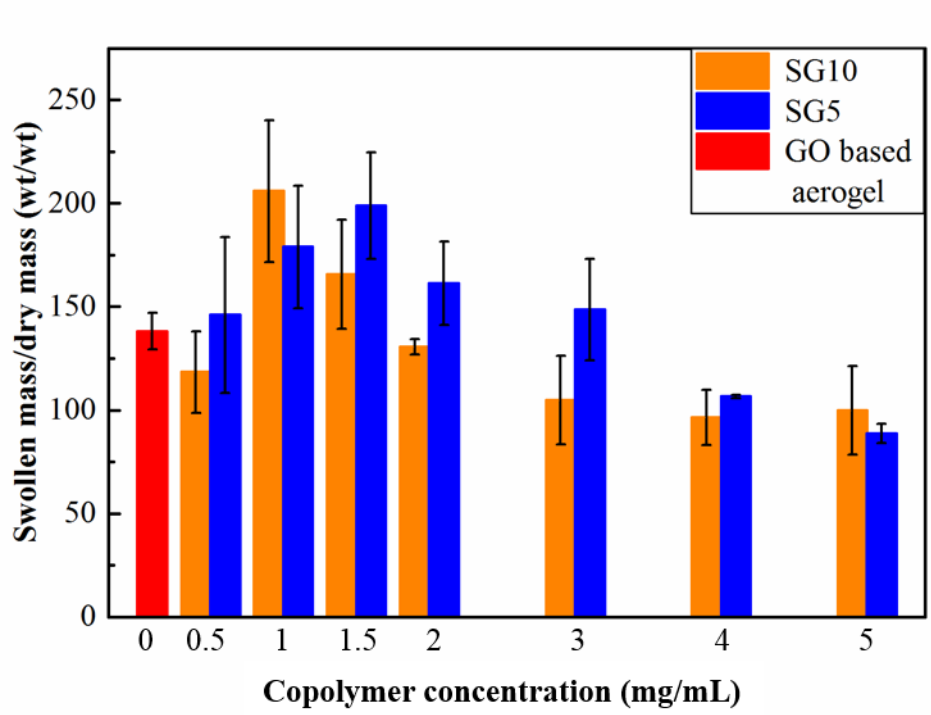

Figure 4.20: Absorption capacities of pGcSt/rGO aerogels for vegetable oil with respect to concentration of styrene and GMA copolymers.

The prepared aerogels were found to have absorption capacities in the range of 90 to 175 g/g for toluene and 90 to 200 g/g for sunflower oil. Higher styrene containing copolymer containing aerogels in general showed higher oil absorption capacities due to the fact that styrene has oleophilic nature. The highest oil absorption values were obtained with aerogels having initial concentrations of 1.5 to 2.0 mg/mL of copolymer. This may be due to unreacted copolymers in the hydrogel synthesis step which were washed out of the gel during washing steps. To assess this, TGA was performed. It can be seen from Figure 4.21 that increase in the copolymer concentration beyond 3 mg/mL do not have any impact on the copolymer amount in the aerogels.

Thermal reduction of graphene oxide can eliminate the aggregation problem that is caused by chemical reduction[100]. Therefore in this study among thermal annealing, microwave treatments, low temperature and solvothermal/hydrothermal reduction methods, low temperature thermal reduction was used. Since the critical temperature

for the chemical changes diminished at the temperature of 150 °C, incubation temperature was set to 150 °C. Therefore, weight losses shown in Figure 4.21 were calculated between 100 °C and 600 °C and reduced graphene oxide does not have a major weight loss between these temperatures. TGA thermograms used to construct Figure 4.21 are provided in Appendix C.

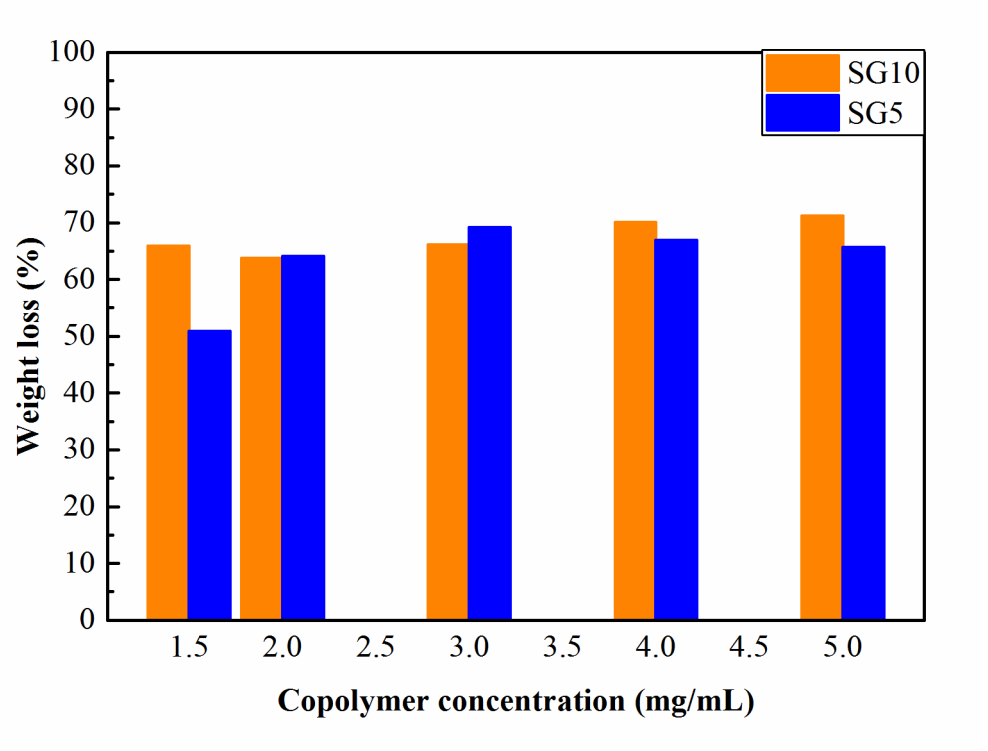

Figure 4.21: Change in weight loss determined by TGA with respect to copolymer concentration.

Aerogels were produced with the purpose of the oil-water separation. Snapshots of a movie that shows the absorption of methyl-red dyed chloroform drop in water by pGcSt/rGO aerogel less than a second are given in Figure 4.22. The figure shows that chloroform can be removed from the bottom of the water easily which indicates that the aerogels produced are promising materials to be used in oil-water separation.

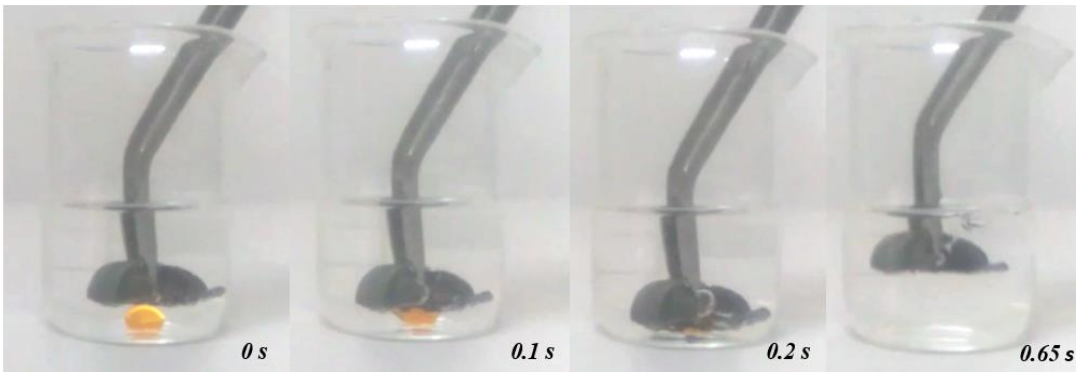

Figure 4.22: Snapshots of a movie that shows the absorption of methyl-red dyed chloroform drop in water by pGcSt/rGO aerogel.

4.3.Reduced Graphene Oxide and 1,3-DAP based Aerogel Production

All of the 1,3-DAP containing dispersions led to hydrogel formation due to the reaction between carboxyl, hydroxyl and epoxide groups of GO and amine groups of 1,3-DAP as illustrated in Figure 3.4.

Addition of 1,3-DAP to graphene oxide dispersions initiated the gel production in a short time. Graphene oxide dispersions without addition of any 1,3-DAP did not form hydrogels at the end of 6 hours of incubation at 95 °C. Vials were held upside down in Figure 4.23 to illustrate gelation behavior upon the addition of 1,3-DAP. Successive washing with ethanol and water mixtures was performed in order to ensure the complete removal of excess amines[161].

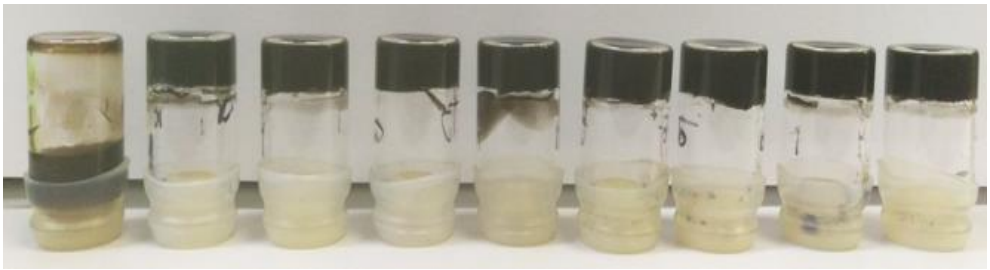

Figure 4.23: GO dispersions at the end of 6 hours of incubation at 95 °C.

SEM images of DAP/rGO aerogels that corresponds to initial GO concentrations of 3, 4, 5 mg/mL were given in Figure 4.24, Figure 4.25 and Figure 4.26, respectively. From SEM images, openness of the pores which enhances the absorbance of the oils can be seen. Pore sizes increase with increasing 1,3-DAP concentration, however in some images there were some regular patterns of larger pores. For all three different concentrations of GO, aerogel with initial 1,3-DAP concentration of 15 mg/mL showed largest pore size among others.

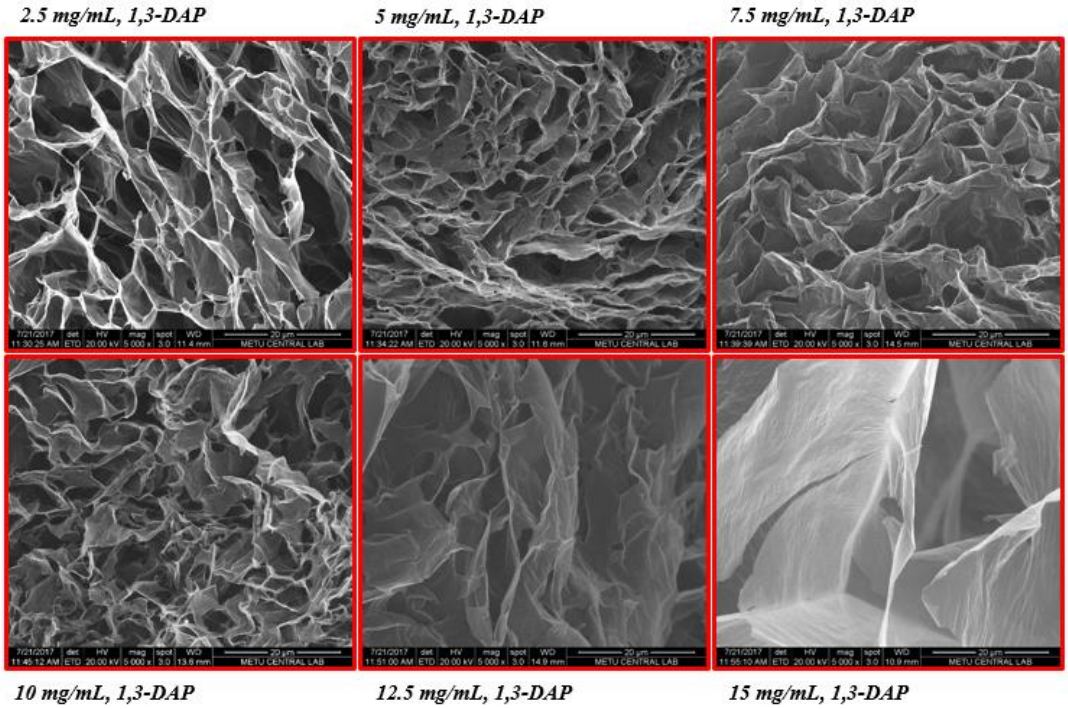

Figure 4.24: SEM images of cross-sections of aerogels of varying concentrations of 1,3-DAP and 3 mg/mL GO.

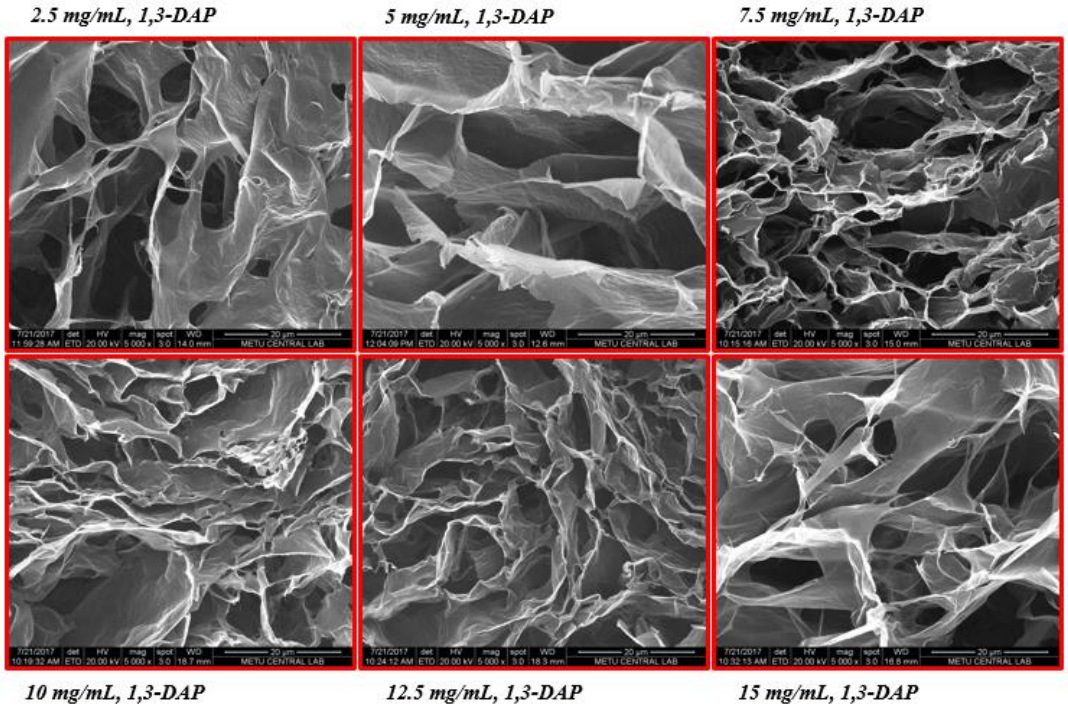

Figure 4.25: SEM images of aerogels of varying concentrations of 1,3-DAP and 4 mg/mL GO.

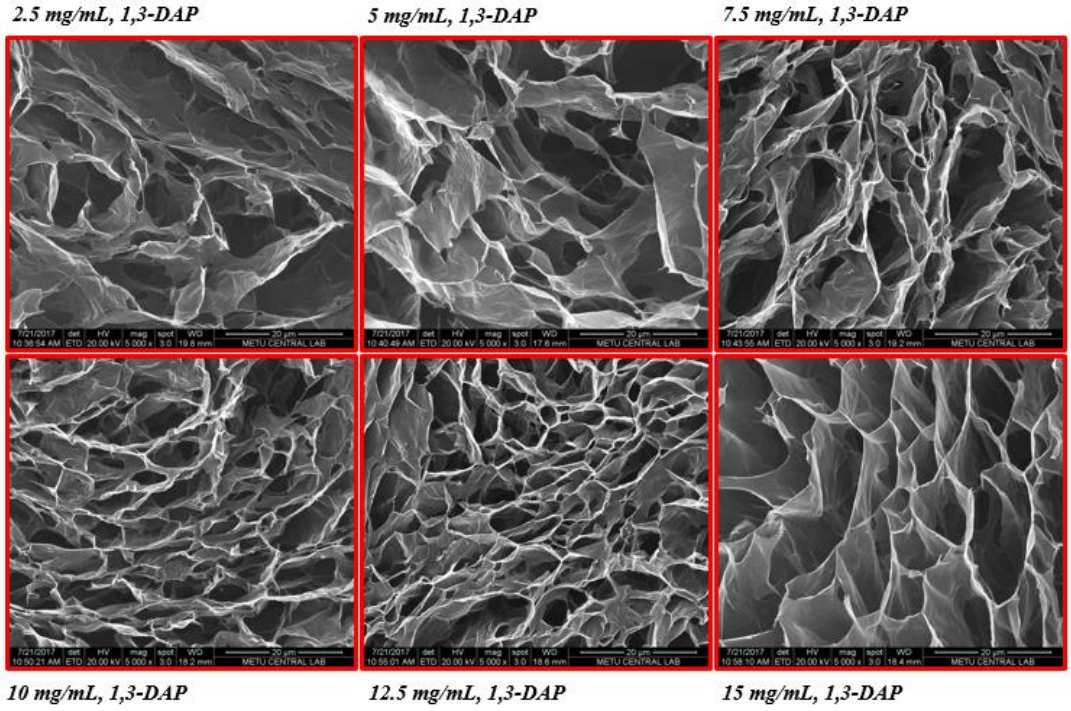

Figure 4.26: SEM images of aerogels of varying concentrations of 1,3-DAP and 5 mg/mL GO.

Absorption experiments were conducted to compare the absorption capacities of the produced aerogels. Based on the experimental observations on change of the mass of wet gel over time, absorption time was fixed at 2 hours for all of the aerogels. For chloroform as illustrated in Figure 4.27, aerogels with the starting GO concentration of 3 mg/mL, gave absorption capacities in the range of 265-534 g/g. Range was in between 280-340 and 230-310 for the aerogels with the starting GO concentration of 4 mg/mL and 5 mg/mL, respectively. It can be seen that the aerogel with 1,3-DAP concentration of 12.5 mg/mL and GO concentration of 3 mg/mL has the highest absorption capacity around 550 g/g. The aerogels with starting GO concentration of 3 mg/mL have an increasing trend until 12.5 mg/mL, and the others have nearly the same absorption capacity for the chloroform.

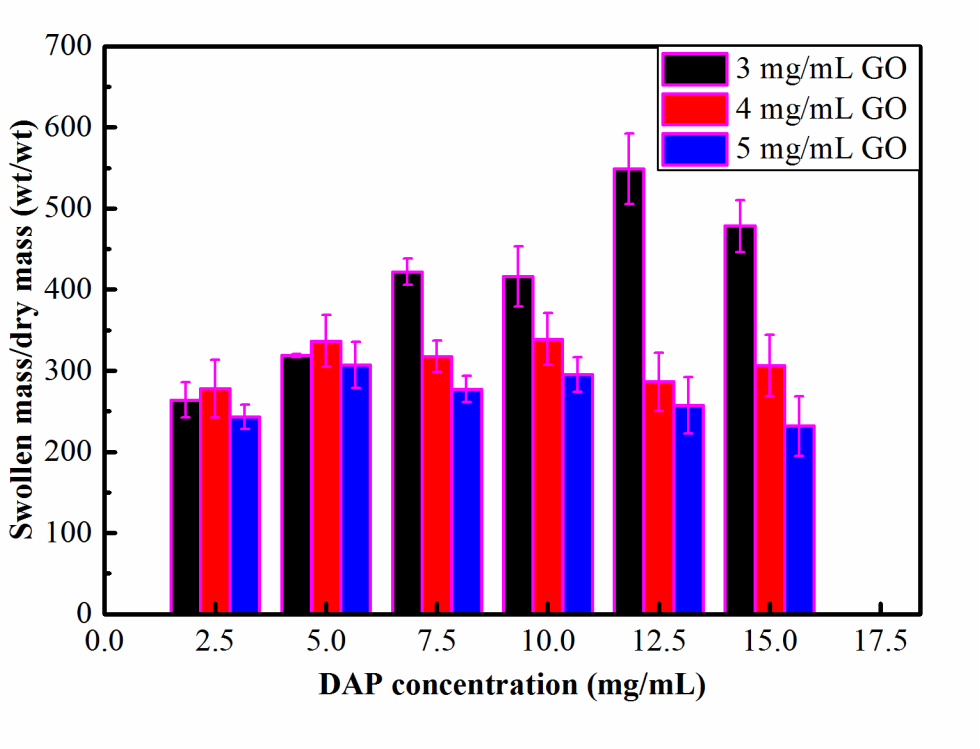

Figure 4.27: Absorption capacities of DAP/rGO aerogels for chloroform with respect to DAP concentration.

DAP/rGO aerogels showed no trend for the absorption of toluene as can be seen from Figure 4.28. On the other hand, aerogels with the lowest GO concentration used in the

synthesis, 3 mg/mL, showed the highest absorption capacity among the others as 202 mg/mg. The absorption capacity ranges were 172 mg/mg to 202 mg/mg, 146 mg/mg to 180 mg/mg, and 109 mg/mg to 159 mg/mg for 3 mg/mL, 4 mg/mL and 5 mg/mL of starting GO concentration, respectively.

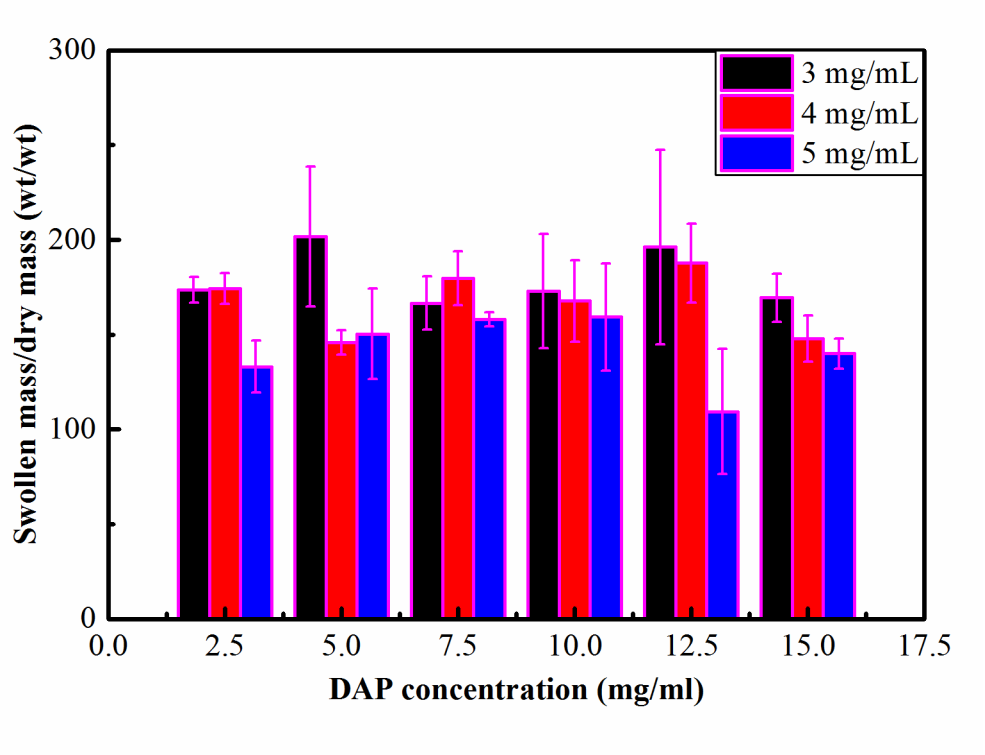

Figure 4.28: Absorption capacities of DAP/rGO aerogels for toluene with respect to DAP concentration.

In the absorption of sunflower oil, there was no trend for 4 mg/mL and 5 mg/mL of starting GO concentration as can be seen from Figure 4.29. Absorption capacity showed an increasing trend upto 270 mg/mg for the aerogels with 3 mg/mL of starting GO concentration until a starting DAP concentration of 7.5 mg/mL. The absorption capacity ranges were 194 mg/mg to 270 mg/mg, 193 mg/mg to 210 mg/mg, and 173 mg/mg to 190 mg/mg for 3 mg/mL, 4 mg/mL and 5 mg/mLof starting GO concentration, respectively. A similar aerogel produced by EDA and graphene oxide can achieve absorption capacities in between 120-250 mg/mg for oils depending on

the liquid density[19]. Most of the DAP/rGO based aerogels exceeds this absorption capacity range in absorbing chloroform.

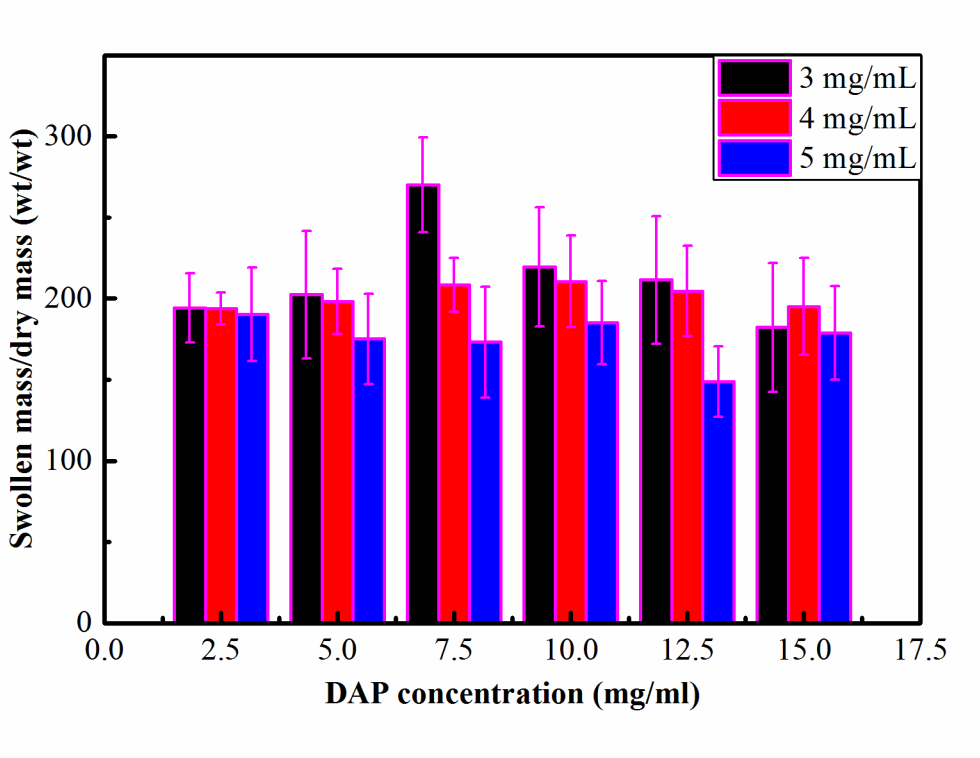

Figure 4.29: Absorption capacities of DAP/rGO aerogels for sunflower oil with respect to DAP concentration.

Snapshots of a movie that shows the absorption of methyl-red dyed chloroform drop in water by DAP/rGO aerogel less than a second are given in Figure 4.30. This shows

that DAP/rGO aerogels can be considered as promising materials to be used in oil-water separation.

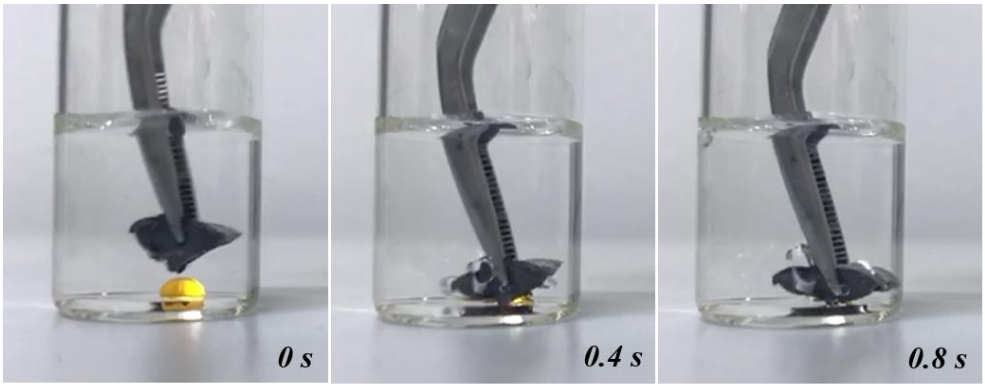

Figure 4.30: Snapshots of a movie that shows the absorption of methyl-red dyed chloroform drop in water by DAP/rGO aerogel.

Ranges of the absorption capacities were from 90 g/g to 315 g/g for reduced graphene oxide and copolymer based aerogels, and from 109 g/g to 534 g/g for reduced graphene oxide and 1,3-diaminopropane based aerogels.

When compared with the literature values of various carbon based materials presented in Table 4.5, produced aerogels are better than most of them in terms of absorption capacity. When the prices of the raw materials are taken into consideration, the ones with CNT have very high cost. Therefore, the routes proposed here can replace many of the aerogels present.

Table 4.5: Comparison of various absorbent materials for oils and organics[162].

Carbon Source	Absorbate	Absorption Capacity (g/g)
CNT	Pump oil, chloroform, ethylene glycol	80-100
GO	Cyclohexane, toluene, vegetable oil...	10-30
GO	Petroleum, toluene, cyclohexane...	5-40
GO	Diesel oil, ethanol, chloroform...	75-154
GO	Pump oil, toluene, chloroform...	60-165
GO and CNT	Compressor oil	80-140
GO and CNT	Motor oil, phenoxin, chloroform...	215-913
GO and CNT	Vegetable oil, gasoline, toluene...	21-35

CHAPTER 5

CONCLUSIONS

GO based materials have arisen great interest in the past decade. In this study, combining the properties of graphene oxide with copolymers of styrene and GMA, and with 1,3-DAP, aerogels were produced for oil-water separation purposes. Styrene as a monomer was chosen since it is known with its oleophilicity, GMA was selected as the crosslinker between graphene oxide and styrene. 1,3-DAP was chosen since it has an ability to promote gelation by forming hydrogen bonds with graphene oxide.

It is seen in this study that copolymers of styrene and GMA can be used as crosslinker for the production of reduced graphene oxide based aerogels. It is also seen that 1,3-diaminopropane can be used with the same purpose. Ranges of the absorption capacities for chloroform were from 145 g/g to 315 g/g for reduced graphene oxide and copolymer based aerogels, and from 230 g/g to 534 g/g for reduced graphene oxide and 1,3-diaminopropane based aerogels. For the absorption of toluene these ranges were from 90 g/g to 175 g/g for reduced graphene oxide and copolymer based aerogels, and from 109 g/g to 202 g/g for reduced graphene oxide and 1,3-diaminopropane based aerogels. And lastly for sunflower oil ranges were from 90 g/g to 200 g/g for reduced graphene oxide and copolymer based aerogels, and from 173 g/g to 270 g/g for reduced graphene oxide and 1,3-diaminopropane based aerogels. Reduced graphene oxide aerogels without the addition of any crosslinker was synthesized at the same experimental conditions with the reduced graphene oxide and copolymers of styrene and GMA based aerogels. It is likely that the mechanism of absorption in the aerogels consists of both imbibition and adsorption of oils/organic liquids onto the aerogel surfaces.

It is seen that increase in copolymer concentration beyond 2 mg/mL does not have effect on the absorption capacity. Comparing the values with the literature, it can be seen that both types are very effective in the absorption of oils and very promising for the use in oil-water separation. On the other hand, when the two routes were compared, reduced graphene oxide and 1,3-diaminopropane based aerogels are more advantageous to use in the oil water separation. Because they can be produced easily when compared to reduced graphene oxide and copolymer based aerogels, they have better absorption capacity.

CHAPTER 6

RECOMMENDATIONS

Based on the studies conducted, there are some recommendations that can be useful for the future work. These can be listed as:

- Different oleophilic ingredients such as oleic acid can be used for the aerogel production.
- Chemicals containing longer amine chains can be used for the aerogel synthesis (such as 1,6-hexanediamine).
- Graphene oxide functionalized with ethylenediamine, 1,3-diaminopropane, 1,6-hexanediamine etc. can be used for the aerogel synthesis
- Microwave reduction can be used for the reduction of aerogels that do not have polymer as one of the ingredient.
- Lastly, both nanoparticles and/or graphene oxide can be modified with oleophilic chemicals and they can be used along with graphene oxide for the production of aerogels.

REFERENCES

1. Wang, H. *et al.* Graphene-based materials: Fabrication, characterization and application for the decontamination of wastewater and wastegas and hydrogen storage/generation. *Adv. Colloid Interface Sci.* **195–196,** 19–40 (2013).

2. Nerín, C. *et al.* Behaviour of different industrial waste oils in a pyrolysis process: Metals distribution and valuable products. *J. Anal. Appl. Pyrolysis* **55,** 171–183 (2000).

3. He, Y. *et al.* An environmentally friendly method for the fabrication of reduced graphene oxide foam with a super oil absorption capacity. *J. Hazard. Mater.* **260,** 796–805 (2013).

4. Who is affected by oil spills. Available at: https://sites.google.com/site/blackoceanspilldisaster/who-is-effected-by-oil-spills. (Accessed: 1st January 2017)

5. Kalam, M. A., Masjuki, H. H., Jayed, M. H. & Liaquat, A. M. Emission and performance characteristics of an indirect ignition diesel engine fuelled with waste cooking oil. *Energy* **36,** 397–402 (2011).

6. Diya'Uddeen, B. H., Abdul Aziz, A. R., Daud, W. M. A. W. & Chakrabarti, M. H. Performance evaluation of biodiesel from used domestic waste oils: A review. *Process Saf. Environ. Prot.* **90,** 164–179 (2012).

7. Shannon, M. A. *et al.* Science and technology for water purification in the coming decades. *Nature* **452,** 301–310 (2008).

8. Felizardo, P. *et al.* Production of biodiesel from waste frying oils. *Waste Manag.* **26,** 487–494 (2006).

9. Xue, Z., Cao, Y., Liu, N., Feng, L. & Jiang, L. Special wettable materials for oil/water separation. *J. Mater. Chem. A* **2,** 2445–2460 (2014).

10. Kharisov, B. I., Dias, H. V. R. & Kharissova, O. V. Nanotechnology-based remediation of petroleum impurities from water. *J. Pet. Sci. Eng.* **122,** 705–718 (2014).

11. Mahajan, Y. R. Nanotechnology-based solutions for oil spills. *Nanotechnol. Insights* **2,** 1–8 (2011).

12. Sun, H., Xu, Z. & Gao, C. Multifunctional, ultra-flyweight, synergistically assembled carbon aerogels. *Adv. Mater.* **25,** 2554–2560 (2013).

13. Sui, Z. Y., Cui, Y., Zhu, J.-H. & Han, B.-H. Preparation of three-dimensional graphene oxide-polyethylenimine porous materials as dye and gas adsorbents. *ACS Appl. Mater. Interfaces* **5,** 9172–9179 (2013).

14. Cheng, C. S. *et al.* Toward 3D graphene oxide gels based adsorbents for high-efficient water treatment via the promotion of biopolymers. *J. Hazard. Mater.* **263,** 467–478 (2013).

15. Jiao, T. *et al.* Self-assembly reduced graphene oxide nanosheet hydrogel fabrication by anchorage of chitosan/silver and its potential efficient application toward dye degradation for wastewater treatments. *ACS Sustain. Chem. Eng.* **3,** 3130–3139 (2015).

16. Yu, B. *et al.* Adsorption behavior of copper ions on graphene oxide-chitosan aerogel. *J. Environ. Chem. Eng.* **1,** 1044–1050 (2013).

17. Wang, J., Song, D., Jia, S. & Shao, Z. Poly(N,N-dimethylaminoethyl methacrylate)/graphene oxide hybrid hydrogels: pH and temperature sensitivities and Cr(VI) adsorption. *React. Funct. Polym.* **81,** 8–13 (2014).

18. Hu, H., Zhao, Z., Wan, W., Gogotsi, Y. & Qiu, J. Ultralight and highly compressible graphene aerogels. *Adv. Mater.* **25,** 2219–2223 (2013).

19. Li, J. *et al.* Ultra-light, compressible and fire-resistant graphene aerogel as a highly efficient and recyclable absorbent for organic liquids. *J. Mater. Chem. A* **2,** 2934–2941 (2014).

20. Wu, F., Xie, A., Sun, M., Wang, Y. & Wang, M. Reduced graphene oxide (RGO) modified spongelike polypyrrole (PPy) aerogel for excellent electromagnetic absorption. *J. Mater. Chem. A* **3,** 14358–14369 (2015).

21. Ha, H., Shanmuganathan, K. & Ellison, C. J. Mechanically stable thermally crosslinked poly(acrylic acid)/reduced graphene oxide aerogels. *ACS Appl. Mater. Interfaces* **7,** 6220–6229 (2015).

22. Zuo, L. *et al. Polymer/carbon-based hybrid aerogels: Preparation, properties and applications*. *Materials* **8,** (2015).

23. Du, A., Zhou, B., Zhang, Z. & Shen, J. A special material or a new state of matter: A review and reconsideration of the aerogel. *Materials (Basel).* **6,** 941–968 (2013).

24. Maleki, H. Recent advances in aerogels for environmental remediation applications: A review. *Chem. Eng. J.* **300,** 98–118 (2016).

25. Hrubesh, L. W. Aerogel applications. *J. Non. Cryst. Solids* **225,** 335–342 (1998).

26. Qian, Y., Ismail, I. M. & Stein, A. Ultralight, high-surface-area, multifunctional graphene-based aerogels from self-assembly of graphene oxide and resol. *Carbon N. Y.* **68,** 221–231 (2014).

27. Wang, X. *et al.* Scalable template synthesis of resorcinol-formaldehyde/graphene oxide composite aerogels with tunable densities and mechanical properties. *Angew. Chemie* **127,** 2427–2431 (2015).

28. Worsley, M. A. *et al.* Synthesis and characterization of highly crystalline graphene aerogels. *ACS Nano* **8,** 11013–11022 (2014).

29. Li, C. & Shi, G. Functional gels based on chemically modified graphenes. *Adv. Mater.* **26,** 3992–4012 (2014).

30. Kistler, S. S. Coherent expanded aerogels and jellies. *Nature* **127,** 741 (1931).

31. Peri, J. B. Infrared study of OH and NH2 groups on the surface of a dry silica aerogel. *J. Phys. Chem.* **70,** 2937–2945 (1966).

32. Dorcheh, A. S. & Abbasi, M. H. Silica aerogel; synthesis, properties and characterization. *J. Mater. Process. Technol.* **199,** 10–26 (2008).

33. Chen, Q., Wang, H. & Sun, L. Preparation and characterization of silica aerogel microspheres. *Materials (Basel).* **10,** 435 (2017).

34. Horiuchi, T. *et al.* High surface area alumina aerogel at elevated temperatures. *J. Chem. Soc. Faraday Trans.* **90,** 2573–2578 (1994).

35. Lermontov, S. A. *et al.* How to tune the alumina aerogels structure by the variation of a supercritical solvent. Evolution of the structure during heat treatment. *J. Phys. Chem. C* **120,** 3319–3325 (2016).

36. Li, X., He, H. & Ren, L. Fabrication and characterization of the monolithic hydrophobic alumina aerogels. *J. Porous Mater.* **24,** 679–683 (2017).

37. Campbell, L. K., Na, B. K. & Ko, E. I. Synthesis and characterization of titania aerogels. *Chem. Mater.* **4,** 1329–1333 (1992).

38. Schneider, M. & Baiker, A. High-surface-area titania aerogels: Preparation and structural properties. **2,** 587–589 (1992).

39. Abecassis-Wolfovich, M. *et al.* Texture and nanostructure of chromia aerogels prepared by urea-assisted homogeneous precipitation and low-temperature supercritical drying. *J. Non. Cryst. Solids* **318,** 95–111 (2003).

40. Rotter, H., Landau, M. V., Carrera, M., Goldfarb, D. & Herskowitz, M. High surface area chromia aerogel efficient catalyst and catalyst support for ethylacetate combustion. *Appl. Catal. B Environ.* **47,** 111–126 (2004).

41. Kucheyev, S. O. *et al.* Electronic structure of chromia aerogels from soft x-ray absorption spectroscopy. *J. Appl. Phys.* **101,** 12315 (2007).

42. Gash, A. E., Satcher, J. H. & Simpson, R. L. Monolithic nickel(II)-based

aerogels using an organic epoxide: The importance of the counterion. *J. Non. Cryst. Solids* **350,** 145–151 (2004).

43. Bi, Y., Ren, H., Chen, B. & Zhang, L. Synthesis and characterization of nickel-based monolithic aerogel via sol-gel method. *Adv. Mater. Res.* **335–336,** 368–371 (2011).

44. Huang, Y., Zhao, B. & Xie, Y. Preparation of zirconia-based acid catalysts from zirconia aerogel of tetragonal phase. *Appl. Catal. A Gen.* **172,** 327–331 (1998).

45. Cao, Y., Hu, J.-C., Hong, Z.-S., Deng, J.-F. & Fan, K.-N. Characterization of high-surface-area zirconia aerogel synthesized from combined alcohothermal and supercritical fluid drying techniques. *Catal. Letters* **81,** 107–112 (2002).

46. Pekala, R. W. Organic aerogels from the polycondensation of resorcinol with formaldehyde. *J. Mater. Sci.* **24,** 3221–3227 (1989).

47. Reuß, M. & Ratke, L. Subcritically dried RF-aerogels catalysed by hydrochloric acid. *J. Sol-Gel Sci. Technol.* **47,** 74–80 (2008).

48. Jin, H., Nishiyama, Y., Wada, M. & Kuga, S. Nanofibrillar cellulose aerogels. *Colloids Surfaces A Physicochem. Eng. Asp.* **240,** 63–67 (2004).

49. Miettunen, K. *et al.* Nanocellulose aerogel membranes for optimal electrolyte filling in dye solar cells. *Nano Energy* **8,** 95–102 (2014).

50. Hoecker, C., Smail, F., Pick, M. & Boies, A. The influence of carbon source and catalyst nanoparticles on CVD synthesis of CNT aerogel. *Chem. Eng. J.* **314,** 388–395 (2017).

51. Gao, Y.-D. *et al.* Graphene oxide aerogels constructed using large or small graphene oxide with different electrical, mechanical and adsorbent properties. *RSC Adv.* **6,** 9851–9856 (2016).

52. Si, W. *et al.* Reduced graphene oxide aerogel with high-rate supercapacitive performance in aqueous electrolytes. *Nanoscale Res. Lett.* **8,** 247 (2013).

53. Mohanan, J. L., Arachchige, I. U. & Brock, S. L. Porous semiconductor chalcogenide aerogels. *Science (80-.).* **307,** 397–400 (2005).

54. Chen, K. *et al.* Low temperature pseudomorphic synthesis of nanocrystalline carbide aerogels for electrocatalysis. *J. Mater. Chem. A* **3,** 11745–11749 (2015).

55. Leventis, N., Chandrasekaran, N., Sadekar, A. G., Sotiriou-Leventis, C. & Lu, H. One-pot synthesis of interpenetrating inorganic/organic networks of CuO/resorcinol-formaldehyde aerogels: nanostructured energetic materials. *J. Am. Chem. Soc.* **131,** 4576–4577 (2009).

56. Jones, S. M. A method for producing gradient density aerogel. *J. Sol-Gel Sci. Technol.* **44,** 255–258 (2007).

57. Cong, H., Wang, P. & Yu, S. Stretchable and self-healing graphene oxide-polymer composite hydrogels: A dual network design. *Chem.* **25,** 3357–3362 (2013).

58. Ye, S., Feng, J. & Wu, P. Highly elastic graphene oxide–epoxy composite aerogels via simple freeze-drying and subsequent routine curing. *J. Mater. Chem. A* **1,** 3495–3502 (2013).

59. Liu, X., Sun, J. & Zhang, X. Novel 3D graphene aerogel-ZnO composites as efficient detection for NO2 at room temperature. *Sensors Actuators, B Chem.* **211,** 220–226 (2015).

60. Jiang, Y., Feng, J. & Feng, J. Synthesis and characterization of ambient-dried microglass fibers/silica aerogel nanocomposites with low thermal conductivity. *J. Sol-Gel Sci. Technol.* **83,** 64–71 (2017).

61. Li, J. *et al.* Improved mechanical and thermal insulation properties of monolithic attapulgite nanofiber/silica aerogel composites dried at ambient pressure. *J. Sol-Gel Sci. Technol.* **82,** 702–711 (2017).

62. Aerotherm aerogel insulation brings space technology to everyday life.

Available at: http://www.innovationintextiles.com/industry-talk/aerotherm-aerogel-insulation-brings-space-technology-to-everyday-life/. (Accessed: 1st July 2017)

63. Hu, H., Zhao, Z., Gogotsi, Y. & Qiu, J. Compressible carbon nanotube-graphene hybrid aerogels with superhydrophobicity and superoleophilicity for oil sorption. *Environ. Sci. Technol. Lett.* **1,** 214–220 (2014).

64. Geim, A. K. & Novoselov, K. S. The rise of graphene. *Nat. Mater.* **6,** 183–191 (2007).

65. Zhu, Y. *et al.* Graphene and graphene oxide: Synthesis, properties, and applications. *Adv. Mater.* **22,** 3906–3924 (2010).

66. Kiew, S. F., Kiew, L. V., Lee, H. B., Imae, T. & Chung, L. Y. Assessing biocompatibility of graphene oxide-based nanocarriers: A review. *J. Control. Release* **226,** 217–228 (2016).

67. Novoselov, K. S. *et al.* Electric field effect in atomically thin carbon films. *Science (80-.).* **306,** 666–669 (2004).

68. Dreyer, D. R., Park, S., Bielawski, C. W. & Ruoff, R. S. The chemistry of graphene oxide. *Chem. Soc. Rev.* **39,** 228–240 (2010).

69. Luo, D., Zhang, G., Liu, J. & Sun, X. Evaluation criteria for reduced graphene oxide. *J. Phys. Chem. C* **115,** 11327–11335 (2011).

70. Pei, S. & Cheng, H. M. The reduction of graphene oxide. *Carbon N. Y.* **50,** 3210–3228 (2012).

71. Sinitskii, A. & Tour, J. M. Chemical approaches to produce graphene oxide and related materials. in *Graphene Nanoelectronics: From Materials to Circuits* (ed. Murali, R.) **9781461405,** (2012).

72. Erickson, K. *et al.* Determination of the local chemical structure of graphene oxide and reduced graphene oxide. *Adv. Mater.* **22,** 4467–4472 (2010).

73. Szabo, T. *et al.* Evolution of surface functional groups in a series of progressively oxidized graphite oxides. **18,** 2740–2749 (2006).

74. He, H., Klinowski, J., Forster, M. & Lerf, A. A new structural model for graphite oxide. *Chem. Phys. Lett.* **287,** 53–56 (1998).

75. Kou, L., He, H. & Gao, C. Click chemistry approach to functionalize two-dimensional macromolecules of graphene oxide nanosheets. *Nano-Micro Lett.* **2,** 177–183 (2010).

76. Gao, W. Graphite oxide: Structure, reduction and applications. (Rice University, 2012).

77. Lee, D. W. *et al.* The structure of graphite oxide: Investigation of its surface chemical groups. *J. Phys. Chem. B* **114,** 5723–5728 (2010).

78. Dreyer, D. R., Todd, A. D. & Bielawski, C. W. Harnessing the chemistry of graphene oxide. *Chem. Soc. Rev.* **43,** 5288 (2014).

79. Brodie, B. C. On the atomic weight of graphite. *Philos. Trans. R. Soc. London* **149,** 249–259 (1859).

80. Talyzin, A. V. *et al.* Colossal pressure-induced lattice expansion of graphite oxide in the presence of water. *Angew. Chemie - Int. Ed.* **47,** 8268–8271 (2008).

81. Tang, G. *et al.* Three dimensional graphene aerogels and their electrically conductive composites. *Carbon N. Y.* **77,** 592–599 (2014).

82. Moo, J. G. S., Khezri, B., Webster, R. D. & Pumera, M. Graphene oxides prepared by Hummers', Hofmann's, and Staudenmaier's Methods: dramatic influences on heavy-metal-ion adsorption. *ChemPhysChem* **15,** 2922–2929 (2014).

83. Lerf, A., He, H., Forster, M. & Klinowski, J. Structure of graphite oxide revisited‖. *J. Phys. Chem. B* **102,** 4477–4482 (1998).

84. Marcano, D. C. *et al.* Improved synthesis of graphene oxide. *ACS Nano* **4,** 4806–4814 (2010).

85. Sudeep, P. M. *et al.* Covalently interconnected three dimensional graphene oxide solids. *ACS Nano* **7,** 7034–7040 (2013).

86. Peng, L. *et al.* An iron-based green approach to 1-h production of single-layer graphene oxide. *Nat. Commun.* **6,** 5716 (2015).

87. Hirata, M., Gotou, T., Horiuchi, S., Fujiwara, M. & Ohba, M. Thin-film particles of graphite oxide 1: High-yield synthesis and flexibility of the particles. *Carbon N. Y.* **42,** 2229–2937 (2004).

88. Kovtyukhova, N. I. *et al.* Layer-by-layer assembly of ultrathin composite films from micron-sized graphite oxide sheets and polycations. *Chem. Mater.* **11,** 771–778 (1999).

89. Nguyen, S. T. *et al.* Morphology control and thermal stability of binderless-graphene aerogels from graphite for energy storage applications. *Colloids Surfaces A Physicochem. Eng. Asp.* **414,** 352–358 (2012).

90. Koch, K. R. Oxidation by Mn2O7: An impressive demonstration of the powerful oxidizing property of dimanganeseheptoxide. *J. Chem. Educ.* **59,** 973–974 (1982).

91. Wahab, H. *et al.* Signatures of different carbon bonds in graphene oxide from soft x-ray reflectometry. *X-Ray Spectrom.* **44,** 468–473 (2015).

92. Compton, O. C. & Nguyen, S. T. Graphene oxide, highly reduced graphene oxide, and graphene: Versatile building blocks for carbon-based materials. *Small* **6,** 711–723 (2010).

93. Kim, F. *et al.* Self-propagating domino-like reactions in oxidized graphite. *Adv. Funct. Mater.* **20,** 2867–2873 (2010).

94. Buchsteiner, A., Lerf, A. & Pieper, J. Water dynamics in graphite oxide investigated with neutron scattering. *J. Phys. Chem. B* **110,** 22328–22338

(2006).

95. Hu, X., Yu, Y., Hou, W., Zhou, J. & Song, L. Effects of particle size and pH value on the hydrophilicity of graphene oxide. *Appl. Surf. Sci.* **273,** 118–121 (2013).

96. Paredes, J. I., Villar-Rodil, S., Martínez-Alonso, A. & Tascón, J. M. D. Graphene oxide dispersions in organic solvents. *Langmuir* **24,** 10560–10564 (2008).

97. Konios, D., Stylianakis, M. M., Stratakis, E. & Kymakis, E. Dispersion behaviour of graphene oxide and reduced graphene oxide. *J. Colloid Interface Sci.* **430,** 108–112 (2014).

98. Shin, H.-J. *et al.* Efficient reduction of graphite oxide by sodium borohydride and its effect on electrical conductance. *Adv. Funct. Mater.* **19,** 1987–1992 (2009).

99. Zhu, Y., Cai, W., Piner, R. D., Velamakanni, A. & Ruoff, R. S. Transparent self-assembled films of reduced graphene oxide platelets. *Appl. Phys. Lett.* **95,** 103104 (2009).

100. Smith, C. T. G. Graphene oxide material interfaces in electronics, energy and environmental membranes. (University of Surrey, 2016).

101. Dua, V. *et al.* All-organic vapor sensor using inkjet-printed reduced graphene oxide. *Angew. Chemie - Int. Ed.* **49,** 2154–2157 (2010).

102. Gao, J. *et al.* Environment-friendly method to produce graphene that employs vitamin C and amino acid. *Chem. Mater.* **22,** 2213–2218 (2010).

103. Fernández-Merino, M. J. *et al.* Vitamin C is an ideal substitute for hydrazine in the reduction of graphene oxide suspensions. *J. Phys. Chem. C* **114,** 6426–6432 (2010).

104. Liu, S., Tian, J., Wang, L. & Sun, X. A method for the production of reduced graphene oxide using benzylamine as a reducing and stabilizing agent and its subsequent decoration with Ag nanoparticles for enzymeless hydrogen peroxide detection. *Carbon N. Y.* **49,** 3158–3164 (2011).

105. Zhou, X. *et al.* Reducing graphene oxide via hydroxylamine: A simple and efficient route to graphene. **115,** 11957–11961 (2011).

106. Tegou, E., Pseiropoulos, G., Filippidou, M. K. & Chatzandroulis, S. Low-temperature thermal reduction of graphene oxide films in ambient atmosphere: Infra-red spectroscopic studies and gas sensing applications. *Microelectron. Eng.* **159,** 146–150 (2016).

107. Sun, H. B., Yang, J., Zhou, Y. Z., Zhao, N. & Li, D. Preparation of reduced graphene oxide films by dip coating technique and their electrical conductivity. *Mater. Technol. Adv. Perform. Mater.* **29,** 14–20 (2014).

108. Zhu, Y. *et al.* Microwave assisted exfoliation and reduction of graphite oxide for ultracapacitors. *Carbon N. Y.* **48,** 2118–2122 (2010).

109. Chen, W., Yan, L. & Bangal, P. R. Preparation of graphene by the rapid and mild thermal reduction of graphene oxide induced by microwaves. *Carbon N. Y.* **48,** 1146–1152 (2010).

110. Wang, K. *et al.* The field emission of vacuum filtered graphene films reduced by microwave. *Appl. Surf. Sci.* **257,** 5808–5812 (2011).

111. Nethravathi, C. & Rajamathi, M. Chemically modified graphene sheets produced by the solvothermal reduction of colloidal dispersions of graphite oxide. *Carbon N. Y.* **46,** 1994–1998 (2008).

112. Murugan, A. V., Muraliganth, T. & Manthiram, A. Rapid, facile microwave-solvothermal synthesis of graphene nanosheets and their polyaniline nanocomposites for energy storage. *Chem. Mater.* **21,** 5004–5006 (2009).

113. Liao, K.-H. *et al.* Aqueous only route toward graphene from graphite oxide.

ACS Nano **5,** 1253–1258 (2011).

114. Zhou, Y., Bao, Q., Tang, L. A. L., Zhong, Y. & Loh, K. P. Hydrothermal dehydration for the 'green' reduction of exfoliated graphene oxide to graphene and demonstration of tunable optical limiting properties. *Chem. Mater.* **21,** 2950–2956 (2009).

115. Li, Y. *et al.* Highly compressible macroporous graphene monoliths via an improved hydrothermal process. *Adv. Mater.* **26,** 4789–4793 (2014).

116. Li, F., Jiang, X., Zhao, J. & Zhang, S. Graphene oxide: A promising nanomaterial for energy and environmental applications. *Nano Energy* **16,** 488–515 (2015).

117. You, S., Luzan, S., Yu, J., Sundqvist, B. & Talyzin, A. V. Phase transitions in graphite oxide solvates at temperatures near ambient. *J. Phys. Chem. Lett.* **3,** 812–817 (2012).

118. Zhou, S. & Bongiorno, A. Origin of the chemical and kinetic stability of graphene oxide. *Sci. Rep.* **3,** 2484 (2013).

119. Yue, H. *et al.* The role of the lateral dimension of graphene oxide in the regulation of cellular responses. *Biomaterials* **33,** 4013–4021 (2012).

120. Zhang, H. *et al.* Uniform ultrasmall graphene oxide nanosheets with low cytotoxicity and high cellular uptake. *ACS Appl. Mater. Interfaces* **5,** 1761–1767 (2013).

121. Li, B. *et al.* Influence of polyethylene glycol coating on biodistribution and toxicity of nanoscale graphene oxide in mice after intravenous injection. *Int. J. Nanomedicine* **9,** 4697–4707 (2014).

122. Guo, X. & Mei, N. Assessment of the toxic potential of graphene family nanomaterials. *J. Food Drug Anal.* **22,** 105–115 (2014).

123. Robinson, J. T., Perkins, F. K., Snow, E. S., Wei, Z. & Sheehan, P. E. Reduced graphene oxide molecular sensors. *Nano Lett.* **8,** 3137–3140 (2008).

124. Furue, R. *et al.* Arsine gas sensor based on gold-modified reduced graphene oxide. *Sensors Actuators B Chem.* **240,** 657–663 (2017).

125. Urbanová, V., Bakandritsos, A., Jakubec, P., Szambó, T. & Zbořil, R. A facile graphene oxide based sensor for electrochemical detection of neonicotinoids. *Biosens. Bioelectron.* **89,** 532–537 (2017).

126. Zhang, Q. *et al.* Mechanically robust honeycomb graphene aerogel multifunctional polymer composites. *Carbon N. Y.* **93,** 659–670 (2015).

127. Feng, B., Xu, K. & Huang, A. Covalent synthesis of three-dimensional graphene oxide framework (GOF) membrane for seawater desalination. *Desalination* **394,** 123–130 (2016).

128. Song, J. J. *et al.* Ultrathin graphene oxide membranes for the removal of humic acid. *Sep. Purif. Technol.* **144,** 162–167 (2015).

129. Lee, J. *et al.* Graphene oxide nanoplatelets composite membrane with hydrophilic and antifouling properties for wastewater treatment. *J. Memb. Sci.* **448,** 223–230 (2013).

130. Chen, X., Qiu, M., Ding, H., Fu, K. & Fan, Y. A reduced graphene oxide nanofiltration membrane intercalated by well-dispersed carbon nanotubes for drinking water purification. *Nanoscale* **8,** 5696–5705 (2016).

131. Hung, W.-S. *et al.* Cross-linking with diamine monomers to prepare composite graphene oxide-framework membranes with varying d-spacing. *Chem. Mater.* **26,** 2983–2990 (2014).

132. Wei, N., Peng, X. & Xu, Z. Understanding water permeation in graphene oxide membranes. *ACS Appl. Mater. Interfaces* **6,** 5877–5883 (2014).

133. Duan, J. *et al.* Graphene oxide aerogel-supported Pt electrocatalysts for methanol oxidation. *J. Power Sources* **285,** 76–79 (2015).

134. Xu, X. *et al.* Self-sensing, ultralight, and conductive 3D graphene/iron oxide aerogel elastomer deformable in a magnetic field. *ACS Nano* **9,** 3969–3977

(2015).

135. Yang, S., Chen, L., Mu, L. & Ma, P.-C. Magnetic graphene foam for efficient adsorption of oil and organic solvents. *J. Colloid Interface Sci.* **430,** 337–344 (2014).

136. Liu, T., Song, W. L. & Fan, L. Z. Alcohol-dependent environments for fabricating graphene aerogels toward supercapacitors. *Electrochim. Acta* **173,** 1–6 (2015).

137. Quan, K. *et al.* Black hemostatic sponge based on facile prepared cross-linked graphene. *Colloids Surfaces B Biointerfaces* **132,** 27–33 (2015).

138. Hu, H., Zhao, Z., Wan, W., Gogotsi, Y. & Qiu, J. Polymer/graphene hybrid aerogel with high compressibility, conductivity, and 'sticky' superhydrophobicity. *ACS Appl. Mater. Interfaces* **6,** 3242–3249 (2014).

139. Fan, Z. *et al.* Thermal and electrical properties of graphene/carbon nanotube aerogels. *Colloids Surfaces A Physicochem. Eng. Asp.* **445,** 48–53 (2014).

140. Mangadlao, J. D. *et al.* Graphene oxide-poly(ethylene glycol) methyl ether methacrylate nanocomposite hydrogels. *Macromol. Chem. Phys.* **217,** 101–107 (2016).

141. Cheng, C. *et al.* Biomimetic assembly of polydopamine-layer on graphene: Mechanisms, versatile 2D and 3D architectures and pollutant disposal. *Chem. Eng. J.* **228,** 468–481 (2013).

142. Li, R. *et al.* A facile approach to superhydrophobic and superoleophilic graphene/polymer aerogels. *J. Mater. Chem. A* **2,** 3057–3064 (2014).

143. Li, Y. *et al.* A robust salt-tolerant superoleophobic alginate/graphene oxide aerogel for efficient oil/water separation in marine environments. *Sci. Rep.* **7,** 46379 (2017).

144. Hao, P. *et al.* Graphene-based nitrogen self-doped hierarchical porous carbon aerogels derived from chitosan for high performance supercapacitors. *Nano*

Energy **15,** 9–23 (2015).

145. Liu, Y. *et al.* Ethylene glycol reduced graphene oxide/polypyrrole composite for supercapacitor. *Electrochim. Acta* **88,** 519–525 (2013).

146. Fan, Z., Gong, F., Nguyen, S. T. & Duong, H. M. Advanced multifunctional graphene aerogel-poly(methyl methacrylate) composites: Experiments and modeling. *Carbon N. Y.* **81,** 396–404 (2015).

147. Felder, R. M. & Rousseau, R. W. *Elementary Principles of Chemical Processes*. *Journal of Chemical Information and Modeling* **1,** (John Wiley&Sons, Inc., 2005).

148. Senatore, A. & Sarno, M. Few-layer graphene oxide in tribology. in *Carbon Nanomaterials Sourcebook: Graphene, Fullerenes, Nanotubes, and Nanodiamonds* (ed. Sattler, K. D.) 111 (Taylor & Francis Group, 2016).

149. Moayeri, A. Cross-linkable matrix materials for nanoporous membranes using nitroxide-mediated polymerization. (McGill University, 2011).

150. IR table. (2001). Available at: http://www.chem.ucla.edu/~bacher/General/30BL/IR/ir.html. (Accessed: 7th July 2017)

151. Zhang, K., Li, H., Xu, X. & Yu, H. Facile and efficient synthesis of nitrogen-functionalized graphene oxide as a copper adsorbent and its application. *Ind. Eng. Chem. Res.* **55,** 2328–2335 (2016).

152. Bo, Z. *et al.* Green preparation of reduced graphene oxide for sensing and energy storage applications. *Sci. Rep.* **4,** 4684 (2014).

153. Yu, L., Yang, H., Wang, Y. & Jiang, W. Magnetically enhanced superhydrophobic functionalized polystyrene foam for the high efficient cleaning of oil spillage. *Powder Technol.* **311,** 257–264 (2017).

154. Canto, L. B. & Pessan, L. A. Determination of the composition of styrene – glycidyl methacrylate copolymers by FTIR and titration. *Polym. Test.* **21,** 35–

38 (2002).

155. Brar, A. S., Yadav, A. & Hooda, S. Characterization of glycidyl methacrylate/styrene copolymers by one- and two-dimensional NMR spectroscopy. *Eur. Polym. J.* **38,** 1683–1690 (2002).

156. Brar, A. S. & Goyal, A. K. Characterization and optimization of poly(glycidyl methacrylate-co-styrene) synthesized by atom transfer radical polymerization. *Eur. Polym. J.* **44,** 4082–4091 (2008).

157. Zulfiqar, S., Paracha, A. & Zulfiqar, M. Reactivity ratios for the copolymerization of styrene and glycidyl methacrylate by nuclear magnetic resonance spectroscopy. *Jour. Chem. Soc. Pak.* **16,** 207–209 (1994).

158. Kim, J.-Y. & Suh, K.-D. Synthesis of poly(styrene-co-GMA) and its application as in situ reactive compatabilizer. *J. Korean Ind. Eng. Chem.* **3,** 499–506 (1992).

159. Abu Hanifah, S., Hamzah, N. & Heng, L. Y. Rapid synthesis of magnetic microspheres poly(glycidyl methacrylate-co-styrene) by photopolymerization. *Sains Malaysiana* **42,** 487–493 (2013).

160. Nardecchia, S., Carriazo, D., Ferrer, M. L., Gutiérrez, M. C. & del Monte, F. Three dimensional macroporous architectures and aerogels built of carbon nanotubes and/or graphene: synthesis and applications. *Chem. Soc. Rev.* **42,** 794–830 (2013).

161. Yan, J. *et al.* Functionalized graphene oxide with ethylenediamine and 1,6-hexanediamine. *New Carbon Mater.* **27,** 370–376 (2012).

162. Chen, B. *et al.* Carbon-based sorbents with three-dimensional architectures for water remediation. *Small* **11,** 3319–3336 (2015).

APPENDIX A

TGA Thermograms of Graphite and Graphene Oxide

TGA thermograms of graphite and graphene oxide produced are given in Figure A- 1 and Figure A- 2, respectively.

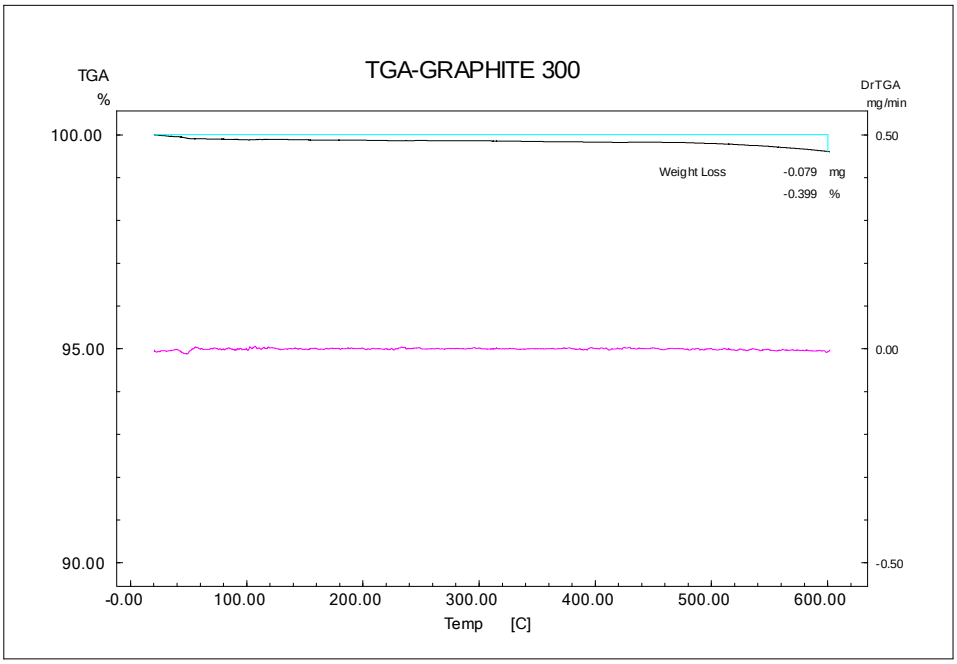

Figure A- 1: TGA thermogram of graphite.

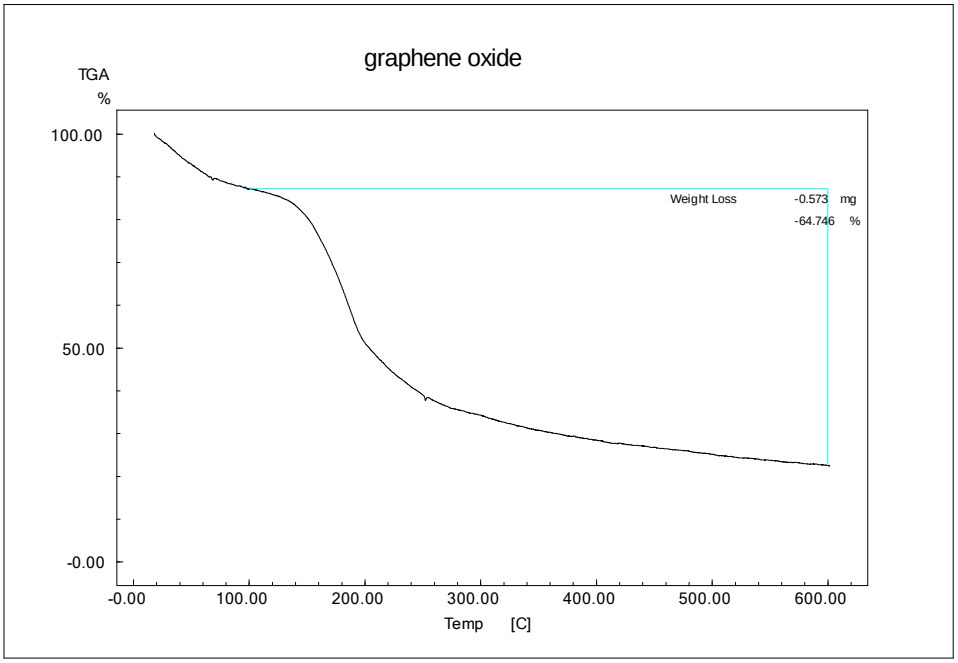

Figure A- 2: TGA thermogram of graphene oxide produced.

APPENDIX B

TGA Thermograms of Copolymers of GMA and Styrene

TGA thermograms of copolymers of GMA and styrene are given in Figure B- 1 and Figure B- 2.

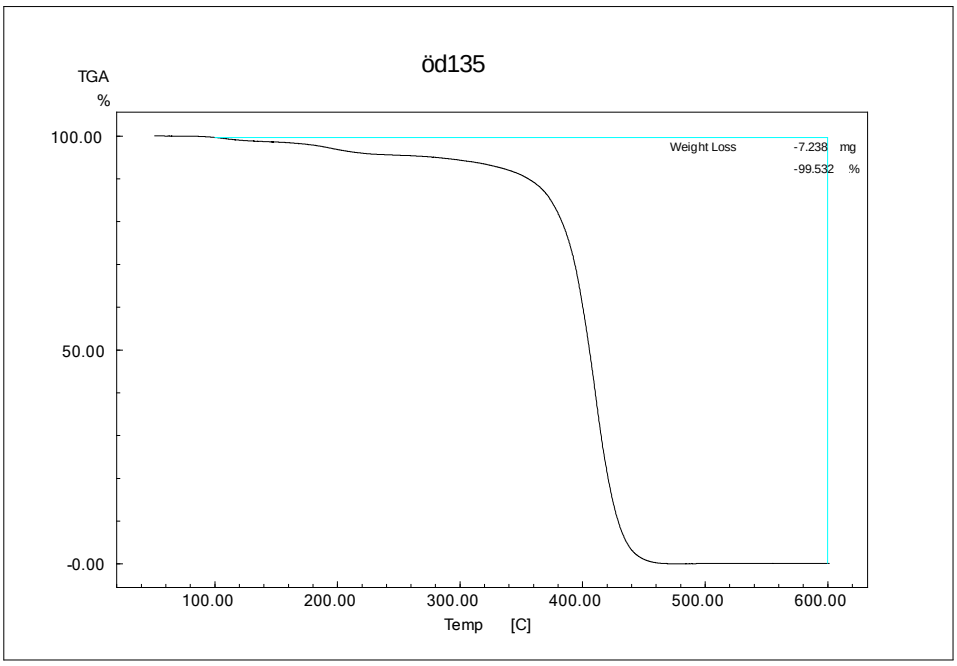

Figure B- 1: TGA thermogram of SG5.

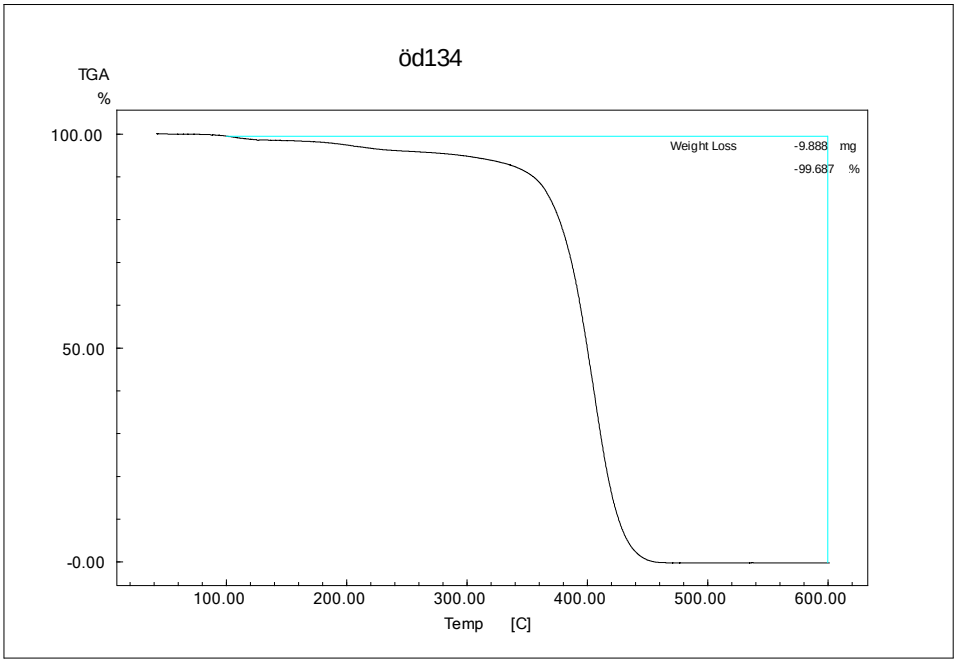

Figure B- 2: TGA thermogram of SG10.

APPENDIX C

TGA Thermograms of Reduced Graphene Oxide and Copolymer Based Aerogels

TGA thermograms of reduced graphene oxide and copolymer based aerogels are given in Figure C- 1 to Figure C- 10.

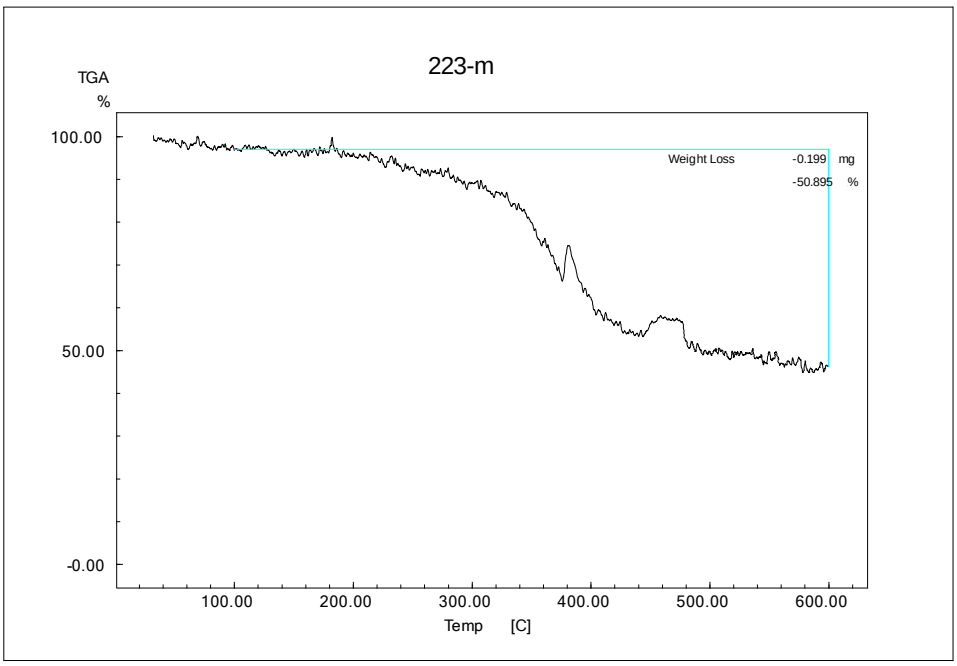

Figure C- 1: TGA thermogram of a reduced graphene oxide and copolymer based aerogel containing 1.5 mg/mL SG5.

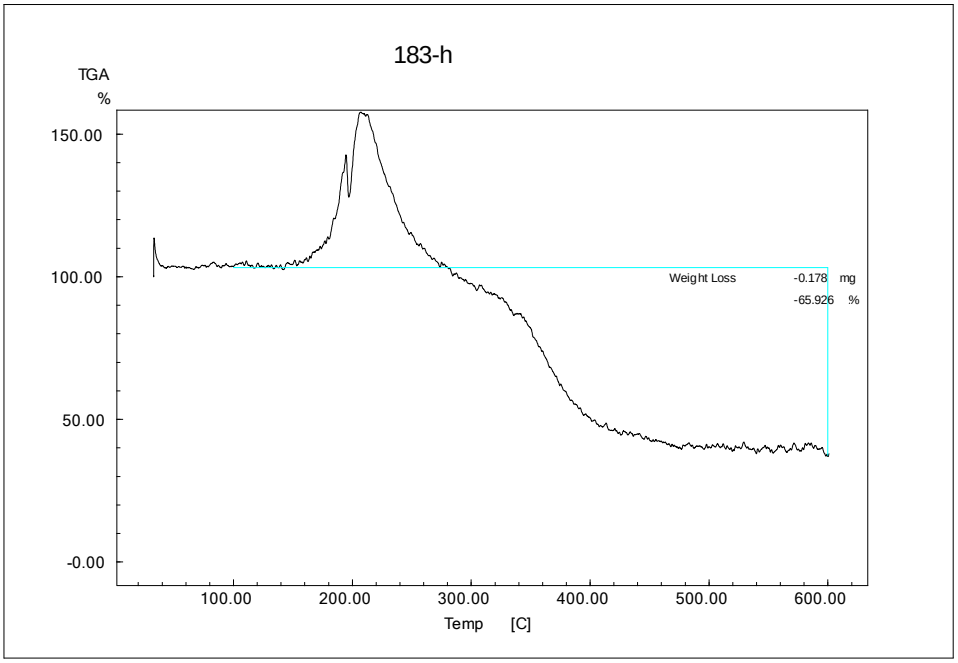

Figure C- 2: TGA thermogram of a reduced graphene oxide and copolymer based aerogel containing 1.5 mg/mL SG10.

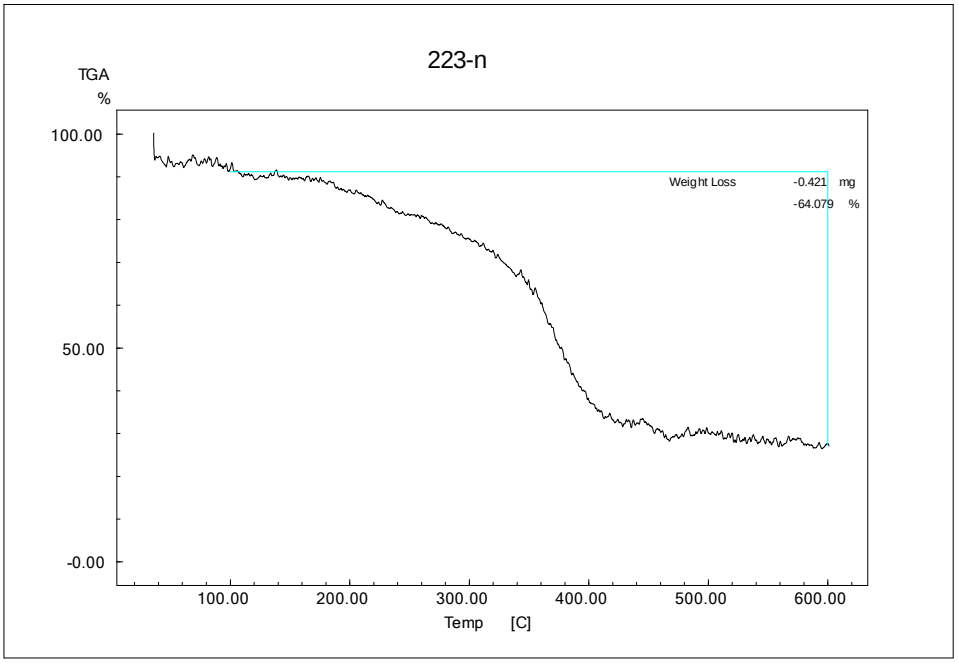

Figure C- 3: TGA thermogram of a reduced graphene oxide and copolymer based aerogel containing 2 mg/mL SG5.

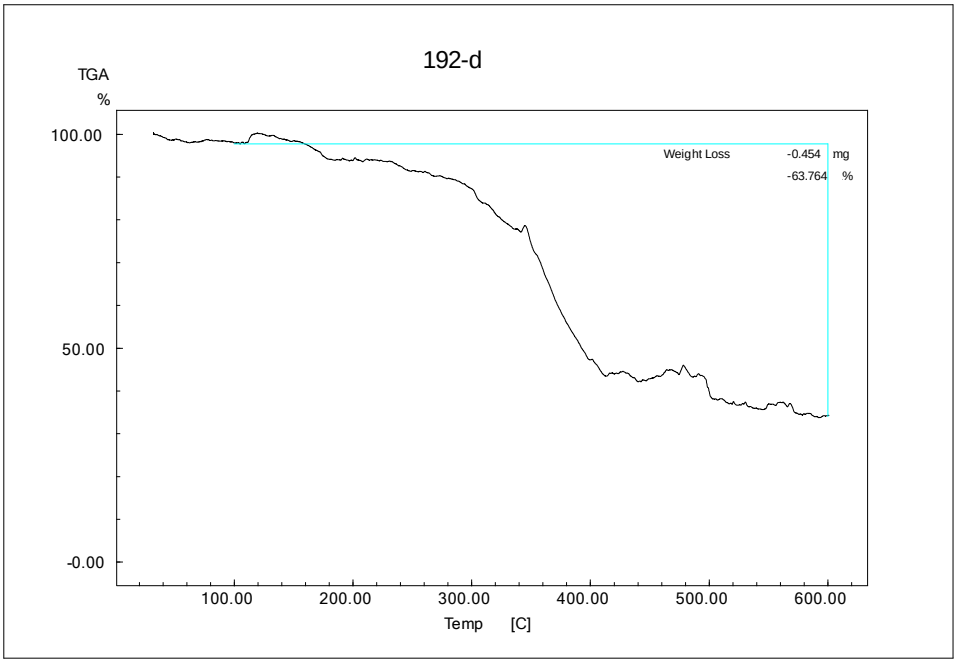

Figure C- 4: TGA thermogram of a reduced graphene oxide and copolymer based aerogel containing 2 mg/mL SG10.

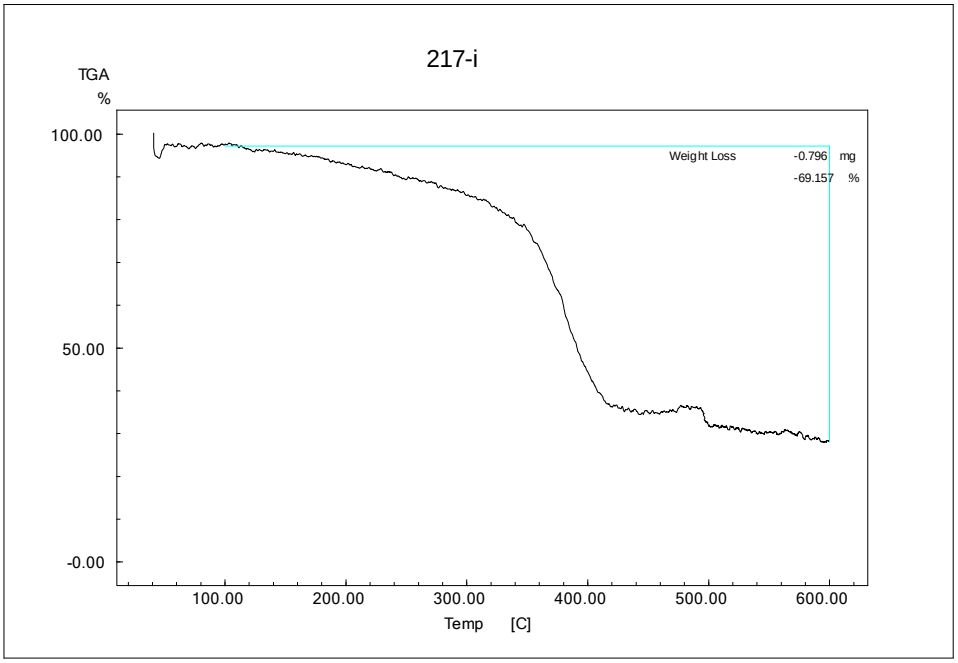

Figure C- 5: TGA thermogram of a reduced graphene oxide and copolymer based aerogel containing 3 mg/mL SG5.

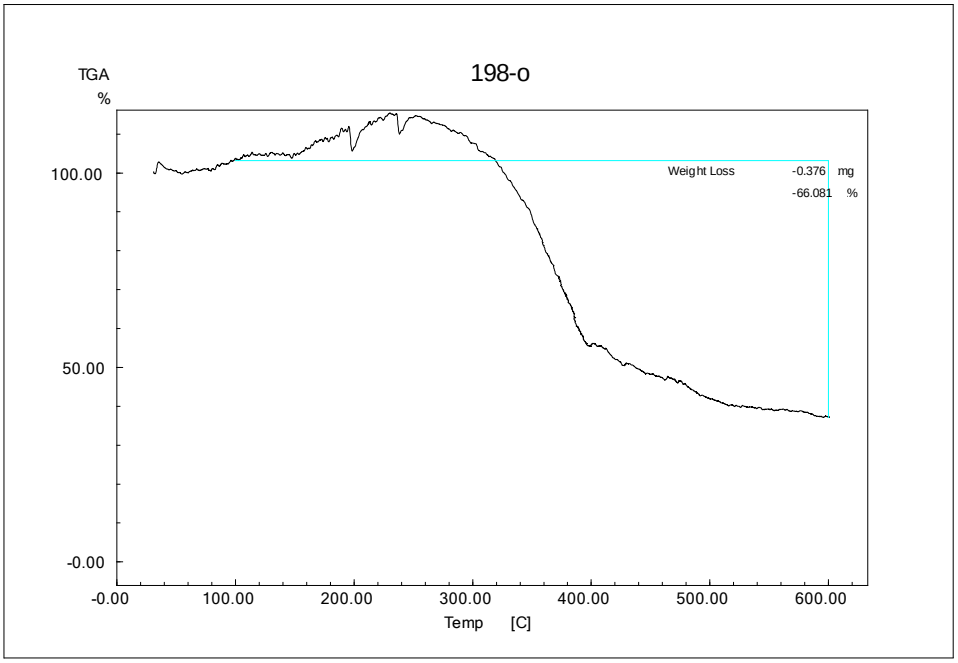

Figure C- 6: TGA thermogram of a reduced graphene oxide and copolymer based aerogel containing 3 mg/mL SG10.

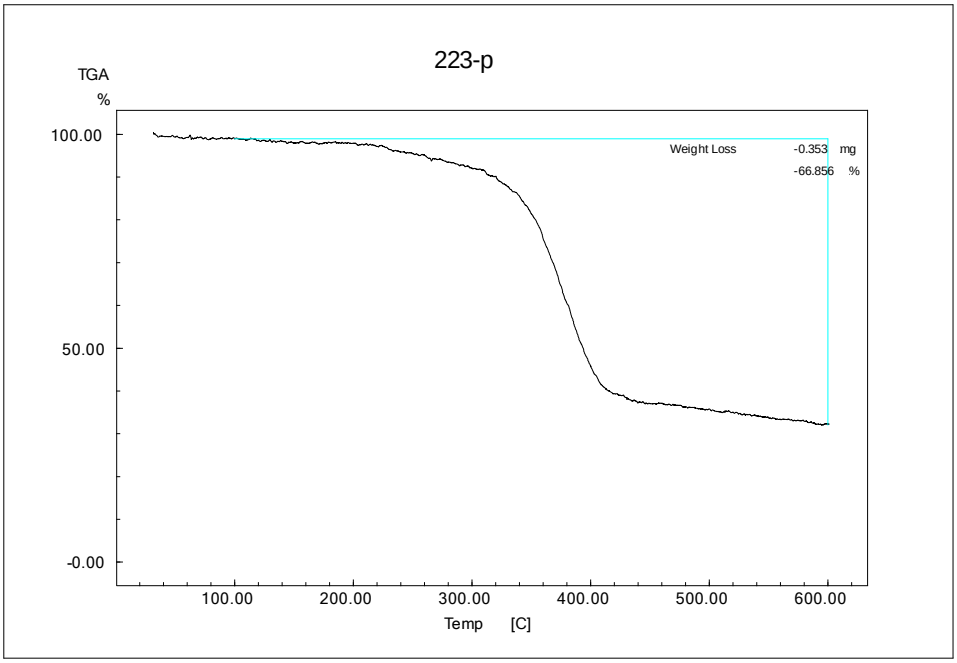

Figure C- 7: TGA thermogram of a reduced graphene oxide and copolymer based aerogel containing 4 mg/mL SG5.

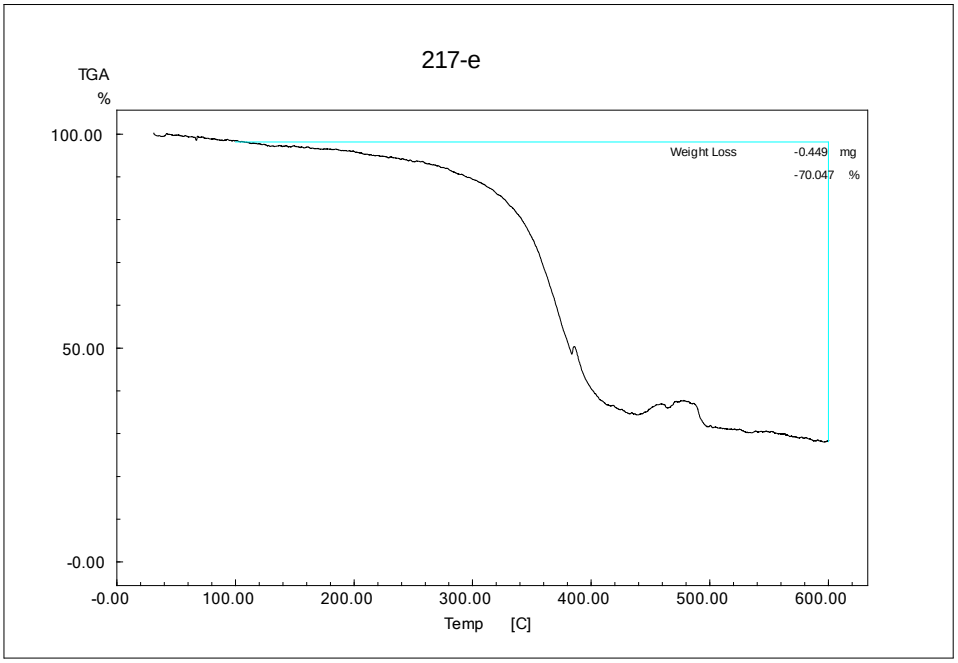

Figure C- 8: TGA thermogram of a reduced graphene oxide and copolymer based aerogel containing 4 mg/mL SG10.

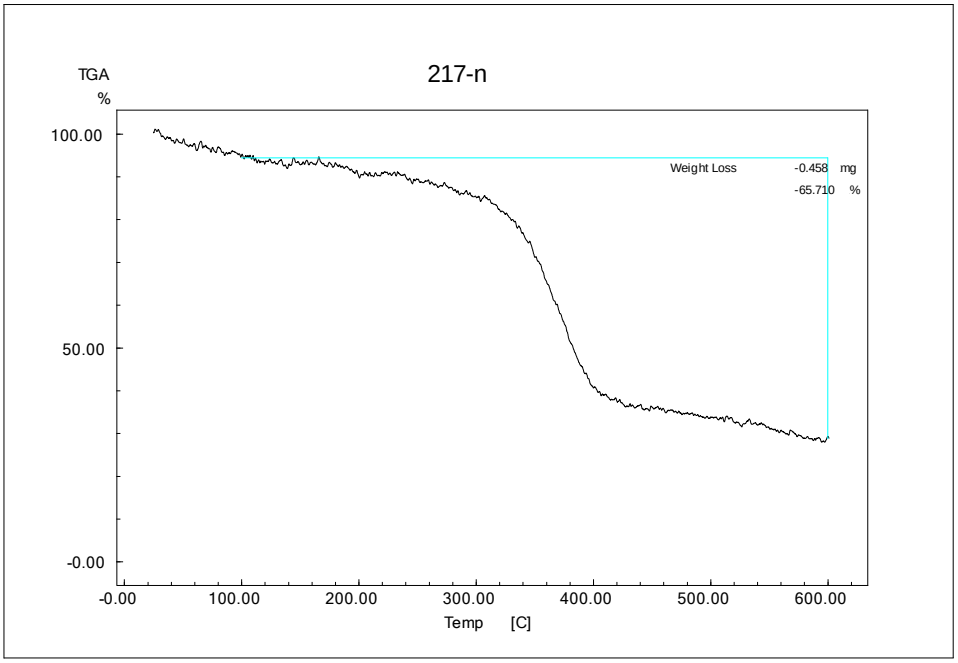

Figure C- 9: TGA thermogram of a reduced graphene oxide and copolymer based aerogel containing 5 mg/mL SG5.

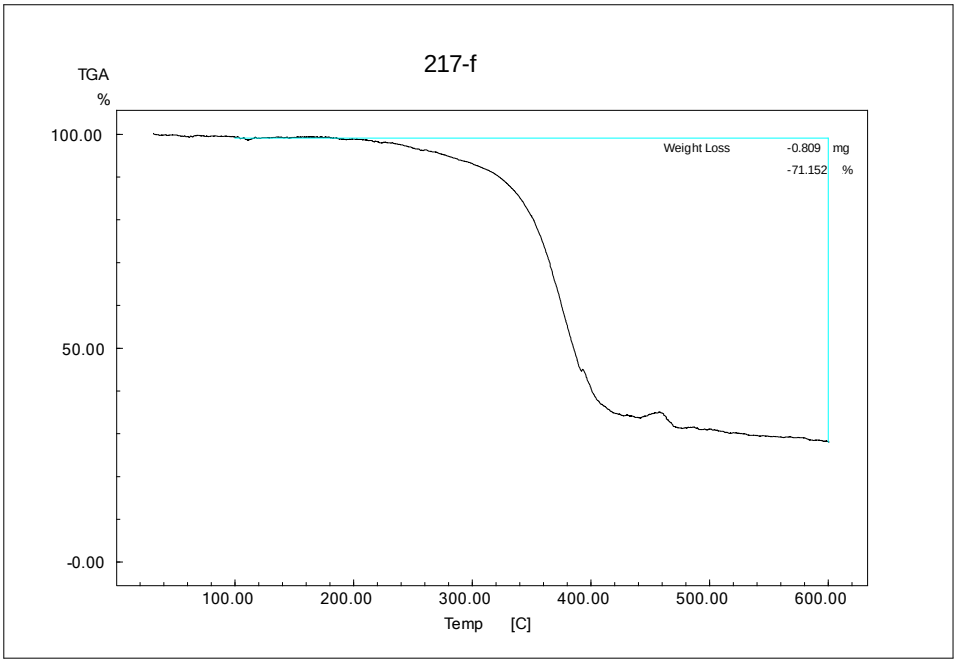

Figure C- 10: TGA thermogram of a reduced graphene oxide and copolymer based aerogel containing 5 mg/mL SG10.